03274-3
DOE/ER/~~02374-3~~

NUCLEAR MOMENTS AND NUCLEAR STRUCTURE

Annual Progress Report

Leon Madansky and Yung Keun Lee

The Johns Hopkins University

Baltimore, Maryland

August 1, 1981 - August 31, 1982

PREPARED FOR THE DEPARTMENT OF ENERGY UNDER CONTRACT

DE-AC02-76 ER03274.A009

DISCLAIMER

The following pages are an exact representation of what is in the original document folder.

DOE/ER/02374-3

DOE/ER/03274--3

DE83 001625

NUCLEAR MOMENTS AND NUCLEAR STRUCTURE

Annual Progress Report

Leon Madansky and Yung Keun Lee

The Johns Hopkins University

Baltimore, Maryland

August 1, 1981 - August 31, 1982

PREPARED FOR THE DEPARTMENT OF ENERGY UNDER CONTRACT

DE-AC02-76 ER03274.A009

THIS PAGE

WAS INTENTIONALLY

LEFT BLANK

RESEARCH STAFF:

Professor Leon Madansky, Co-Research Director

Professor Yung Keun Lee, Co-Research Director

Professor James Calvin Walker

Dr. Edward K. McIntyre, Jr.	Postdoctoral Fellow
Mr. Timothy J. Hallman	Research Assistant
Mr. Ron Levin	Research Assistant
Mr. Allan Posner	Research Assistant

THIS PAGE

WAS INTENTIONALLY

LEFT BLANK

TABLE OF CONTENTS

THIS PAGE

WAS INTENTIONALLY

LEFT BLANK

INTRODUCTION

This report is a review of the activities of the period from August 1, 1981 through August 31, 1982. The final analysis of pi-zero production in heavy ion collisions representing experiments at the Bevalac with a system previous described is completed. The main results involve cross sections for central collisions resulting in the production of pi-zeros, charged pions, and proton multiplicities, and some results of correlations and low energy gamma radiation.

Results from the alpha-alpha experiment at the CERN ISR are included in the form of a published paper and an outline of papers that are in press. A short report of a collision effect in an "anomalon" experiment is included as well.

The energetic particle spectra from μ^--capture in medium heavy nuclei were studied at TRIUMF, using the large scintillation counters for neutron and proton detection and multiple Ge(Li) and NaI(Tl) counters. The preliminary analysis indicates the presence of such an unusual energetic component. The measurement of the particle and γ-ray correlation in π^--capture in ^{165}Ho was completed during this year, and the data analysis is continuing in order to elucidate the discrete spectral features, high spin generation and other correlations. A measurement was finished in our search for a new type of strong perturbation of pionic x-ray by the use of coincidences between pionic x-rays and γ-rays from a deformed nuclei.

RESUMÉ OF RESULTS FROM EXPERIMENT E399H

T. Hallman and L. Madansky

The experimental apparatus employed in experiment 399H—an experiment designed to search for threshold phenomena in central collisions of relativistic heavy ions—has been described previously in Annual Report, DOE/ER/02374-2 (1981). Following is a brief synopsis describing selected analyses which have already been completed. Specifically, the charged particle multiplicity, rate of neutral pion production, and low energy gamma ray yields found to characterize central collisions of relativistic ^{12}C and ^{40}Ar on Pb have been discussed briefly to indicate the character of the results afforded by this research. Furthermore, the associated rate of charged pion production and characteristic 2-particle correlations will be discussed as well. The analysis of these data has been completed and a detailed account of the results of experiment 399H will be presented in the doctoral dissertation of T. Hallman as well as in a forthcoming publication. It is thought that these data are among the most comprehensive taken to date insofar as a great many characteristic parameters have been examined simultaneously. As a consequence, these results are of particular interest and, hopefully, will provide a more complete description of relativistic heavy ion collisions than any available thus far.

Using a 40-element dE/dx scintillator array, it was possible to determine statistically the average number of charged reaction products associated with a given heavy ion collision. The multiplicity distributions from which average values have been extracted are shown in Fig. 1a-h.

While the upstream and total multiplicity distributions are generally symmetric, even gaussian in appearance, the downstream distributions exhibit

Figure 1 Charged Particle Multiplicity Distributions

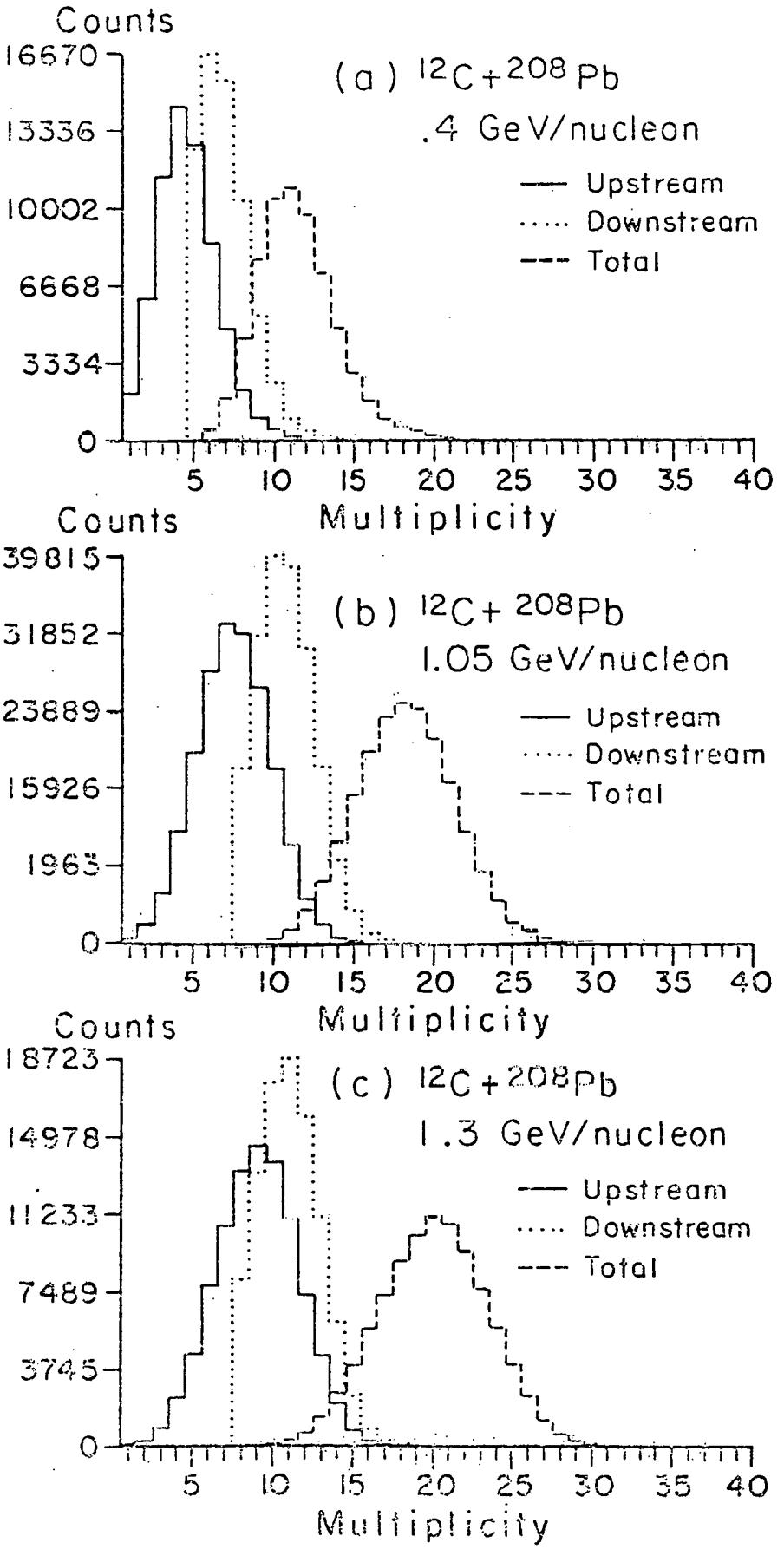

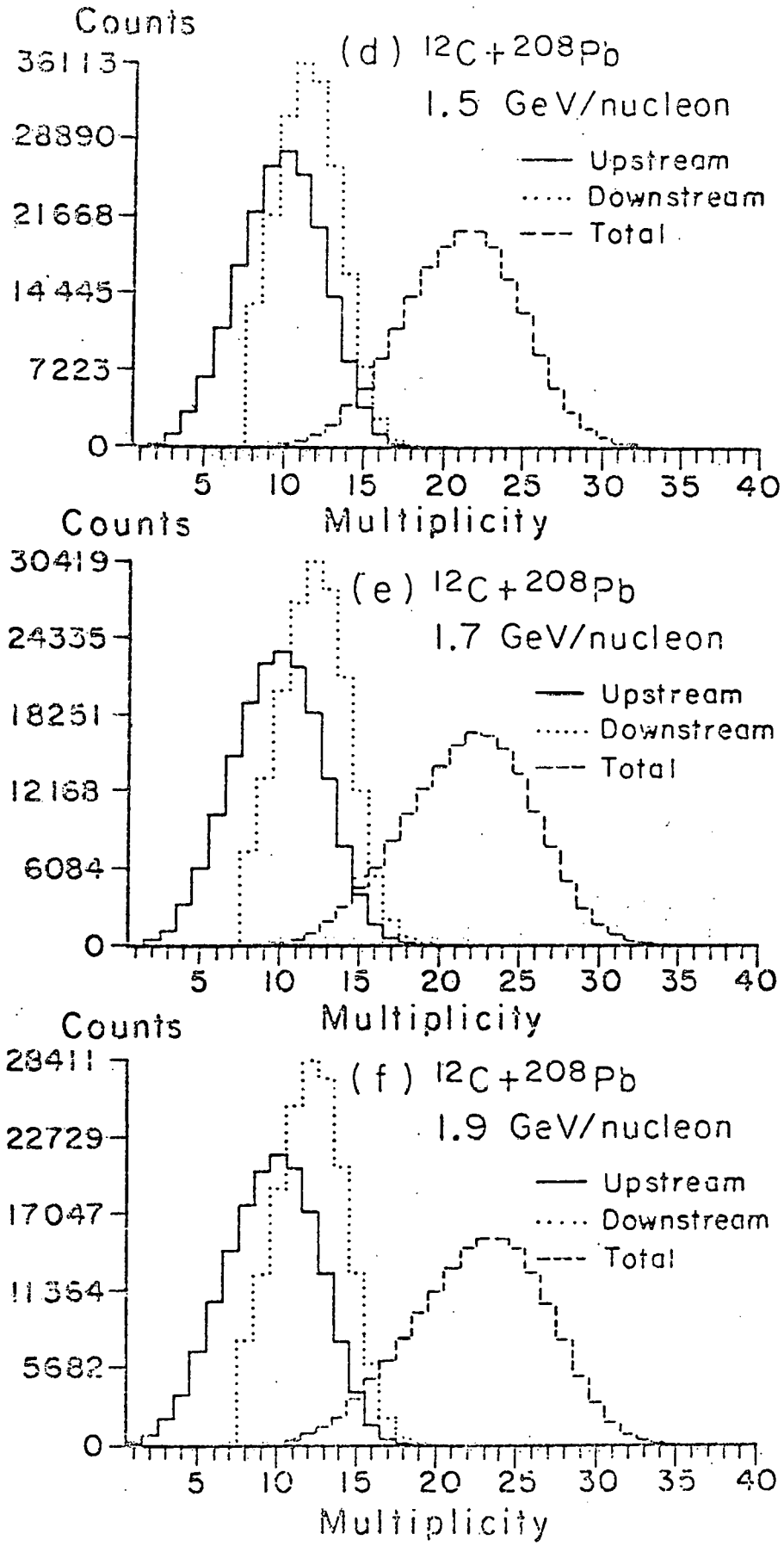
Counts
(d) $^{12}C+^{208}Pb$
1.5 GeV/nucleon
Upstream
Downstream
Total
36113
28890
21668
14445
7223
0
5 10 15 20 25 30 35 40
Multiplicity
Counts
(e) $^{12}C+^{208}Pb$
1.7 GeV/nucleon
Upstream
Downstream
Total
30419
24335
18251
12168
6084
0
5 10 15 20 25 30 35 40
Multiplicity
Counts
(f) $^{12}C+^{208}Pb$
1.9 GeV/nucleon
Upstream
Downstream
Total
28411
22729
17047
11364
5682
0
5 10 15 20 25 30 35 40
Multiplicity

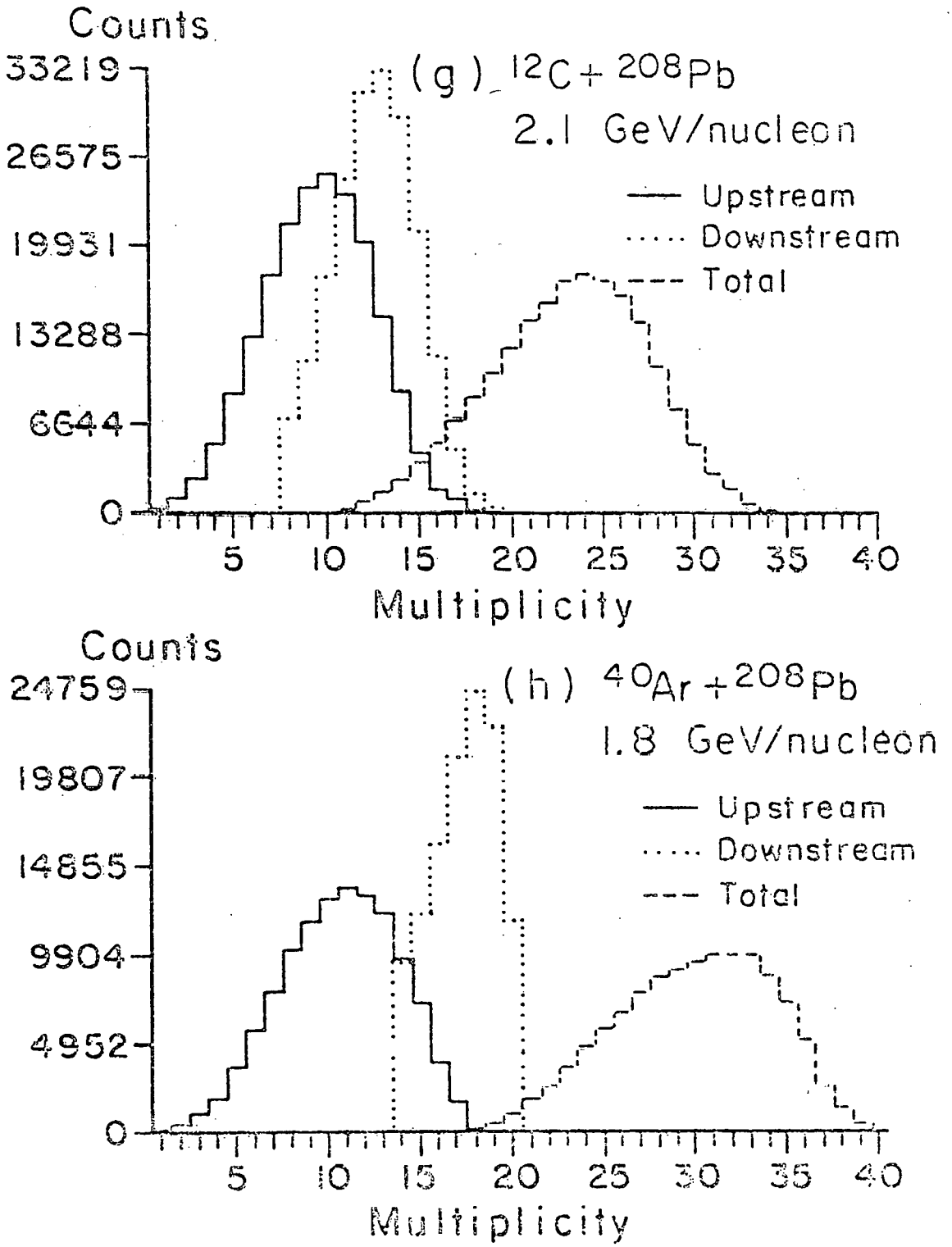
Counts
33219
26575
19931
13288
6644
0
(g) $^{12}C + ^{208}Pb$
2.1 GeV/nucleon
Upstream
Downstream
Total
5
10
15
20
25
30
35
40
Multiplicity
Counts
24759
19807
14855
9904
4952
0
(h) $^{40}Ar + ^{208}Pb$
1.8 GeV/nucleon
Upstream
Downstream
Total
5
10
15
20
25
30
35
40
Multiplicity

TABLE I: Charged Particle Multiplicity

I Energy (GeV/n)	II Beam	III Target	IV <m> measured upstream	V <m> measured downstream	VI <m> real upstream (a) $M \pm ((\Delta M)^2)^{\frac{1}{2}} \frac{\Delta M}{M}$	VI (b) M	VII <m> real downstream (a)	VII (b)	VIII <m> real total*	IX <m> real total†	X <m> real total††
.4	^{12}C	^{208}Pb	4.5	6.9	5.1 ± 2.4	.47	5.3	8.8 ± 1.7	8.8	14.1	14.8	15.7
1.05	^{12}C	^{208}Pb	7.4	10.7	9.3 ± 3.2	.34	9.6	15.6 ± 1.4	16.0	25.6	27.0	28.4
1.3	^{12}C	^{208}Pb	9.0	11.0	12.0 ± 4.1	.34	12.3	16.4 ± 1.9	16.8	29.1	30.6	32.2
1.5	^{12}C	^{208}Pb	9.7	11.4	13.4 ± 4.6	.34	13.7	16.9 ± 2.3	17.5	31.2	32.8	34.5
1.7	^{12}C	^{208}Pb	9.7	12.0	13.6 ± 4.8	.35	13.8	18.4 ± 3.6	19.2	33.0	34.7	36.5
1.9	^{12}C	^{208}Pb	10.6	12.1	15.5 ± 5.5	.35	15.7	18.7 ± 3.1	19.3	35.0	36.9	38.7
2.1	^{12}C	^{208}Pb	10.5	12.6	15.3 ± 5.6	.37	15.5	20.1 ± 3.9	20.7	36.2	38.1	40.0
1.8	^{40}Ar	^{208}Pb	12.6	17.3	20.4 ± 8.4	.41	20.7	———	39.7	60.4	63.6	67.2

* Corrected for coincidence summing only.

† Corrected additionally for missing detector acceptance.

†† Corrected additionally for proton low energy threshold.

somewhat greater asymmetry due to a low multiplicity cutoff used to eliminate non target-associated background events. From Fig. 1 however, it is clear that the asymmetry introduced in this manner is minimal and the associated error made in evaluating the downstream average is small. Nevertheless, it is noted that, because of the low multiplicity cutoff made, values of the downstream multiplicity extracted from these distributions must be regarded as representing an upper limit.

Values of the average real multiplicity of charged reaction products derived from the distributions shown in Fig. 1 are listed in column 10 of Table I. These results have been corrected for coincidence summing, missing detector acceptance, and a low energy threshold imposed by the construction of the multiplicity detector itself. Upon further subtracting, where possible, the number of compton electrons, charged pions and electron showers estimated to contribute to the values quoted in Table I, the estimated number of nucleonic charged secondaries denoted in Table II is arrived at. One notes that values of the average multiplicity of nucleonic charges so derived are in fair agreement with those predicted by the fireball model[1] (column 1, Table II) although it is also noted that as the beam energy is increased for a given target-projectile combination, the model does not appear to reproduce the attendant increase in the multiplicity of nucleonic charges observed experimentally.

In addition to being of intrinsic interest, the multiplicity information measured in experiment 399H was also used to parameterize other quantities of interest, e.g., the rate of charged pion production.

It is by now generally supposed that, as the impact parameter of

TABLE II: Estimated Nucleonic Charges

I Beam Energy (GeV/n)	II Projectile Ion	III Target Nucleus	IV Total Charges Observed per Event	V Estimated Non-nucleonic Charged Particles per Event	VI Estimated Nucleonic Charged Particles per Event	VII Predicted Proton Multiplicity per Event (Fireball,b=0)
1.05	^{12}C	^{208}Pb	28.4	2.8 - 3.0	25.6 - 25.4	24
2.1	^{12}C	^{208}Pb	40.0	7.1 - 7.8	32.9 - 32.2	24
1.8	^{40}Ar	^{208}Pb	67.2	14.8 - 17.9	52.4 - 49.3	55

a collision between two relativistic heavy nuclei decreases, the resultant multiplicity of charged secondaries will increase although an exact relationship between the two variables has not yet been established. Consequently, to investigate the role impact parameter may play in heavy ion collisions, the data of experiment 399H were investigated as a function of multiplicity as well as bombarding energy.

To accomplish this parameterization of the data, each event was established, according to its associated multiplicity, as belonging to one or more of five different populations. The multiplicity requirements specific to each category are listed in Table III as a function of beam energy and projectile mass. It is noted that in this context multiplicity refers to the number of dE/dx scintillators registering a count in a given event. Populations I, II, and III contain, respectively, events of successively higher multiplicity, while population IV consists primarily of events having a low associated multiplicity. Population Ø contains all events, subject only to a downstream background multiplicity cut. The regions of the upstream and downstream multiplicity distributions so defined are illustrated in Fig. 2.

To measure the production of high energy gamma rays emanating from π° decay the modular NaI system shown in Fig. 3 was employed. Two 5" thick by 10" diameter NaI crystals were placed behind a 12" x 12" x ¼" charged particle veto scintillator, a 1" thick (~one radiation length) NaI gamma ray converter with 10" diameter, and a 5" diameter ¼" thick scintillator paddle. This NaI system was located at an angle of $\theta = 90^\circ$ with respect to the beam axis at a distance of $\cong$ 27" from the target. A high energy gamma ray entering this acceptance would not be detected by

TABLE III: Multiplicity Criteria

Beam Energy (GeV/n)		.4	1.05	1.3	1.5	1.7	1.9	2.1	1.8
Projectile Ion		^{12}C	^{12}C	^{12}C	^{12}C	^{12}C	^{12}C	^{12}C	^{40}Ar
Target Nucleus		^{208}Pb	^{208}Pb	^{208}Pb	^{208}Pb	^{208}Pb	^{208}Pb	^{208}Pb	^{208}Pb
Required multiplicity* for:									
Cut Ø	Upstream	≥ 0	≥ 0	≥ 0	≥ 0	≥ 0	≥ 0	≥ 0	≥ 0
	Downstream	≥ 5	≥ 8	≥ 8	≥ 8	≥ 8	≥ 8	≥ 8	≥ 14
Cut 1	Upstream	≥ 2	≥ 5	≥ 6	≥ 6	≥ 7	≥ 8	≥ 8	≥ 10
	Downstream	≥ 5	≥ 8	≥ 9	≥ 10	≥ 10	≥ 10	≥ 10	≥ 15
Cut 2	Upstream	≥ 4	≥ 7	≥ 9	≥ 9	≥ 10	≥ 11	≥ 11	≥ 14
	Downstream	≥ 6	≥ 10	≥ 11	≥ 12	≥ 12	≥ 12	≥ 13	≥ 18
Cut 3	Upstream	≥ 7	≥ 10	≥ 12	≥ 12	≥ 13	≥ 14	≥ 14	≥ 17
	Downstream	≥ 8	≥ 13	≥ 13	≥ 14	≥ 14	≥ 14	≥ 15	≥ 19
Cut 4	Upstream	≤ 4	≤ 7	≤ 9	≤ 9	≤ 10	≤ 11	≤ 11	≤ 14
	Downstream	$\leq 6, \geq 5$	$\leq 10, \geq 8$	$\leq 11, \geq 8$	$\leq 12, \geq 8$	$\leq 12, \geq 8$	$\leq 12, \geq 8$	$\leq 13, \geq 8$	$\leq 18, \geq 14$

*Multiplicity, in this instance, refers to the number of dE/dx scintillators registering a count. The highest possible multiplicity therefore is 20 upstream, and 20 downstream.

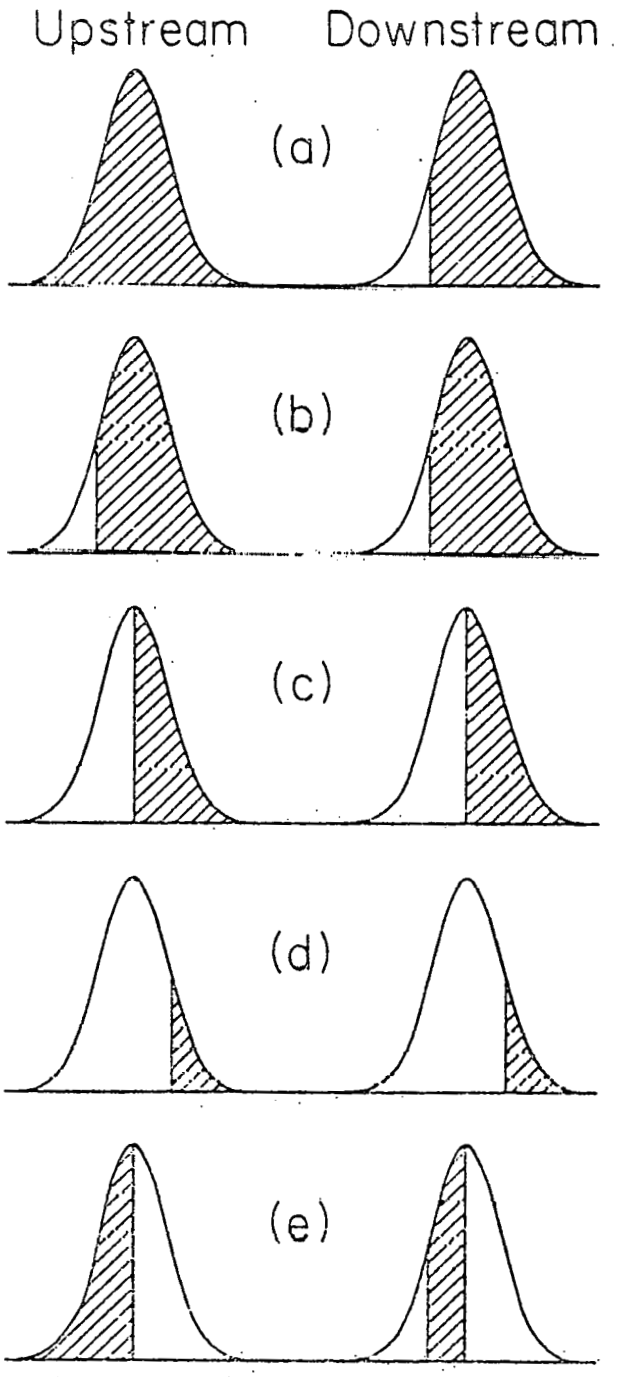

Fig 2 Regions of the upstream and downstream multiplicity distributions defining a) Cut ϕ, b) Cut 1, c) Cut 2, d) Cut 3, e) Cut 4 at each beam energy

Fig 3 High Energy Gamma Ray

NaI Detector System

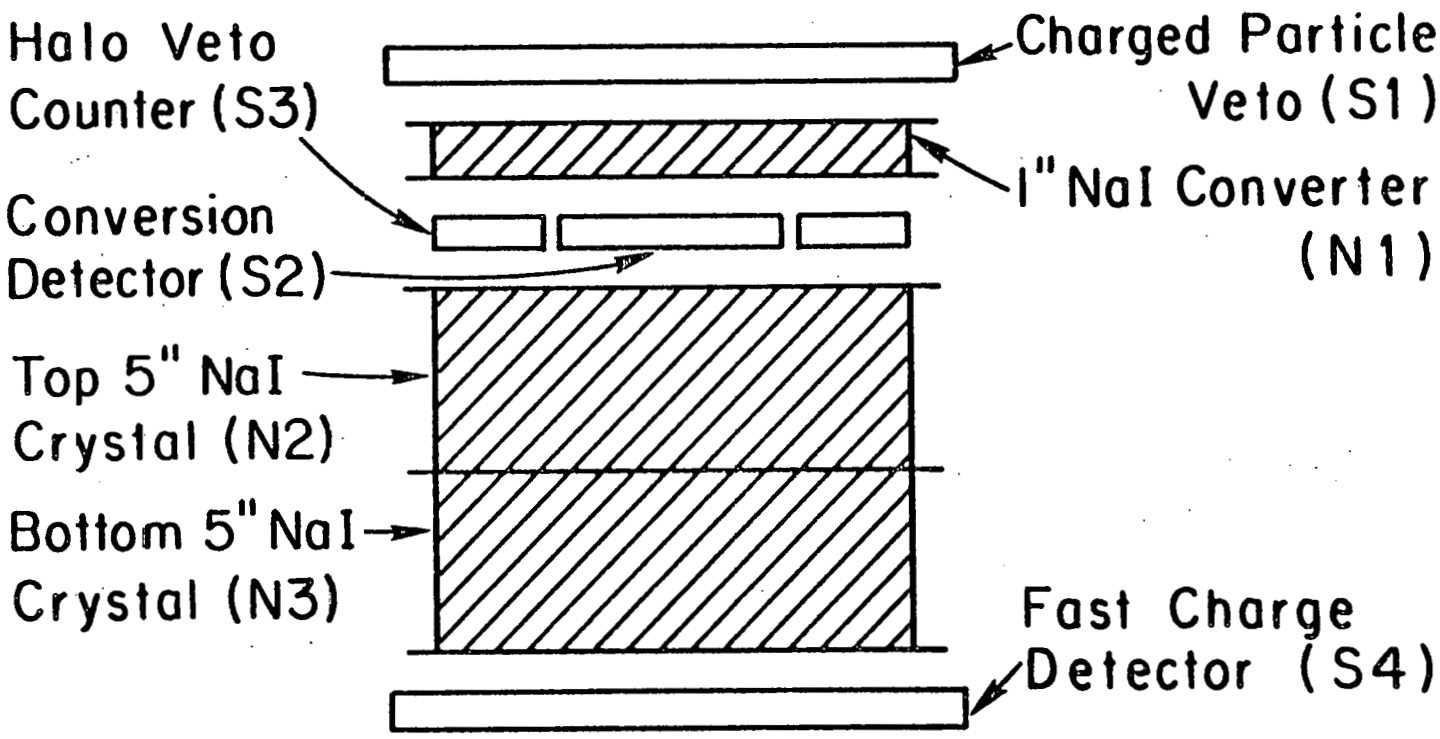

the uppermost charged particle veto, but approximately 50% of the time would subsequently convert to an electron shower in the 1" thick NaI crystal and be observed by the 5" diameter scintillator paddle. The shower would then deposit its remaining energy in the final 10" of NaI. By summing the pulse heights from all three crystals, the total gamma ray energy could be determined. The uppermost veto scintillator effectively eleiminated charged particle contamination from this measurement, and the small probability that a neutron would interact in the 1" thick NaI crystal limited this source of background to less than $\cong$ 1.5%. The overall resolution of this detector system was determined to be $\cong$ 17% at $\cong$ 130 MeV.

For three of the reactions which encompass the range of variation one might expect to observe in the present experiment, namely 1.05 and 2.1 GeV/n ^{12}C + ^{208}Pb, and 1.8 GeV/n ^{40}Ar + ^{208}Pb, the gamma ray pulse height distributions and absolute double differential single photon inclusive spectra $d^2\sigma/dEd\Omega$ at 90^o have been presented in Figs. 4-6 and Figs. 7-9, respectively. Several features of these spectra require explanation.

Although it is not immediately obvious in every instance, the shape of these spectra is flawed. Due to a problem with overflow counts in the top 5" NaI crystal at $\cong$ 170 MeV, the spectra shown in Figs. 4-6 are "bunched up" in the intermediate energy region (140-230 MeV) and consequently fall off too quickly in the high energy region $\gtrsim$ 300 MeV. This effect is most pronounced for the 2.1 GeV/n ^{12}C + ^{208}Pb data, actually giving the semblance of structure to the final distributions. As a result of this difficulty, the <u>detailed</u> behavior of those spectra above $\cong$ 140 MeV should be regarded as suspect, although aside from this problem they are thought

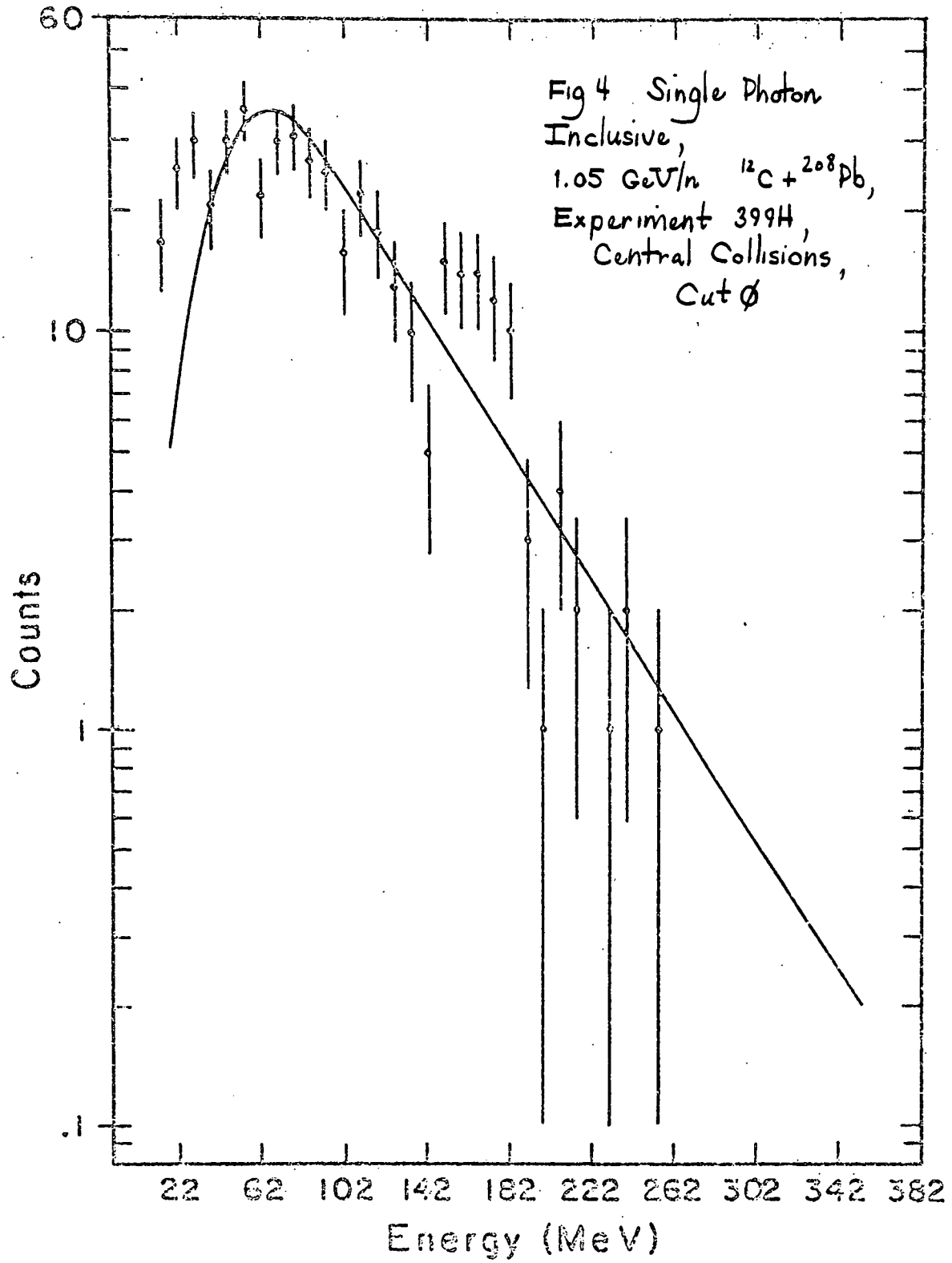

Fig 4 Single Photon Inclusive, 1.05 GeV/n $^{12}C + ^{208}Pb$, Experiment 399H, Central Collisions, Cut Ø

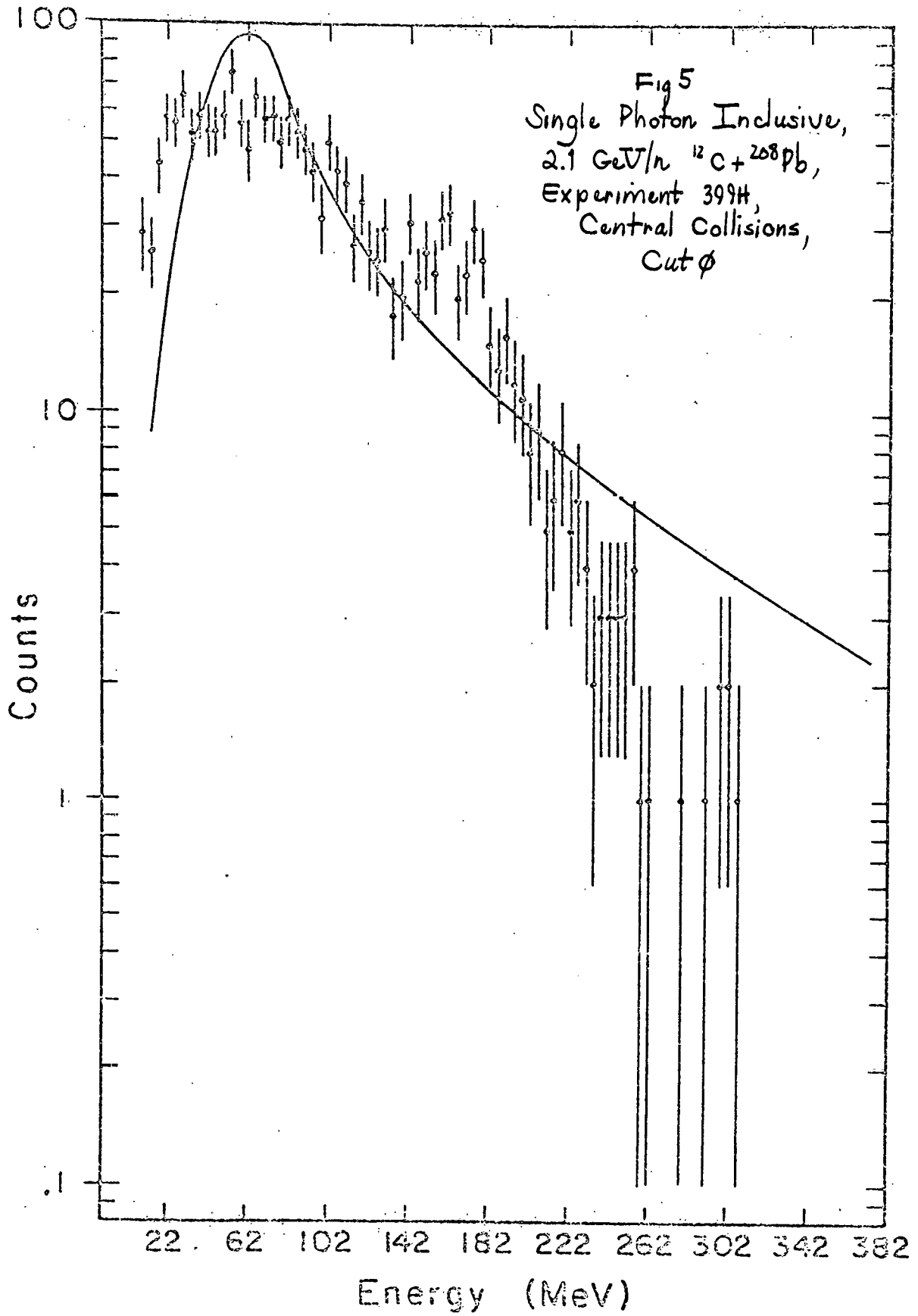

Fig 5
Single Photon Inclusive,
2.1 GeV/n $^{12}C + ^{208}Pb$,
Experiment 399H,
Central Collisions,
Cut ϕ

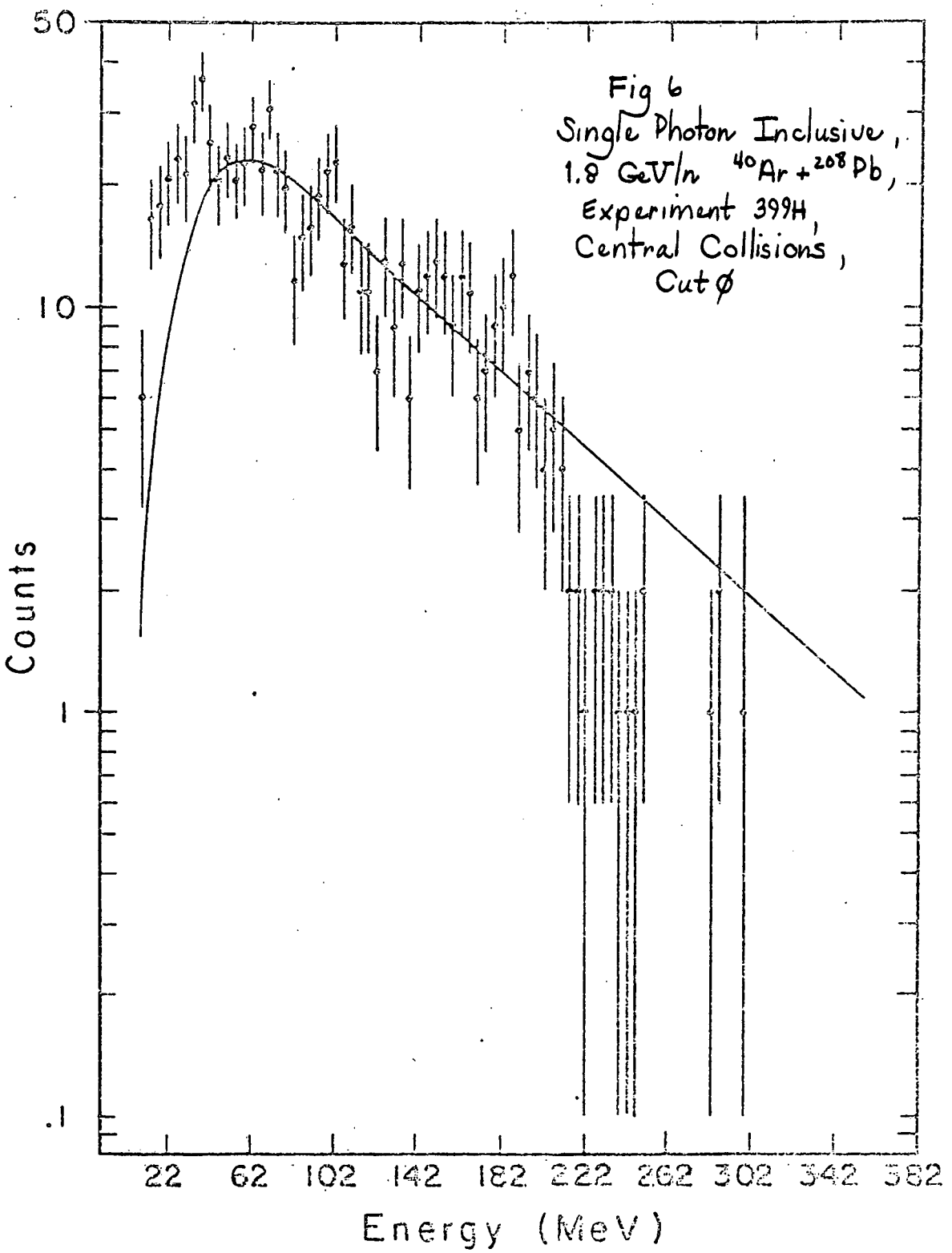

Fig 6
Single Photon Inclusive,
1.8 GeV/n $^{40}Ar + ^{208}Pb$,
Experiment 399H,
Central Collisions,
Cut ϕ

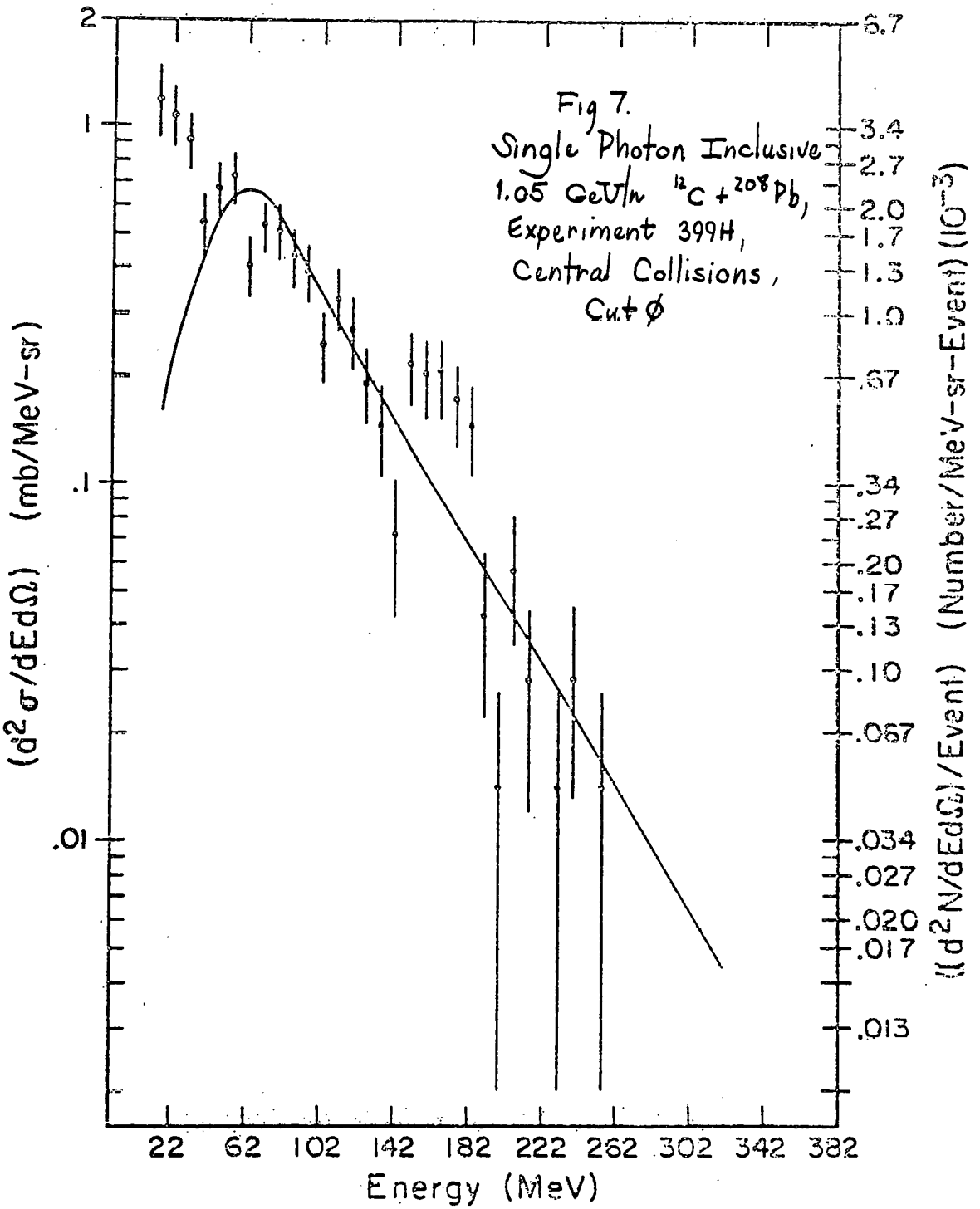
Fig 7.
Single Photon Inclusive
1.05 GeV/n $^{12}C + ^{208}Pb$,
Experiment 399H,
Central Collisions,
Cut ϕ
$(d^2\sigma/dEd\Omega)$ (mb/MeV-sr)
$((d^2N/dEd\Omega)/Event)$ (Number/MeV-sr-Event) (10^{-3})
2
1
.1
.01
6.7
3.4
2.7
2.0
1.7
1.3
1.0
.67
.34
.27
.20
.17
.13
.10
.067
.034
.027
.020
.017
.013
22 62 102 142 182 222 262 302 342 382
Energy (MeV)

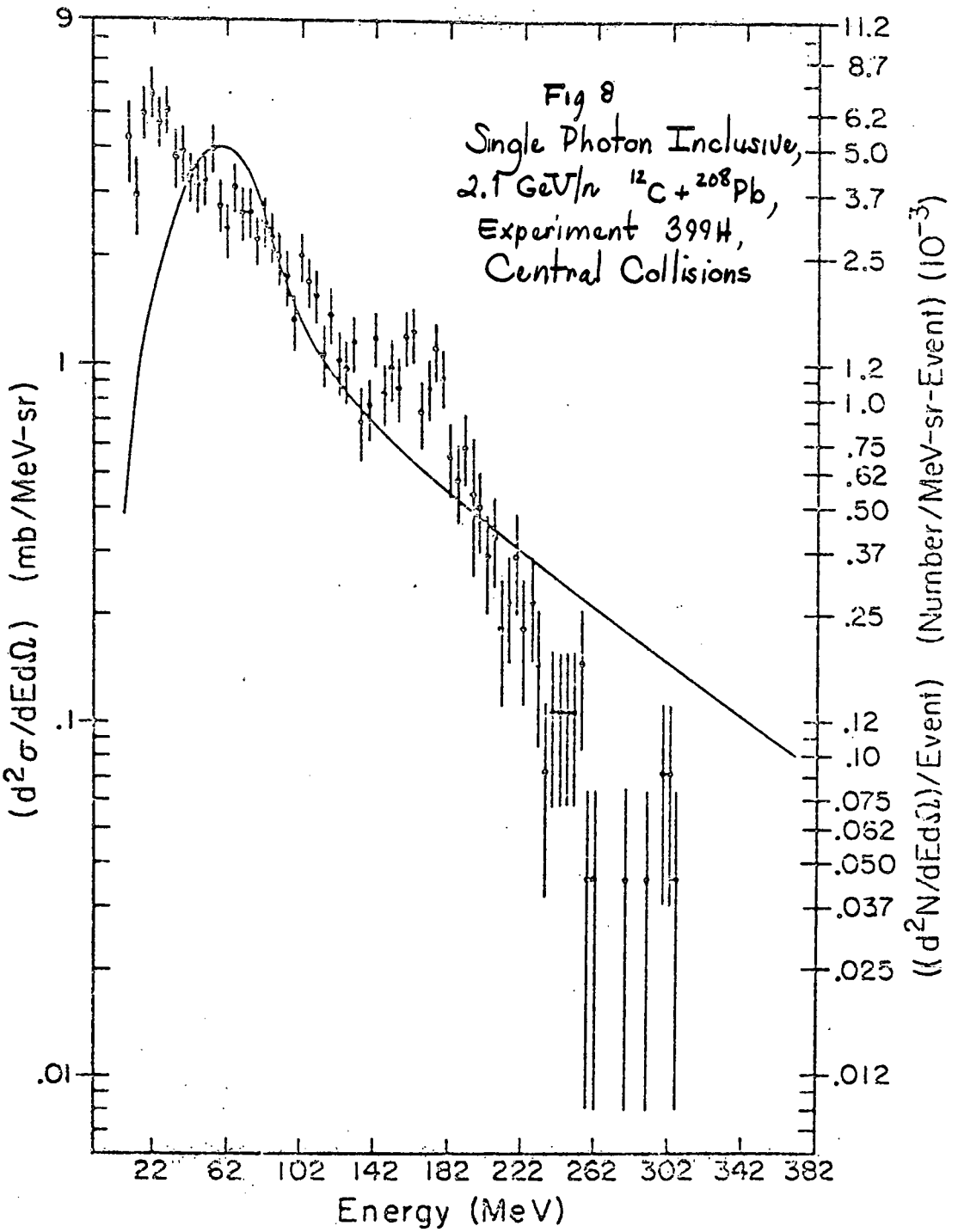
Fig 8
Single Photon Inclusive,
2.1 GeV/n $^{12}C + ^{208}Pb$,
Experiment 399H,
Central Collisions
$(d^2\sigma/dEd\Omega)$ (mb/MeV-sr)
$((d^2N/dEd\Omega)/Event)$ (Number/MeV-sr-Event) (10^{-3})
9
1
.1
.01
11.2
8.7
6.2
5.0
3.7
2.5
1.2
1.0
.75
.62
.50
.37
.25
.12
.10
.075
.062
.050
.037
.025
.012
22
62
102
142
182
222
262
302
342
382
Energy (MeV)

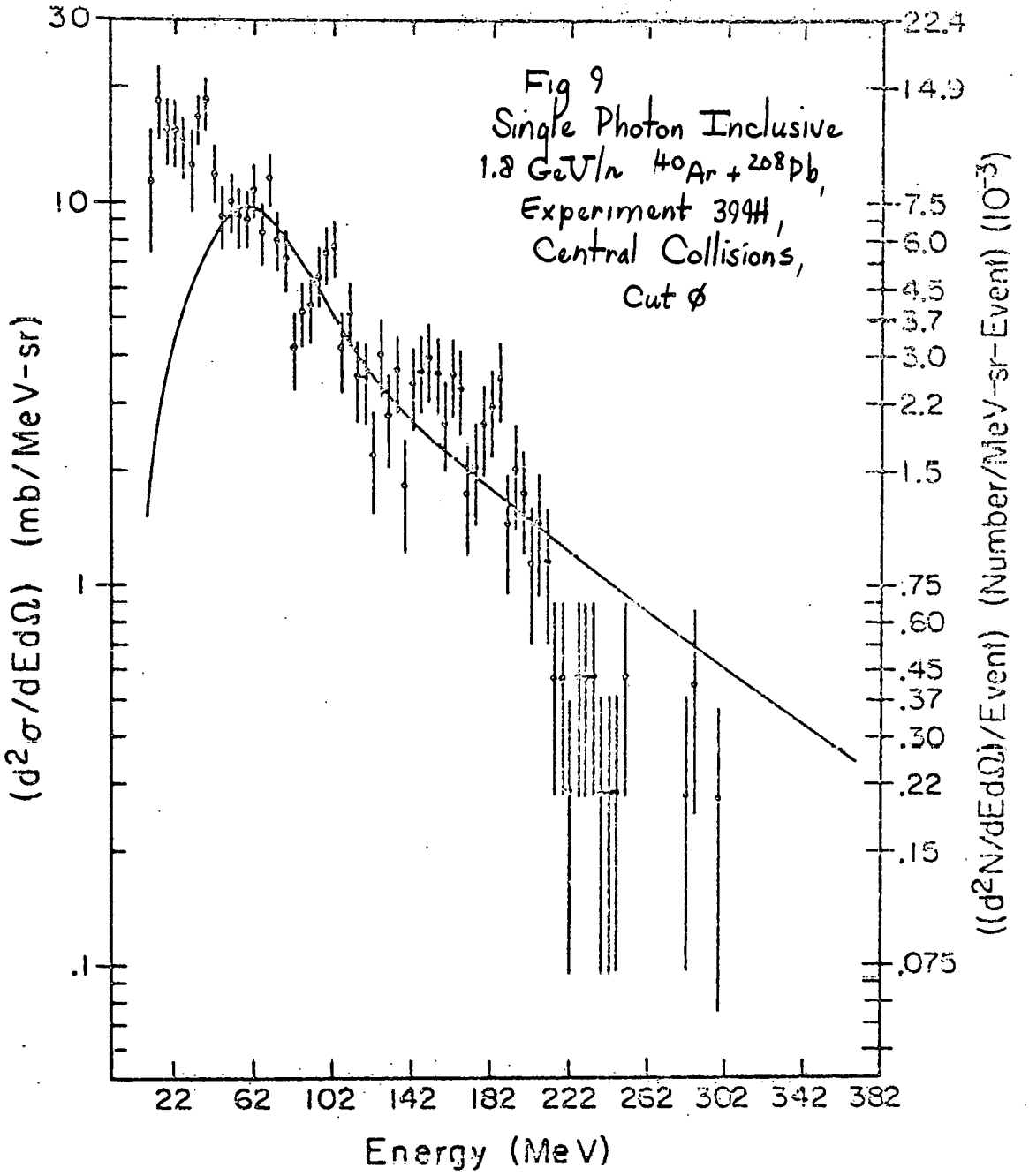
Fig 9
Single Photon Inclusive
1.8 GeV/n $^{40}Ar + ^{208}Pb$,
Experiment 394H,
Central Collisions,
Cut ∅
$(d^2\sigma/dEd\Omega)$ (mb/MeV-sr)
$((d^2N/dEd\Omega)/Event)$ (Number/MeV-sr-Event) (10^{-3})
Energy (MeV)
30
10
1
.1
22.4
14.9
7.5
6.0
4.5
3.7
3.0
2.2
1.5
.75
.60
.45
.37
.30
.22
.15
.075
22
62
102
142
182
222
262
302
342
382

to be accurate to 20-25%.

In order to indicate how the true shape of these spectra would appear were there no difficulty with overflow counts, corresponding data from a subsequent experiment (E486H) have been presented in Figs. 10-12 for central collisions of 1.8 GeV/n ^{40}Ar + ^{208}Pb. In this experiment, the NaI system used to record data was identical to the one presently under discussion. However, the central collision trigger employed was a scintillation counter located downstream of the target, similar to that used at the triggered streamer chamber facility of the Bevalac. As expected, the curves shown in Figs. 10-12 give no indication of structure in the intermediate energy region, and do not exhibit the precipitous drop in cross section above $\cong$ 200 MeV, observed in the results of the present experiment.

The errors shown in Figs. 7-9 and 12 reflect the error due to counting statistics, an assumed error of $\cong$ 8% in conversion efficiency and an estimated 7% error in trigger cross section. The uncertainty due to the conversion of γ-rays within the target has not been included since it would not influence the shape of the observed distributions. It is important to note, therefore, that the absolute double differential spectra presented are additionally uncertain by $\cong$ 15%. Overall, cross section data derived from the present experiment are thought to be accurate within 20-25% aside from the overflow difficulty discussed above. Alternatively, for reasons beyond the scope of this work, absolute cross sections derived from experiment 486H are only accurate within a factor of two, although in this instance the shape of the double differential spectra is thought to be correct.

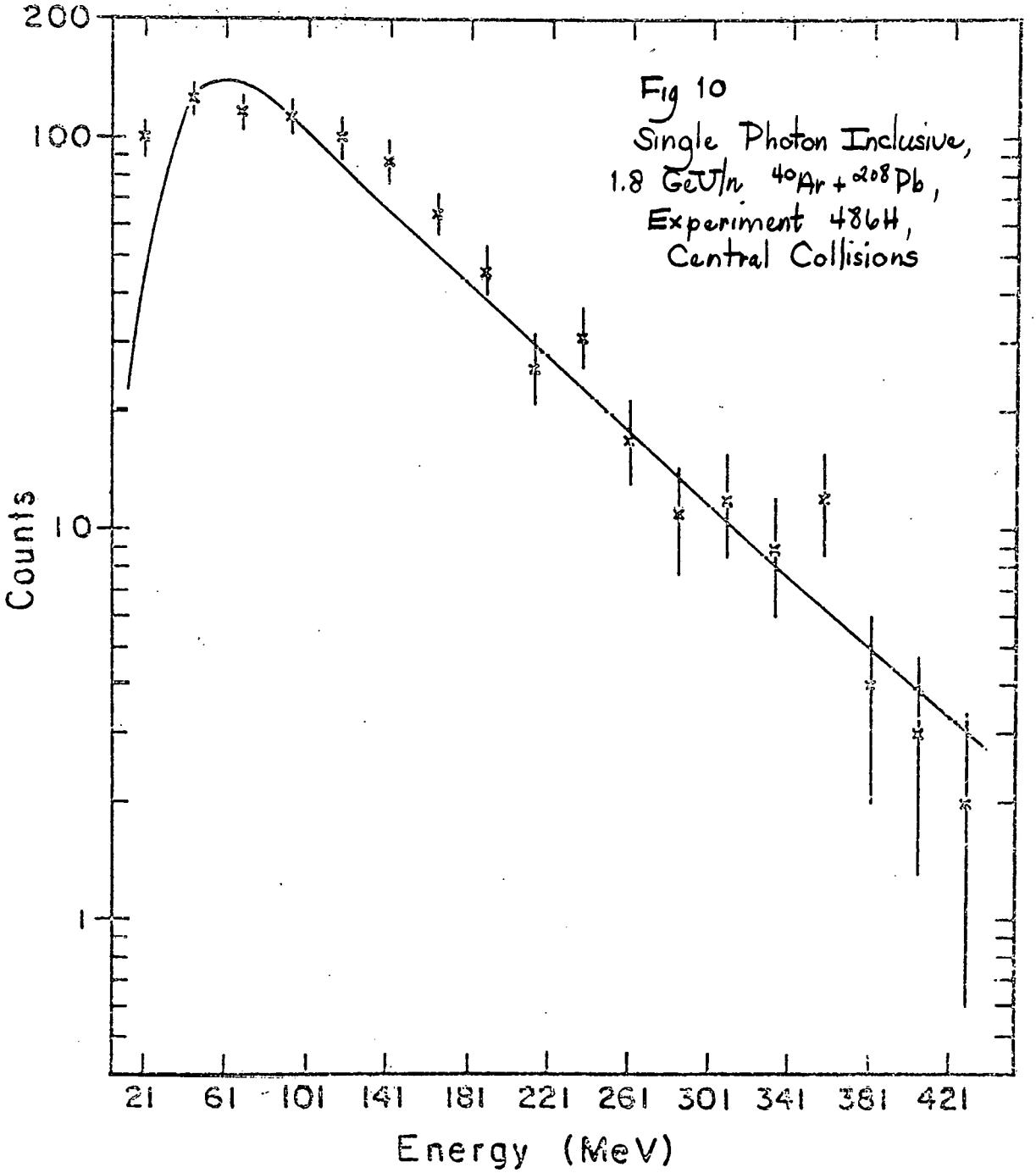

Fig 10
Single Photon Inclusive,
1.8 GeV/n $^{40}Ar + ^{208}Pb$,
Experiment 486H,
Central Collisions

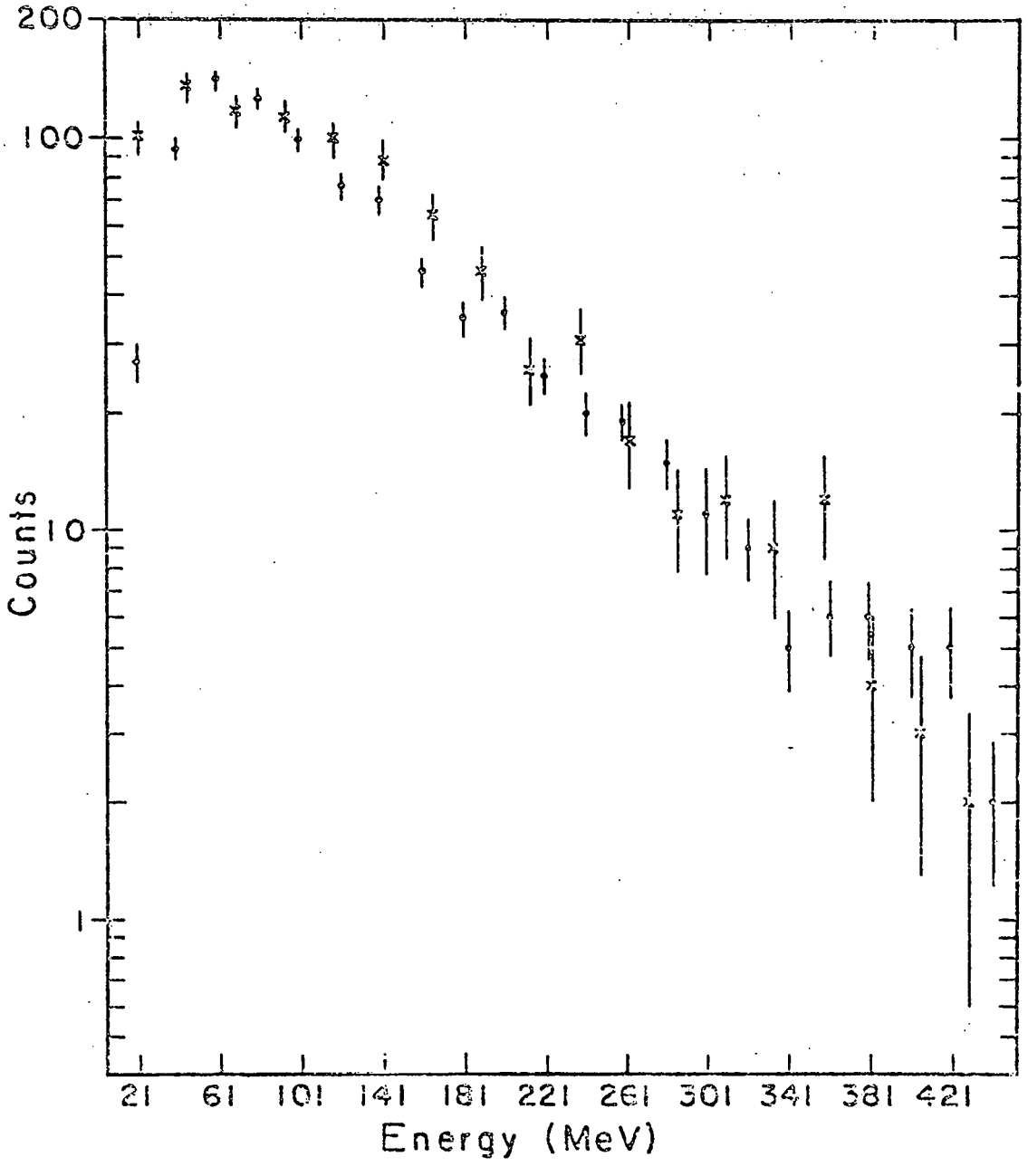

Fig 11. Single Photon Inclusive, 1.8 GeV/n $^{40}Ar + ^{208}Pb$, Experiment 486H, Central Collisions; x = data, • = thermal model having $\rho = .6$, $\tau = 100$ MeV.

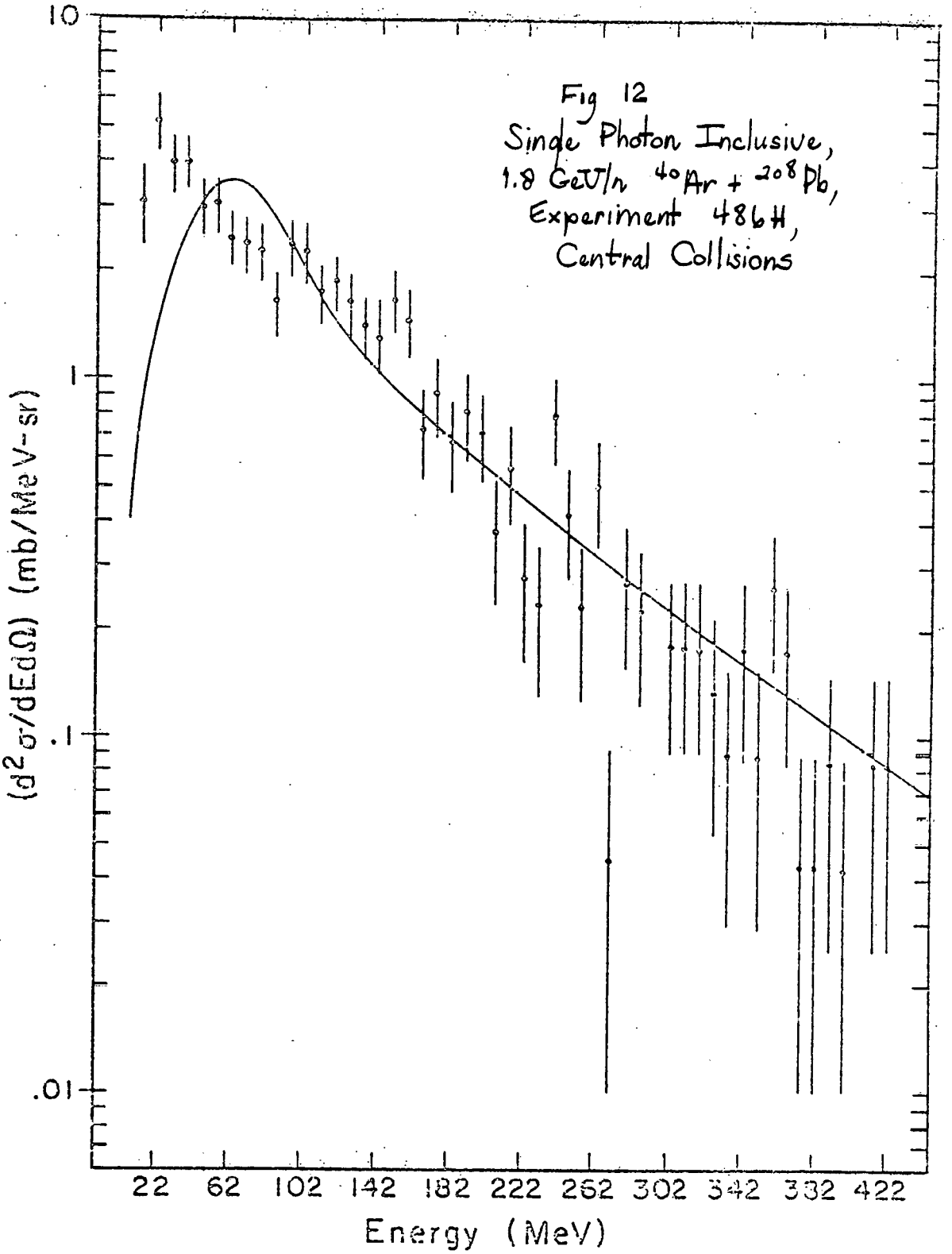

Fig 12
Single Photon Inclusive,
1.8 GeV/n $^{40}Ar + ^{208}Pb$,
Experiment 486H,
Central Collisions

For each of the distributions which has been presented, the results of a Monte Carlo calculation taking an assumed momentum distribution of π° mesons into account has been presented as well (solid line curve). The normalizations used are arbitrary and are intended to represent the best fit by eye. In the instance of 1.05 GeV/n ^{12}C + ^{208}Pb, the inclusive data of Nagamiya[2] for .8 GeV/n ^{12}C + $^{208}Pb \rightarrow \pi^-$ + Y have been used for comparison, while π^- data from a similar stream chamber experiment[3] have been used to interpret the 2.1 GeV/n ^{12}C + ^{208}Pb and 1.8 GeV/n ^{40}Ar + ^{208}Pb results. To make the predictions of the Monte Carlo as accurate as possible, the number of computational π° mesons thrown per event was determined by a poisson distribution having a realistic average estimated from other experimental results. Specifically, for the three reactions discussed above, the average number of computational π° mesons thrown per event was 1, 2, and 5 respectively. It is also noted that the characteristic resolution function for the NaI system was not unfolded in determining the double differential spectra presented above, and, therefore, had to be included as part of the Monte Carlo calculation.

Upon inspection of Figs. 7-9 and 12, it appears that while the predictions of the Monte Carlo generally reproduce the overall trend of the data, serious discrepancies do exist, notwithstanding the overflow difficulty discussed above.

One problem is that the observed spectra do not turn over below ~60 MeV as one might expect if π° decay were the sole source of gamma rays in this energy range. This is partially due to the poor resolution characterizing the 1" NaI crystal in this region. However, it was also determined using a 3" x 3" NaI crystal that there is an exponential low

energy gamma component which makes a substantial contribution to the observed cross section below ~22 MeV. To ascertain whether or not the low energy component might resolve the discrepancy noted above, an extrapolated low energy gamma ray spectrum "smeared" with an 80% resolution function was subtracted from each double differential single photon inclusive spectrum under consideration. The results indicate that the low energy component cannot account for the excess of gamma rays observed in the 20-50 MeV energy range. Consequently, assuming there are no systematic errors which have not been anticipated, one is led to consider the possibility that the excess is real and important, although to be certain of these conclusions, further experimentation with an improved 1" NaI crystal would be required.

A second observation is that although the Monte Carlo does suggest, for example, that the double differential single photon inclusive spectrum associated with the 1.8 GeV/n ^{40}Ar + ^{208}Pb reaction should fall off more slowly than that associated with the 1.05 GeV/n ^{12}C + ^{208}Pb reaction, the data do not follow the detailed spectral shape which is predicted. This is equally true of the curve generated for the 2.1 GeV/n ^{12}C + ^{208}Pb reaction. In this instance, the discrepancy between the Monte Carlo and the observed spectra could be an indication that the momentum distribution characterizing the emission of neutral π° mesons differs substantially from that characterizing charged pion production. If so, this disparity would tend to support heavy ion collision theories which invoke the existence of hydrodynamic effects, e.g., nuclear "blast waves." Unfortunately, to be certain of this conclusion would once again require further experimentation with an improved 1" NaI crystal, as well as a thorough investigation of the Monte Carlo program itself.

Using a Monte Carlo developed to interpret the results of the present experiment, it was determined by throwing 1 computational π° meson per event, that for the .8 GeV/n $^{12}C + ^{208}Pb \rightarrow \pi^- + Y$ reaction, the NaI system would have detected $\cong$ .15% of all the π° mesons thrown. Additionally, similar calculations for 2.1 GeV/n $^{12}C + Pb_3O_4 \rightarrow \pi^- + Y$, and 1.8 GeV/n $^{40}Ar + Pb_3O_4 \rightarrow \pi^- + Y$ yielded corresponding efficiencies of $\cong$ .13% and .14% respectively. Assuming the .8 GeV/n efficiency to remain applicable at 1.05 GeV/n, the intermediate efficiency data listed in Table IV as a function of beam energy and projectile mass were estimated by interpolating between the .8 GeV/n and 2.1 GeV/n results. For the .4 GeV/n $^{12}C + ^{208}Pb$ reaction, however, the procedure outlined above was not followed. In this instance, the efficiency was determined by assuming the emission of gamma rays to be approximately isotropic in the laboratory. Noting, therefore, that the NaI system subtended $\cong$ .26% of the available solid angle, and two gamma rays are emitted per π° decay, the efficiency in this instance was estimated to be $\cong$ .15%, assuming that the 1" NaI crystal converted $\cong$ .30% of the gamma rays entering its acceptance.

Using the efficiency data listed in Table IV, the rate of high energy ($\gtrsim$ 50 MeV) gamma ray production measured by the NaI system was translated, for each reaction under study, into an average number of π° mesons produced per central collision. These results have been presented in Table V as a function of beam energy, projectile mass, and multiplicity cut. For reference, the associated absolute π° production cross sections have been noted in Table V as well. The errors shown for the $\langle N_{\pi^\circ} \rangle$ results reflect the error due to counting statistics and an assumed 8% error in conversion efficiency. For the absolute cross section data which have been presented, the errors shown include an additional 7% error in trigger cross section,

TABLE IV: Estimated Absolute Efficiency; NaI System

Beam Energy (GeV/n)	Projectile Ion	Target Nucleus	Estimated Total Absolute Efficiency for Detecting π° Mesons (%)
.4	^{12}C	^{208}Pb	.154
1.0	^{12}C	^{208}Pb	.150
1.3	^{12}C	^{208}Pb	.145
1.5	^{12}C	^{208}Pb	.142
1.7	^{12}C	^{208}Pb	.138
1.9	^{12}C	^{208}Pb	.134
2.1	^{12}C	^{208}Pb	.130
1.8	^{40}Ar	^{208}Pb	.140

as well as an estimated 15% uncertainty due to the target correction discussed above. It is noted that the uncertainty due to the target correction has not been included in estimating the error associated with the $\langle N_{\pi^\circ} \rangle$ results, since it would not affect the dependence of the rate of π° production on multiplicity.

From the data listed in Table V, it would appear that, for the $^{12}C + ^{208}Pb$ reaction, the number of π° mesons produced per central collision exhibits a generally smooth increase from $\cong (1.17 \pm .06)$ at 1.05 GeV/n (Cut Ø) to $\cong (2.845 \pm .10)$ at 2.1 GeV/n (Cut Ø). For 1.8 GeV/n $^{40}Ar + ^{208}Pb$, the corresponding rate of production is $\cong (4.82 \pm .19)$ π° mesons per central collision. These results compare favorably with those of similar streamer chamber experiments,[3] in which the number of π^- mesons produced per central collision was estimated to be $\cong (1.79 \pm .16)$ for 2.1 GeV/n $^{12}C + Pb_3O_4$ and $\cong 5.6$ for 1.8 GeV/n $^{40}Ar + Pb_3O_4$. It is observed from Table V that the rate of π° production is a moderately strong function of the "centrality" of the collision. Consequently, discrepancies noted above between the results of the present experiment and those of similar experiments may be partially due to differences in trigger criteria. Additionally, discrepancies between the observed rate of high energy gamma ray production and the predictions of the Monte Carlo program may constitute another contributing factor. It is also observed that the smooth increase with beam energy noted in Table V for the rate of π° production is consistent with cascade model predictions[4] of the behavior expected to characterize charged pion production.

A second observation afforded by the data presented in Table V is that as the charged particle multiplicity increases and the collision

TABLE V: $\langle N_{\pi^\circ} \rangle$; NaI System

Beam Energy (GeV/n)	Projectile Ion	Target Nucleus	Cut IV		Cut Ø		Cut I		Cut II		Cut III	
			$\langle N_{\pi^\circ} \rangle$	σ_{π° (mb)	$\langle N_{\pi^\circ} \rangle$	σ_{π° (mb)	$\langle N_{\pi^\circ} \rangle$	σ_{π° (mb)	$\langle N_{\pi^\circ} \rangle$	σ_{π° (mb)	$\langle N_{\pi^\circ} \rangle$	σ_{π° (mb)
.4	^{12}C	^{208}Pb	———		(.025±.016)	(.15±.09)	(.026±.017)	(.13±.09)	(.023±.021)	(.07±.06)	———	
1.05	^{12}C	^{208}Pb	(.96±.11)	(84±17)	(1.17±.06)	(347±60)	(1.17±.07)	(289±50)	(1.19±.09)	(161±29)	(1.29±.35)	(12.4±4.0)
1.3	^{12}C	^{208}Pb	(1.60±.17)	(255±50)	(1.72±.11)	(685±121)	(1.77±.12)	(587±99)	(2.02±.20)	(274±52)	(1.57±.51)	(24.9±9.0)
1.5	^{12}C	^{208}Pb	(1.73±.13)	(335±61)	(1.85±.08)	(916±156)	(1.90±.09)	(685±117)	(1.95±.14)	(313±56)	(2.29±.41)	(51.4±12.5)
1.7	^{12}C	^{208}Pb	(1.99±.15)	(488±88)	(2.10±.09)	(1265±215)	(2.14±.11)	(976±167)	(2.39±.16)	(514±91)	(1.77±.36)	(56.7±14.9)
1.9	^{12}C	^{208}Pb	(2.52±.17)	(716±127)	(2.70±.11)	(1877±317)	(2.75±.13)	(1411±241)	(2.70±.18)	(673±120)	(3.07±.48)	(123 ±28)
2.1	^{12}C	^{208}Pb	(2.56±.15)	(940±163)	(2.85±.10)	(2279±383)	(2.99±.12)	(1824±305)	(3.35±.19)	(856±149)	(4.07±.56)	(152 ±33)
1.8	^{40}Ar	^{208}Pb	(4.12±.24)	(3465±565)	(4.82±.19)	(6459±1015)	(5.10±.23)	(4559±720)	(5.59±.40)	(1737±291)	(7.84±1.07)	(477±98)

presumably becomes more central the measured rate of π° production appears to increase substantially. This effect becomes more pronounced as the beam energy and/or projectile mass are raised, being only slightly evident for 1.05 GeV/n ^{12}C + ^{208}Pb ($.95\pm.22 \rightarrow 1.29\pm.35$), more apparent for 2.1 GeV/n ^{12}C + ^{208}Pb ($2.56\pm.15 \rightarrow 4.07\pm.56$), and quite dramatic for 1.8 GeV/n ^{40}Ar + ^{208}Pb ($4.12\pm.24 \rightarrow 7.84\pm1.07$). The origin of this increase is not immediately apparent. It cannot, for example, be accounted for by increased isotropy of the π° momentum distribution. Since, however, the "explosiveness" of the collision is thought to increase as the impact parameter decreases, the observed effect might be partially due to an increase in the average number of nucleon-nucleon collisions or an increased "survival rate" for the π° mesons which are produced.

It is gratifying to note that the estimated rate ($.025\pm.016$) of π° production for .4 GeV/n ^{12}C + ^{208}Pb is consistent with the rate estimated by Bertsch[5] for threshold pion production in similar heavy ion collisions. It is estimated, for example, by extrapolating the calculated results for ^{16}O + ^{238}U, that at .4 GeV/n the number of π mesons produced a priori should be ~(1/2.5). Assuming the production of π° mesons accounts for one-third the total, and allowing as well for an "escape" probability of $\cong$ 1/3, the observed rate of π° production would be $\cong$ .044 per collision. Scaling this rate of production by the mass of ^{12}C relative to ^{16}O (.75), one would expect the measured rate of π° production for .4 GeV/n ^{12}C + ^{208}Pb to be $\cong$ .033 per collision which agrees, within statistics, with the experimental result. It is thought, therefore, that the NaI data presented above contain little or no background, and truly reflect the rate of π° production which occurs in central collisions of relativistic ^{12}C and ^{40}Ar on ^{208}Pb.

To provide an independent measurement of the production of high energy gamma rays from π° decay, two walls of lead glass blocks, one on either side of the beam line, were also employed. Each wall consisted of twelve pieces of lead glass, configured as 3 rows of 4 blocks each. Eighty-one percent of each lead glass hodoscope was shielded by an upstream Cerenkov telescope, which eliminated spurious counts due to fast charged particles.

Using the inclusive data of Nagamiya[2] for .8 GeV/n $^{12}C + {}^{208}Pb \rightarrow \pi^- + Y$, and data from similar streamer chamber experiments[3] for 2.1 GeV/n $^{12}C + Pb_3O_4 \rightarrow \pi^- + Y$, a Monte Carlo program taking an assumed momentum distribution of π° mesons into account was developed in order to interpret the response of the lead glass detector system.

From the results of the Monte Carlo program, it was determined by throwing 1 computational π° meson per event, that for the .8 GeV/n $^{12}C + {}^{208}Pb \rightarrow \pi^- + Y$ reaction the upstream lead glass columns under study would have detected $\cong$ 3.5% of all the π° mesons thrown. Additionally, similar calculations for 2.1 GeV/n $^{12}C + Pb_3O_4 \rightarrow \pi^- + Y$ and 1.8 GeV/n $^{40}Ar + {}^{208}Pb \rightarrow \pi^- + Y$ yielded corresponding efficiencies of $\cong$ 2.9% and 3.1% respectively. Assuming the .8 GeV/n efficiency to remain applicable at 1.05 GeV/n, intermediate efficiency data were estimated by interpolating between the .8 GeV/n and 2.1 GeV/n results. The efficiency for .4 GeV/n $^{12}C + {}^{208}Pb$ was determined by extrapolating below .8 GeV/n.

Using the efficiency data derived in this manner the rate of high energy (~50 MeV) gamma ray production measured by the upstream lead glass columns was translated for each reaction under study, into an average number of π° mesons produced per central collision. The results have been presented

in Table VI as a function of beam energy, projectile mass, and multiplicity cut. For reference, the associated absolute π° production cross sections have been noted in Table VI as well. The errors shown reflect the error due to counting statistics, as well as an estimated 5% uncertainty due to the target corrections.

From the data listed in Table VI, it would appear that several observations previously noted from measurements made with the NaI system apply to the results of the lead glass measurement as well.

For the $^{12}C + ^{208}Pb$ reaction, the number of π° mesons produced per central collision exhibits a generally smooth increase from $\cong (.99 \pm .05)$ at 1.05 GeV/n (Cut Ø), to $\cong (2.92 \pm .15)$ at 2.1 GeV/n (Cut Ø). For 1.8 GeV/n $^{40}Ar + ^{208}Pb$, the corresponding rate of production is $\cong (5.37 \pm .27)$ π° mesons per central collision. These results compare favorably with those of similar stream chamber experiments,[3] in which the number of π^- mesons produced per central collision was estimated to be $\cong (1.79 \pm .16)$ for 2.1 GeV/n $^{12}C + Pb_3O_4$ and $\cong 5.6$ for 1.8 GeV/n $^{40}Ar + Pb_3O_4$. It is noted from the literature that in determining the latter streamer chamber result, special care was taken to insure that the events analyzed were acutely central, having $b \lesssim 4.5$ fm in an ideal geometric picture. However, in specifying the results for 2.1 GeV/n $^{12}C + Pb_3O_4$, the trigger is described as "inelastic," rejecting only the most noninteractive collisions. Consequently, since the rate of pion production in general is thought to be a moderately strong function of impact parameter, the relatively large discrepancy observed above the 2.1 GeV/n $^{12}C + ^{208}Pb$ reaction might be a reflection of differing trigger criteria.

TABLE VI: $\langle N_{\pi^o} \rangle$ Lead Glass System

Beam Energy (GeV/n)	Projectile Ion	Target Nucleus	Cut IV		Cut Ø		Cut I		Cut II		Cut III	
			$\langle N_{\pi^o} \rangle$	σ_{π^o} (mb)	$\langle N_{\pi^o} \rangle$	σ_{π^o} (mb)	$\langle N_{\pi^o} \rangle$	σ_{π^o} (mb)	$\langle N_{\pi^o} \rangle$	σ_{π^o} (mb)	$\langle N_{\pi^o} \rangle$	σ_{π^o} (mb)
1.05	^{12}C	^{208}Pb	(.89±.05)	(77.5±7.1)	(.99±.05)	(294±25)	(1.01±.05)	(248±22)	(1.04±.06)	(141±12)	(1.00±.10)	(9.6±1.1)
1.3	^{12}C	^{208}Pb	(1.43±.08)	(223±20)	(1.51±.03)	(603±52)	(1.56±.08)	(487±42)	(1.61±.09)	(219±19)	(1.73±.16)	(27.5±3.2)
1.5	^{12}C	^{208}Pb	(1.43±.08)	(280±25)	(1.68±.09)	(832±70)	(1.75±.09)	(633±54)	(1.87±.10)	(301±26)	(2.17±.15)	(48.9±4.7)
1.7	^{12}C	^{208}Pb	(1.92±.10)	(471±40)	(2.19±.11)	(1321±111)	(2.33±.12)	(1063±89)	(2.46±.13)	(528±44)	(2.75±.18)	(88.0±8.3)
1.9	^{12}C	^{208}Pb	(2.20±.12)	(623±54)	(2.59±.13)	(1795±150)	(2.75±.14)	(1414±118)	(3.00±.16)	(747±64)	(3.39±.21)	(135 ± 12)
2.1	^{12}C	^{208}Pb	(2.46±.13)	(901±76)	(2.92±.15)	(2339±196)	(3.14±.16)	(1921±162)	(3.54±.18)	(906±76)	(3.74±.23)	(140 ± 13)
1.8	^{40}Ar	^{208}Pb	(4.20±.22)	(3609±205)	(5.37±.27)	(7193±402)	(5.86±.30)	(4955±279)	(7.19±.38)	(2236±127)	(8.22±.48)	(501 ± 32)

A second observation afforded by the data presented in Table VI is that as the charged particle multiplicity increases, and the collision becomes more central, the rate of π° production increases substantially. Furthermore, this effect becomes more pronounced as the beam energy and/or projectile mass are raised, being only slightly evident for 1.05 GeV/n ^{12}C + ^{208}Pb ($.89\pm.05 \rightarrow 1.00\pm.1$), but quite dramatic for 1.8 GeV/n ^{40}Ar + ^{208}Pb ($4.29\pm.22 \rightarrow 8.22\pm.48$). Since both of the trends were also observed in measurements made with the NaI system (Table V) it would appear that they are real and important, although, once again, the origin of the increased rate of π° production is not immediately clear. It is possible that as the impact parameter of the collision decreases, either the average number of nucleon-nucleon collisions becomes larger, or the "survival rate" for π° mesons which are produced increases.

The rate of π° production for .4 GeV/n ^{12}C + ^{208}Pb has not been presented in Table VI since the associated total absolute efficiency is somewhat uncertain. It is observed, however, that were the .4 GeV/n efficiency noted above correct, the corresponding rate of π° production would be .2-.4 per event under the present assumptions. This results is too high by approximately a factor of 10 if measurements made with the NaI system are regarded as correct.

One possible explanation is that because .4 GeV is near the threshold for π° production, kinematic correlations may cause the back to back upstream lead glass columns to be more efficient than expected. Alternatively, the disparity noted above could be due to a neutral background component which is only significant for the .4 GeV/n ^{12}C + ^{208}Pb reaction. Although it is not satisfying to propose a separate background to account

for the results of one measurement, it is true, for example, that the np total and nC inelastic cross sections would become substantially larger as the average neutron energy decreased, increasing the overall possibility of interaction within the detector system. Unfortunately, although plausible explanations can be rendered for the excessive signature rate observed for .4 GeV/n ^{12}C + ^{208}Pb, it is not possible to proffer a decisive interpretation of this discrepancy without further experimentation.

It is, however, gratifying to note that the lead glass results quoted in Table VI compare very well with the data presented previously for the NaI detector system (Table V). The excellent agreement between the two, despite the relatively large difference in the number and magnitude of the corrections taken into account suggests that the interpretation given to the measured rate of high energy gamma ray production is correct for both detector systems.

A 3" x 3" NaI crystal, located at 90^{o} with respect to the beam, provided an inclusive measurement of the spectrum of low energy gamma rays (.7 MeV $\lesssim$ E $\lesssim$ 7 MeV) associated with central collisions of relativistic heavy ions.

For three reactions which encompass the range of variation one might expect to observe in the present experiment, 1.05 and 2.1 GeV/n ^{12}C + ^{208}Pb and 1.8 GeV/n ^{40}Ar + ^{208}Pb, the absolute double differential single photon inclusive spectra $d^2\sigma(90^{o})/dEd\Omega$ associated with the Cut Ø data sample have been presented in Figs. 13, 15 and 17. To illustrate the dependence of these results on charged particle multiplicity, corresponding spectra associated with the Cut II data sample are shown in Figs. 14, 16 and 18. Several features of these spectra require explanation.

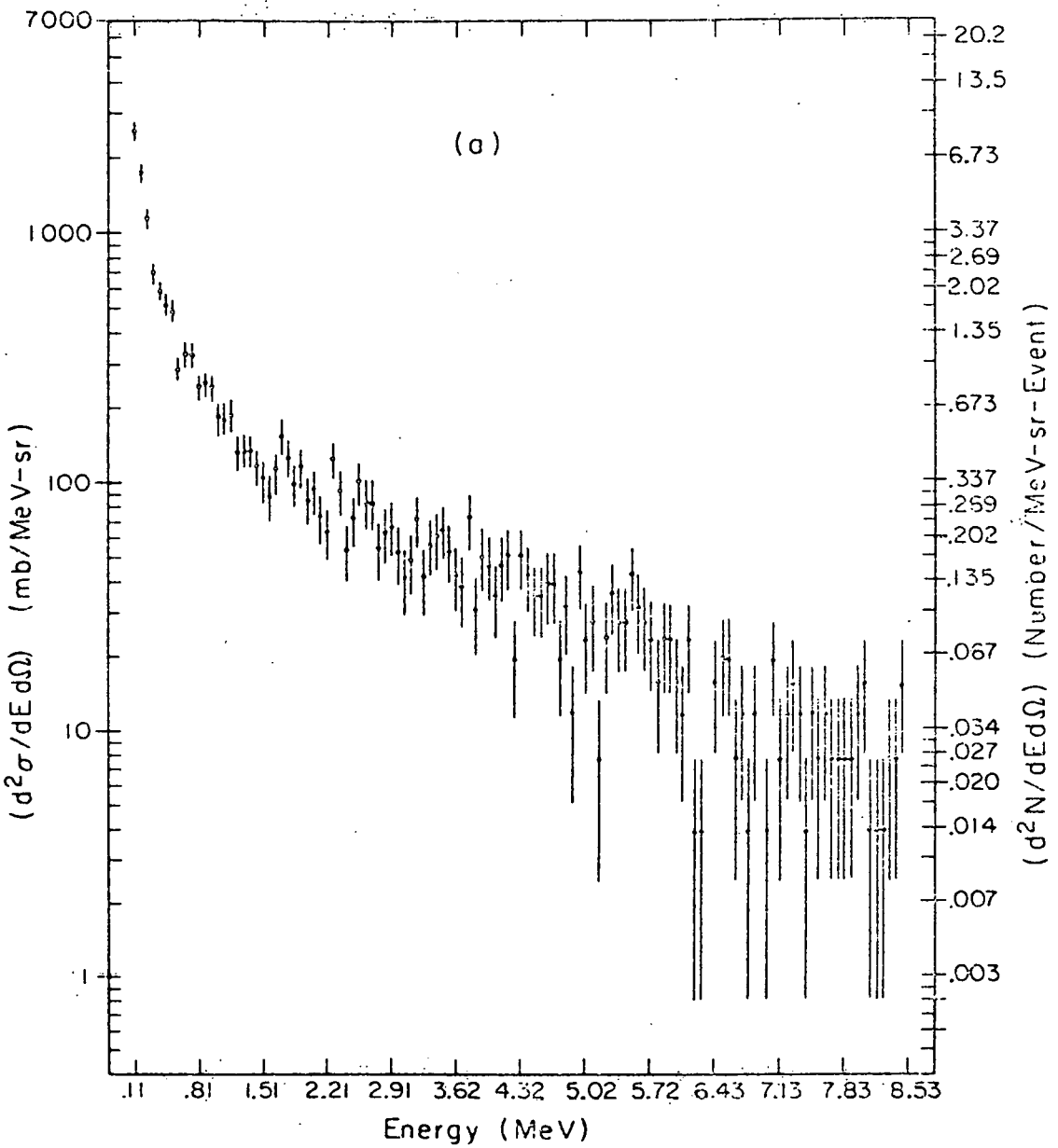

Fig 13 Single Photon Inclusive, 1.05 GeV/n $^{12}C + ^{208}Pb$, Experiment 399H, Central Collisions, Cut ø

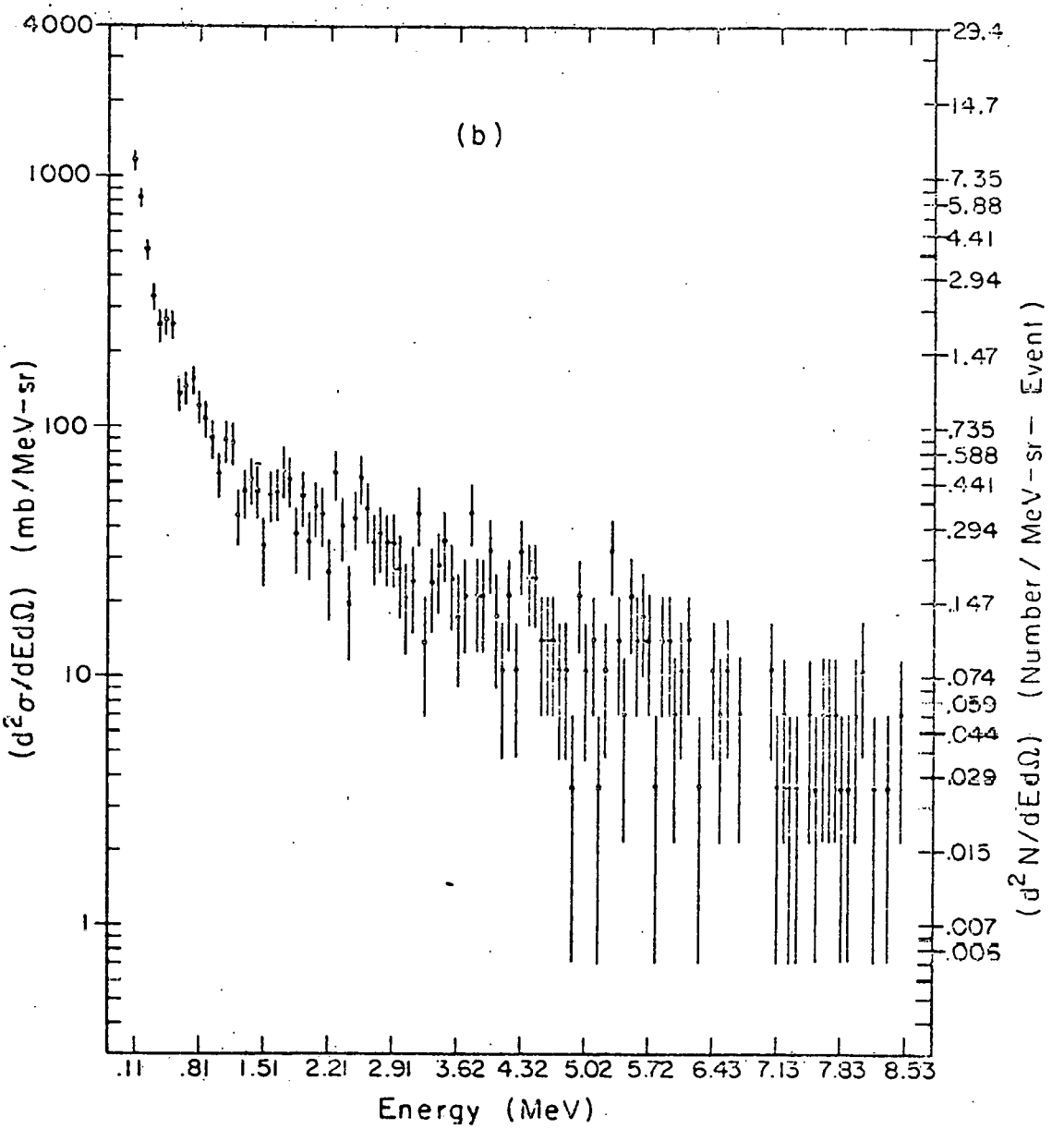

Fig 14. Single Photon Inclusive, 1.05 GeV/n $^{12}C + ^{208}Pb$, Experiment 399H, Central Collisions, Cut II

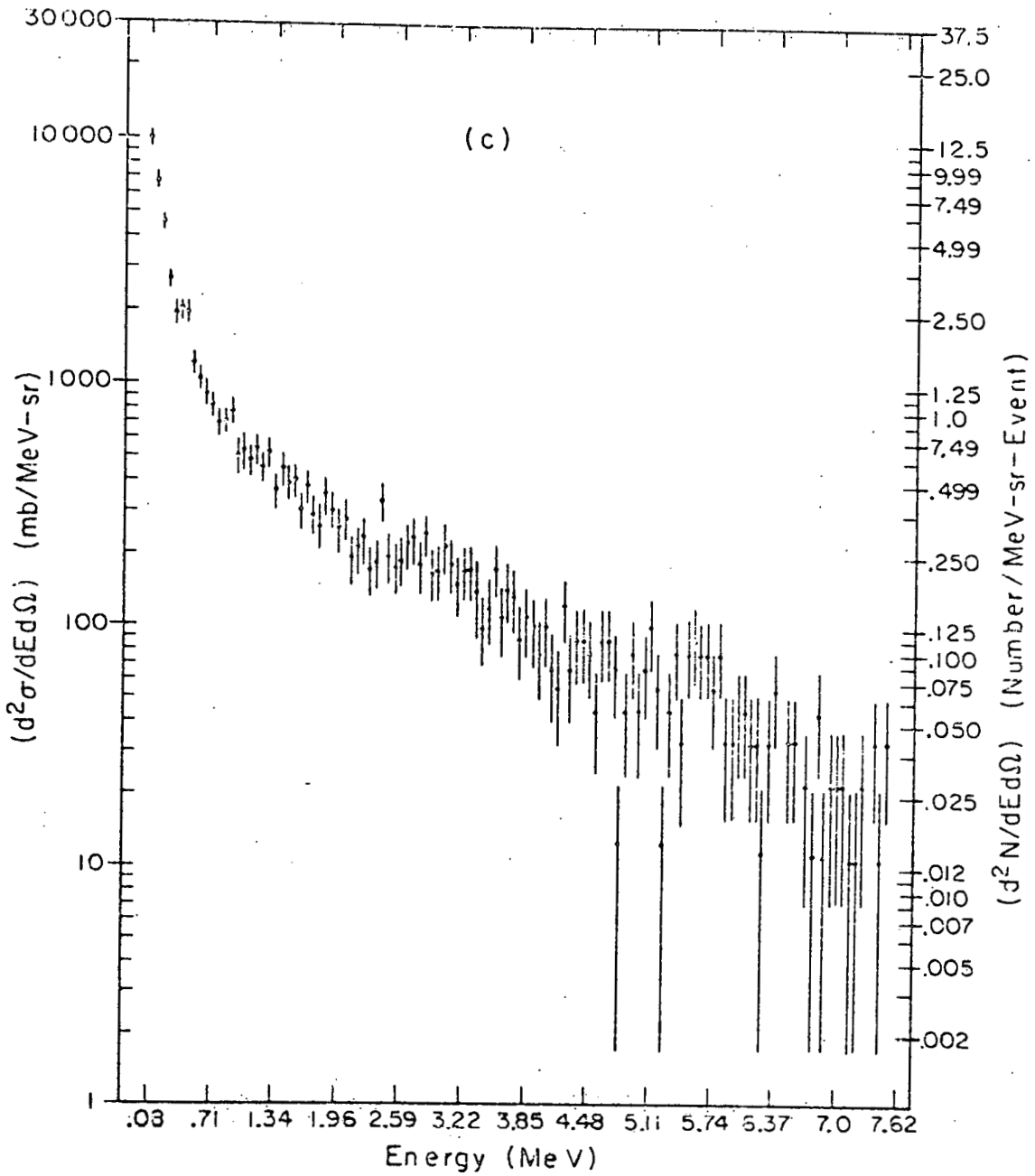

Fig 15. Single Photon Inclusive, 2.1 GeV/n $^{12}C + ^{208}Pb$, Experiment 399H, Central Collisions, Cut ϕ

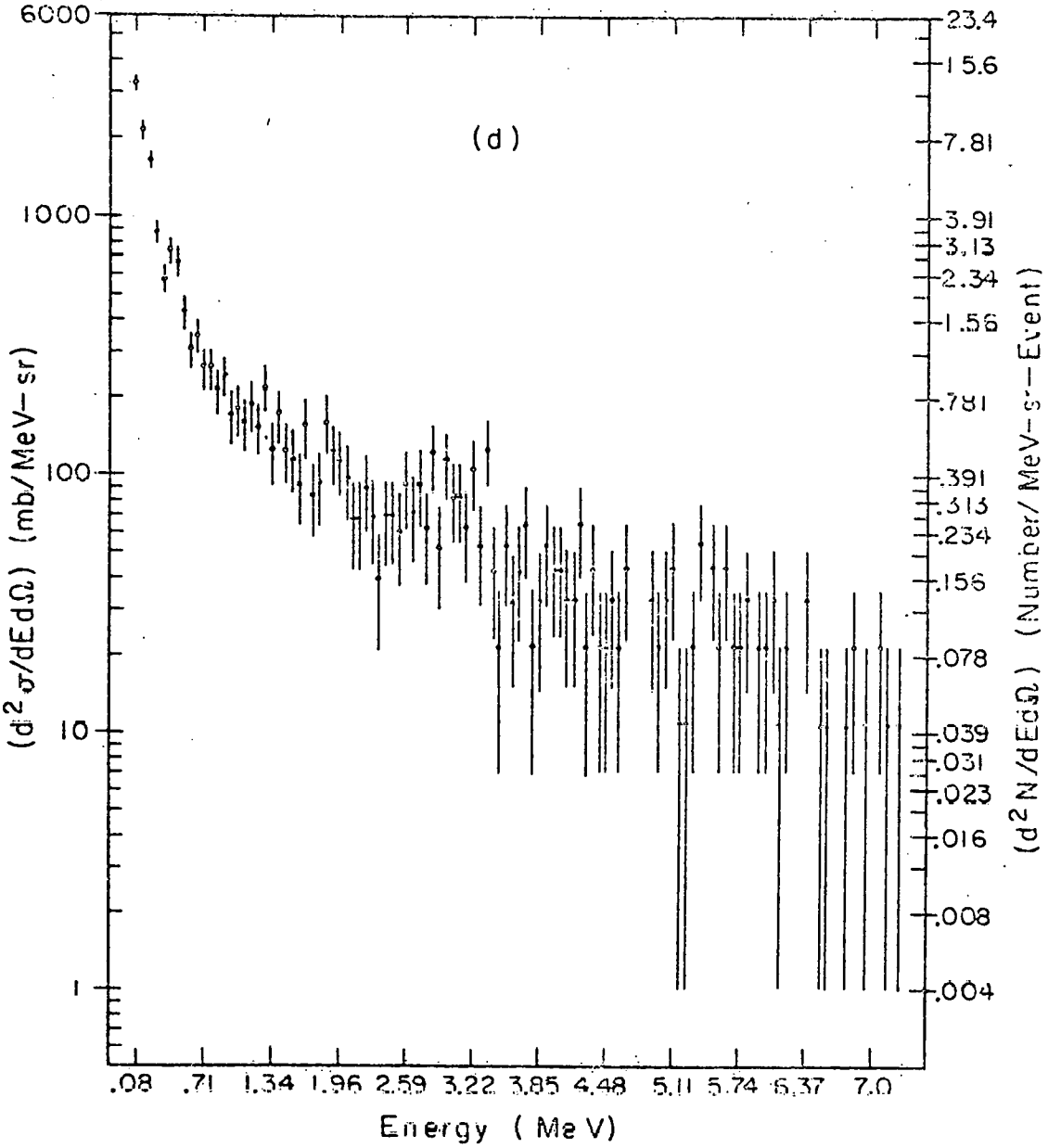

Fig 16. Single Photon Inclusive, 2.1 GeV/n $^{12}C + ^{208}Pb$, Experiment 399H, Central Collisions, Cut II

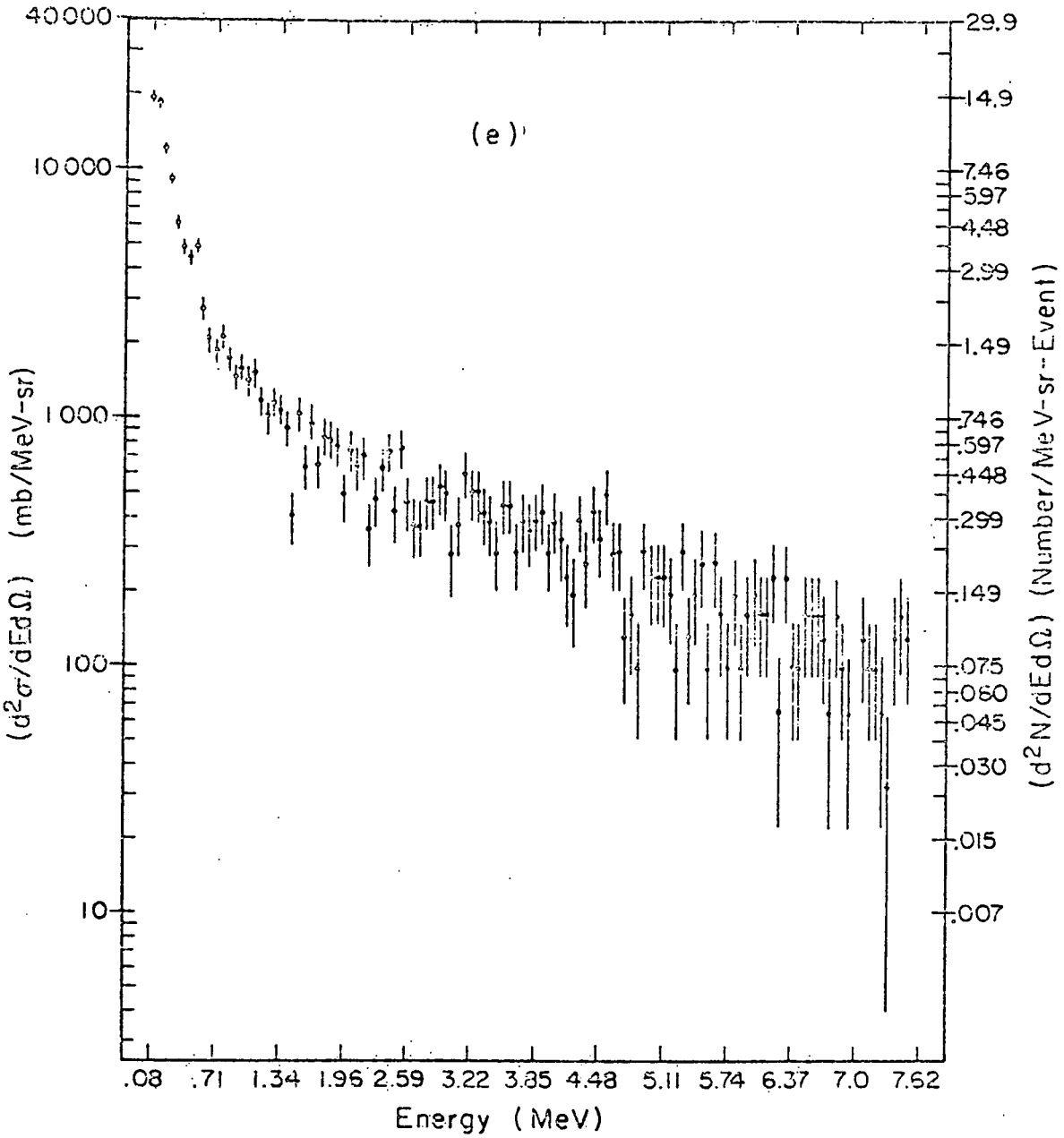

Fig 17 Single Photon Inclusive, 1.8 GeV/n $^{40}Ar + ^{208}Pb$, Experiment 399H, Central Collisions, Cut ø

The data shown in Figs. 13-18 were calculated by dividing the observed gamma ray pulse height distributions by the total absolute efficiency characterizing a 3" x 3" NaI crystal loacted at a distance of ≅ 23" from a radiating point source. Additionally, a veto correction was made to correct for the possibility of an accidental coincidence between a charged particle and a low energy gamma ray. It was not possible to correct these data for neutron background which is therefore estimated to comprise ≅ (10-15)% of the low energy gamma ray spectra presented. Furthermore, in calculating the results shown in Figs. 13-18, the characteristic resolution (≅7% at ≅ 1.2 MeV) of the 3" x 3" NaI crystal was not unfolded, this type of reconstruction being unwarranted in view of the statistical accuracy of the data. The errors shown reflect the error due to counting statistics, and an estimated 7% uncertainty in trigger cross section.

Upon inspection of the spectra presented in Figs. 13-18, several qualitative observations can be made.

It will be noted first, for example, that in general the spectra of low energy gamma rays associated with central collisions of relativistic ^{12}C and ^{40}Ar on ^{208}Pb decrease monotonically, showing no apparent signs of structure, subject to the intrinsic resolution of the 3" x 3" NaI crystal. This behavior would appear to be consistent with the results of similar in-beam nuclear gamma ray studies[6] which indicate that discrete transitions are only observed in peripheral collisions of relativistic heavy ions where the energy and momentum transferred to the target nucleus are small.

A second observation afford by the data presented in Figs. 13-18 is that the spectra generally appear to consist of two components, one

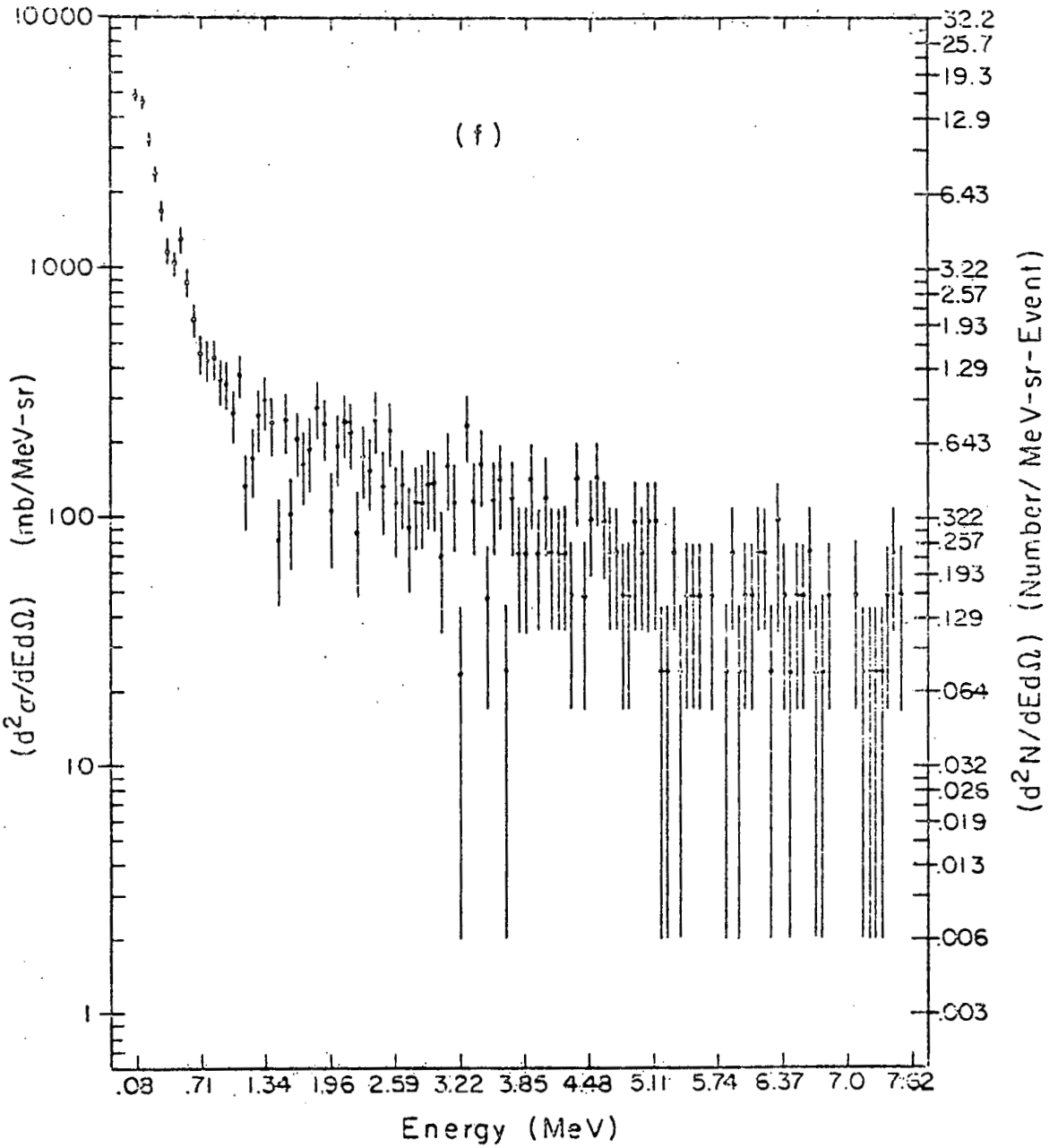

Fig 18. Single Photon Inclusive, 1.8 GeV/n $^{40}Ar + ^{208}Pb$, Experiment 399H, Central Collisions, Cut II

component having a large decay constant and ranging up to ≅ 1 MeV, the other extending to higher photon energies and falling off more slowly. The low energy component was not investigated in the current study, since this region of the observed spectra is most subject to the effects of neutron background, and is close as well to the end of the dynamic range of the ADC used to interpret pulse height information. Upon examination of the high energy component, however, it was observed that this region of the low energy gamma ray spectra is well fit by an exponential, representative curves being presented in Figs. 19a-c for the three reactions under study. The apparent structure shown in Fig. 19 for the 2.1 GeV/n ^{12}C + ^{208}Pb reaction is thought to arise from counting statistics, since this feature was not observed in the corresponding 1.9 GeV/n ^{12}C + ^{208}Pb spectra, nor in a similar 2.1 GeV/n ^{12}C + ^{208}Pb gamma ray spectrum measured in a subsequent experiment. Values of the inverse decay constant derived from this fitting procedure are presented in Table VII along with associated values of the reduced chi square.

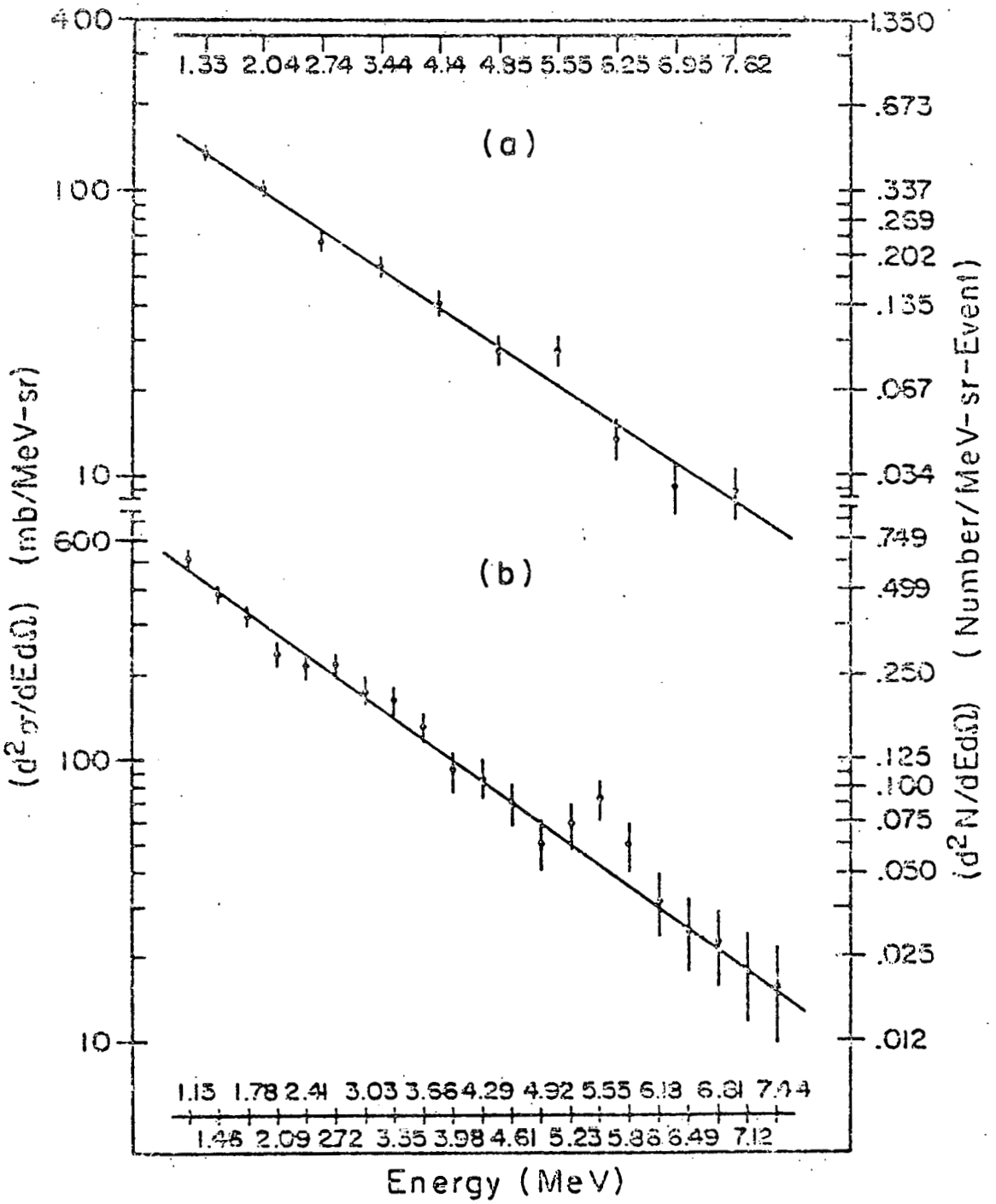

Fig 19 Single Photon Inclusive for a) 1.05 GeV/n $^{12}C + ^{208}Pb$, b) 2.1 GeV/n $^{12}C + ^{208}Pb$, c) 1.8 GeV/n $^{40}Ar + ^{208}Pb$; Straight line curves represent best fit to a $\sigma = \sigma_0 e^{-aE}$ functional form.

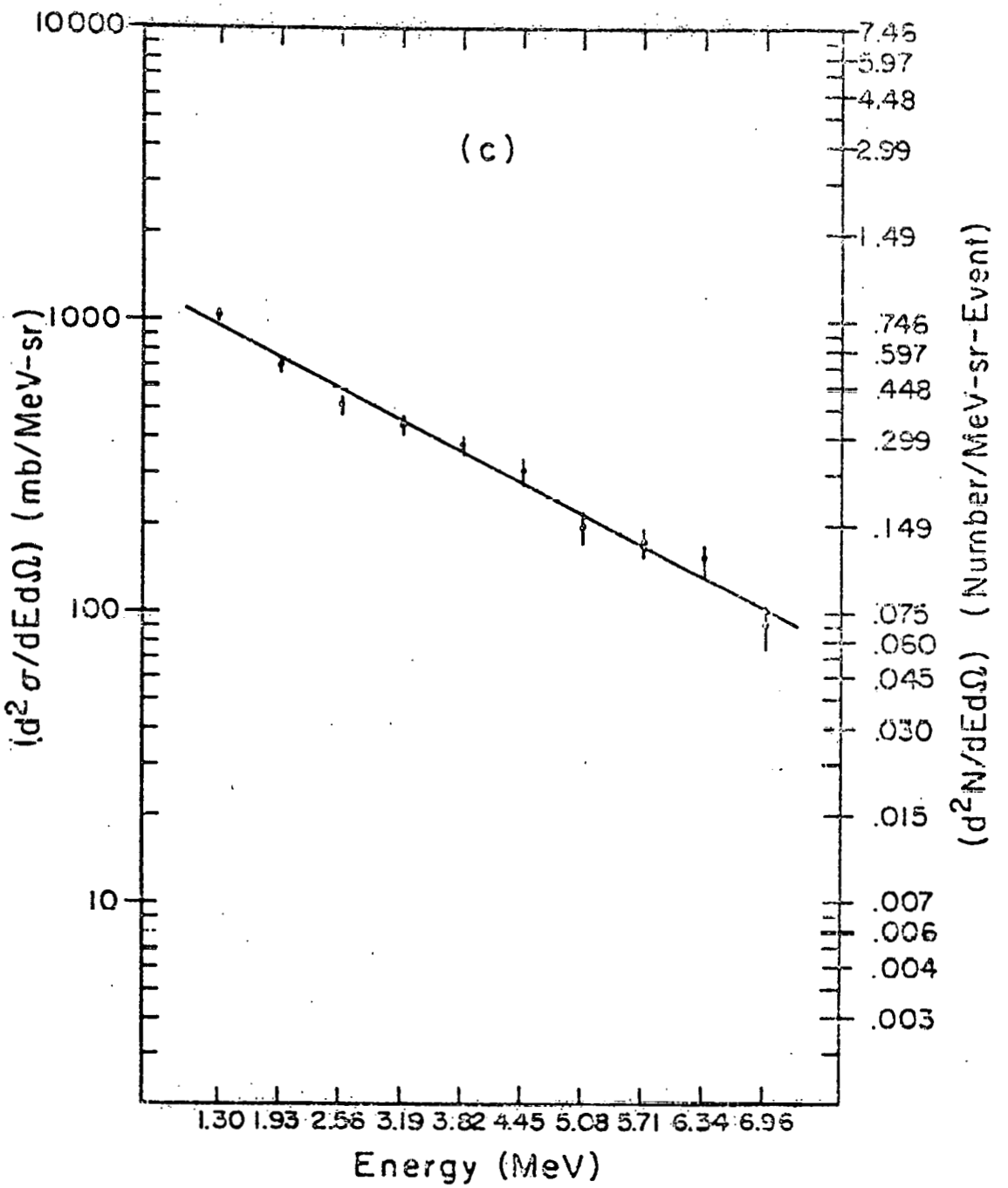
10000
1000
100
10
(c)
7.46
5.97
4.48
2.99
1.49
.746
.597
.448
.299
.149
.075
.060
.045
.030
.015
.007
.006
.004
.003
(d²σ/dEdΩ) (mb/MeV-sr)
(d²N/dEdΩ) (Number/MeV-sr-Event)
1.30 1.93 2.56 3.19 3.82 4.45 5.08 5.71 6.34 6.96
Energy (MeV)

TABLE VII: Fitted Values of the Slope of Typical Low Energy Gamma Ray Spectra

Beam Energy (GeV/n)	Projectile Ion	Target Nucleus	a^{-1} * $(MeV)^{-1}$	χ^2/NDF
1.05	^{12}C	^{208}Pb	2.23	7.98/8
2.1	^{12}C	^{208}Pb	1.83	11.24/16
1.8	^{40}Ar	^{208}Pb	2.51	10.81/8

* Spectra fitted to $\sigma = \sigma_o\ e^{-aE}$

It will be recalled from previous work[7] that to measure the production of energetic charged pi mesons, two octagonal arrays of lucite Cerenkov telescopes were employed. Each telescope consisted of two 1¼" thick pieces of UVT plastic separated by a removable sheet of ¼" thick lead. With the lead converters removed, charged pions having energies $\geq$ 70 MeV would Cerenkov radiate in the UVT lucite and be detected simultaneously in both elements of a given Cerenkov telescope. In terms of the notation developed previously, the rate per event of charged pion production measured by a given telescope would therefore be expressed,

$$R_{\pi}(1,1), \qquad (1)$$

the first index referring to the inner Cerenkov counter, the second to the outer Cerenkov detector, and the "1", (as opposed to "0"), denoted for both counters indicating that each had registered a count. (Primed signature rates, e.g. R'(0,0) represent measurements made with the lead converter sheets inserted.) However, before the raw coincidence rates denoted by expression 1 could be interpreted properly, several substantial corrections had to be taken into account.

It should also be pointed out that, since the downstream lucite Cerenkov telescopes were subject to substantially higher levels of background than the corresponding upstream detectors, only pion data provided by the latter have been treated in the discussion which follows.

Accounting for the possibility of an accidental coincidence between a noise signature, (1,0), and a high energy gamma-ray signature, (0,1),

constituted one correction important to a proper interpretation of the response of this detector system. This correction was accomplished in the standard manner by noting that if the measured rate of noise signatures were R(1,0), and the corresponding rate of high energy gamma-ray signatures R(0,1), the probability of an accidental coincidence between the two was approximately

$$R_c \cong (R(1,0) \times R(0,1)). \qquad (2)$$

The true rate of charged pion production would therefore be calculated

$$R_{\pi\ TRUE}(1,1) = R_{\pi\ measured}(1,1) - (R(1,0) \times R(0,1)) \qquad (3)$$

This method of correcting for accidental coincidences is an approximation, since the measured rates themselves require correction. However, from the sample data listed in Table VIII, it would appear that the R(1,0) and R(0,1) signature rates both remain small compared to unity for all the reactions under study, and as a consequence this method of correction can be considered valid. The magnitude of the correction itself appears to range from $\cong$ 12.5% for 1.05 GeV/n $^{12}C + {}^{208}Pb$ to $\cong$ 8.5% for 1.8 GeV/n $^{40}Ar + {}^{208}Pb$.

A second important correction consisted of estimating the percentage of π° gamma rays which were converted to electron pairs within the target, and subsequently emulated the (1,1) charged pion signature.

Taking the acceptance of the upstream lucite Cerenkov telescopes into account, it was determined that, for the $^{12}C + {}^{208}Pb$ reactions (target thickness $\cong$ .015"), the average pathlength of lead traversed by a gamma ray within the target was $\cong$ .29 radiation lengths, a radiation length of lead being $\cong$ .25". Noting therefore that the probability of conversion is $\cong$ 7/9 per radiation length in this energy range, it was estimated that $\cong$ 22%

TABLE VIII: Upstream Cerenkov Telescope Cut Ø Production Rates,

Lead Converter Removed

Beam Energy (GeV/n)	Projectile Ion	Target Nucleus	$R_{\pi}(1,1)$ uncorrected (per event)	$R_{NOISE}(1,0)$ uncorrected (per event)	$R_{\gamma}(0,1)$ uncorrected (per event)	$R_{\pi}(1,1)$ corrected (per event)	% Reduction of Charged Pion Signature
1.05	^{12}C	^{208}Pb	(.0425±.0003)	(.0911±.0006)	(.0605±.0004)	(.0372±.0003)	12.5
2.1	^{12}C	^{208}Pb	(.1033±.0004)	(.1343±.0005)	(.0807±.0004)	(.0928±.0004)	10.1
1.8	^{40}Ar	^{208}Pb	(.1999±.0012)	(.1786±.0011)	(.0998±.0008)	(.1828±.0012)	8.5

of the gamma rays entering the acceptance of an upstream lucite Cerenkov telescope should have converted within the target. A similar analysis for the $^{40}Ar + ^{208}Pb$ reaction in which a thicker target (.042") was used, indicated a corresponding conversion rate of $\cong$ 34%.

Having calculated the percentage of gamma rays which should have converted within the target, the number of gamma rays per event entering the acceptance of an upstream Cerenkov telescope was estimated using the π° production rates presented in the previous section.

Using the inclusive data of Nagamiya[2] for .8 GeV/n $^{12}C + ^{208}Pb \rightarrow \pi^- + Y$, and data from a similar streamer chamber experiment[3] for 2.1 GeV/n $^{12}C + Pb_3O_4 \rightarrow \pi^- + Y$, and 1.8 GeV/n $^{40}Ar + Pb_3O_4 \rightarrow \pi^- + Y$, a Monte Carlo program taking an assumed momentum distribution of π° mesons into account was developed to determine the geometric efficiency of an upstream lucite Cerenkov telescope for detecting high energy gamma rays emanating from π° decay. The efficiency data derived in this manner are listed in Table IX as a function of beam energy and projectile mass. Using these results, it was possible for each reaction under study to translate the rate of π° production indicated in Table VI into the average number of high energy gamma rays entering the acceptance of the upstream Cerenkov detector system per event. The conversion probabilities discussed above were then used to estimate the rate, per event, of false (1,1) charged pion signatures due to gamma-ray conversion within the target. The magnitude of this correction is indicated by the sample data presented in Table X from which it is noted that subtraction of the false (1,1) signature rate due to this source of error generally reduces the observed "charged pion" signature rate by

TABLE IX: The Estimated Geometric Efficiency of an Upstream Cerenkov Telescope for Detecting Gamma Radiation Emanating from π° Decay

Beam Energy (GeV/n)	Projectile Ion	Target Nucleus	Estimated Geometric Efficiency (%)
1.05	^{12}C	^{208}Pb	2.24
1.3	^{12}C	^{208}Pb	2.18
1.5	^{12}C	^{208}Pb	2.12
1.7	^{12}C	^{208}Pb	2.07
1.9	^{12}C	^{208}Pb	2.01
2.1	^{12}C	^{208}Pb	1.96
1.8	^{40}Ar	^{208}Pb	1.94

≅ 25% for the $^{12}C + ^{208}Pb$ reactions, and ≅ 40% for the $^{40}Ar + ^{208}Pb$ reaction.

A third correction essential to a proper interpretation of the response of the Cerenkov telescope detector system consisted of estimating the background due to protons energetic enough to emulate the (1,1) charged pion signature.

Using standard formulae[8] to calculate the ionization energy loss expected for a proton traversing a given thickness of material, it was estimated that at 90° a proton would require ≅ 350 MeV to be above the effective threshold for detection by the lucite Cerenkov telescope counters. Furthermore, it was noted from the inclusive data of Nagamiya[2] for .8 GeV/n $^{12}C + ^{208}Pb \rightarrow p + X$ that the measured laboratory proton inclusive spectrum was fit quite well by an exponential having an inverse decay constant of ≅ $(107\ MeV)^{-1}$. Consequently, assuming that in the energy range of interest in the present experiment the proton spectra for the $^{12}C + ^{208}Pb$ reactions might be characterized by an exponential having a decay constant of ≅ $(115\ MeV)^{-1}$, it was calculated taking the Cerenkov efficiency into account that ≅4.8% of the protons produced should have been energetic enough to duplicate the (1,1) charged pion signature and effectively 17.3% of these should have been detected by the lucite Cerenkov telescopes. A similar analysis for the $^{40}Ar + ^{208}Pb$ reaction indicated that ≅ 18.2% of the protons above 350 MeV (≅ 5.4% of the total spectrum) should have produced false pion signatures. Using the multiplicity information provided by the dE/dx counter system, it was therefore possible to estimate and subtract the rate per event of false (1,1) signatures due to this source of background. Some indication of the magnitude of this correction may be obtained from the

TABLE X: The Production of False (1,1) Charged Pion Signatures Due to the Conversion of High Energy Gamma Rays within the Target

Beam Energy (GeV/n)	Projectile Ion	Target Nucleus	$R_{\pi}(1,1)=R_{\pi}(1,1)-(R_N(1,0)xR_{\gamma}(0,1))$ TRUE (per event)	False (1,1) Signatures Due to γ-ray Conversion within the Target (per event)	Percentage Reduction of (1,1) Signature Rate Due to Conversion Correction (%)
1.05 (Cut Ø)	^{12}C	^{208}Pb	(.0372±.0003)	(.0099±.0009)	26.6
2.1 (Cut Ø)	^{12}C	^{208}Pb	(.0933±.0006)	(.0254±.0022)	27.2
1.8 (Cut Ø)	^{40}Ar	^{208}Pb	(.1828±.0012)	(.0715±.0062)	39.1

sample data listed in Table XI, from which one notes that this source of background appears to range from ≅ 8% of the observed charged pion signature rate for 1.05 GeV/n ^{12}C + ^{208}Pb to ≅ 4% of the corresponding rate for 1.8 GeV/n ^{40}Ar + ^{208}Pb.

The measured rate of (1,1) charged pion signatures was also corrected for background due to knock-on electrons and the "preconversion" of high energy gamma rays in the first lucite Cerenkov counter of a given telescope.

To effect the latter correction, the mass attenuation coefficient for a 65 MeV photon was noted[9] to be ≅ $1.65 \times 10^{-2} cm^2/gm$ and $1.50 \times 10^{-2} cm^2/gm$ for ^{12}C and ^{1}H respectively. Therefore, observing the chemical formula for lucite to be $C_5H_8O_2$, and its molecular weight ≅ 6.7 gms/mole, the corresponding mass attenuation coefficient for lucite was estimated to be .016 cm^2/gm using the relationship

$$\left(\frac{\mu}{\rho}\right)_{\text{lucite}} = W_{^{12}C}\left(\frac{\mu}{\rho}\right)_{^{12}C} + W_{^{1}H}\left(\frac{\mu}{\rho}\right)_{^{1}H} + W_{^{16}O}\left(\frac{\mu}{\rho}\right)_{^{16}O} \qquad (4)$$

and assuming the mass attenuation coefficient for ^{16}O to be the same as that for ^{12}C. The factors W_i appearing in equation 4 represent the percentage by weight, of lucite made up by the ith element.

Having estimated the mass attenuation coefficient of lucite, it was assumed that if a high energy gamma ray converted to an electron pair before it came within 1 cm of the back surface of the first lucite Cerenkov of a given telescope, it would be detected in both the first and second lucite Cerenkov counters and thereby duplicate the charged pion signature. Noting that this assumption implied an average pathlength of ≅ 2.25 cm for

TABLE XI: The Production of False (1,1) Charged Pion Signatures Due to Energetic Protons

Beam Energy (GeV/n)	Projectile Ion	Target Nucleus	$R_\pi(1,1)=R_T(1,1)-(R_N(1,0)\times R_Y(0,1))$ TRUE (per event)	False (1,1) Signatures Due to Energetic Protons (per event)	Percentage Reduction of (1,1) Signature Rate Due to Proton Correction
1.05 (Cut Ø)	^{12}C	^{208}Pb	(.0372±.0003)	(.0030±.0002)	8.0%
2.1 (Cut Ø)	^{12}C	^{208}Pb	(.0933±.0006)	(.0045±.0002)	4.8%
1.8 (Cut Ø)	^{40}Ar	^{208}Pb	(.1828±.0012)	(.0066±.0003)	3.6%

a gamma ray traversing the first counter of a given upstream telescope, it was calculated that

$$\left(1 - \frac{I}{I_o}\right) = \left(1 - \exp[-.016\frac{cm^2}{gm} \times 2.25 \text{ cm} \times 1.17\frac{g}{cm^3}]\right) \cong .042 \quad (5)$$

or 4.2% of the high energy gamma rays incident upon the upstream Cerenkov telescope system should have produced false (1,1) signatures due to "preconversion" in the first lucite Cerenkov detector. Using the π° production rates presented in Table VI and the geometric efficiency data of Table IX, it was then possible to reduce the observed rate of charged pion production by the background (1,1) signature rate due to this source of error—a relatively constant correction of approximately 5%.

To estimate the level of background due to delta (δ), or knock-on electrons, it was necessary to calculate, for a proton or a pion of a given energy, the average number of energetic knock-on electrons produced in traversing one of the 1¼" thick lucite Cerenkov counters.

For a "heavy" charged particle (e.g. pion, proton) traversing a thickness dx (in cm) of a given medium, the number of knock-on electrons produced having kinetic energies in a range dT about the energy T may be expressed as

$$\frac{dN}{dTdx} = \frac{1}{2}D\left(\frac{Z_{med}}{A_{med}}\right)\left(\frac{Z^2_{proj}}{\beta^2}\right) \rho_{med} \frac{1}{T^2} \quad (6)$$

where $D = 4\pi N_A r_e^2 m_e c^2 = .3070$ MeV-cm^2/gm. Z_{med} and A_{med} are respectively the effective charge and mass numbers of the medium, ρ_{med} is its density (g/cm^3), and Z_{proj} and β are respectively the charge and speed of the incident charged particle. T is the kinetic energy of the knock-on electron

and m_e its mass. Physically, the kinetic energy of a knock-on electron is constrained to be much greater than the average ionization potential, I, of the medium ($\cong$ 65.6 ev for lucite). Kinematically, it must be less than the maximum energy transferable from the incident charged particle, namely

$$T_{max} = \frac{2m_e c^2 \beta^2 \gamma^2}{1 + 2\gamma(\frac{m_e}{m_{proj}}) + (\frac{m_e}{m_{proj}})^2} \qquad (7)$$

where m_{proj} is the mass of the incident charged particle.

In the particular instance of a proton or a pion incident upon one of the lucite Cerenkov counters employed in the present experiment, $\rho_{med} \cong 1.17$ g/cm^3, $Z_{proj} = 1$, and

$$\frac{Z_{med}}{A_{med}} = \sum_i W_i \frac{Z_i}{A_i} \cong .54, \qquad (8)$$

where W_i is the percentage by weight of the i^{th} element making up the compound $C_5H_8O_2$. Consequently, assuming that the lucite detectors in question are "thin" with respect to the energy of the incident charged particle (i.e. β is approximately constant), and integrating equation 6 to obtain the total number of knock-on electrons produced between an arbitrary low energy cutoff, T_0, ($\gg$I), and the maximum allowable transfer energy, T_{max}, it was calculated that

$$N = \frac{1}{2}D\left(\frac{Z_{med}}{A_{med}}\right)\frac{Z_{proj}^2}{\beta^2}\rho_{med}(x)\left(\frac{1}{T_0} - \frac{1}{T_{max}}\right) \cong \frac{.097(x)}{\beta^2}\left(\frac{1}{T_0} - \frac{1}{T_{max}}\right) \qquad (9)$$

However, it was also noted with regard to the false (1,1) signature rate, that the only electrons of real interest were those which produced sufficient Cerenkov radiation to be detected with some efficiency.

Empirically this constraint was found to imply that, in fact, only knock-on electrons having energies $\gtrsim$ .84 MeV contributed to this source of background, even though theoretically, the Cerenkov threshold for an electron in this type of plastic was $\cong$ 174 keV. Furthermore, observing that the range of an .84 MeV electron in lucite is $\cong$ .33 cm, it was assumed that effectively, only energetic electrons produced before the incident charged particle came within ~.3 cm of the back surface of a given Cerenkov counter contributed to this source of background, making the functional thickness of lucite $x \cong 2.8$ cm. Introducing this information into equation 9, the average number of effective knock-on electrons produced per incident charged particle, or equivalently, the probability per incident charged particle of registering a false Cerenkov count due to this source of background may be expressed,

$$N_\delta(E) = P_\delta(E)_{(1,(0+1))} = P_\delta(E)_{((0+1),1)} \cong \frac{.276}{\beta^2}\left(\frac{1}{.84} - \frac{1}{T_{max}}\right), \quad (10)$$

with T_{max} defined as above. The plus sign, "+", appearing in the subscripts (1,(0+1)), and ((0+1),1) shown above is intended to represent a logical "or". Consequently, the expression $P_\delta(E)_{(1,(0+1))}$, for example, denotes the probability, per charged particle, as a function of the energy of the incident charged particle, that the first element of a given lucite Cerenkov telescope registers a count due to the production of a knock-on electron, regardless of whether the second element does or not. For purposes of illustration, this probability is graphed in Fig. 20 as a function of proton kinetic energy along with associated values of the maximum allowable transfer energy, T_{max}.

Having calculated, as a function of energy, the probability for a

Fig 20

(a) —— The number (N_δ), per incident proton, of effective knock-on electrons produced ($.84\,MeV \lesssim T_e \lesssim T_{max}$) in an upstream lucite Cerenkov counter, plotted as a function of proton kinetic energy. Equivalently, the probability ($P_\delta(1,(0+1))$), per incident proton, of producing an effective knock-on electron in an upstream lucite Cerenkov counter, plotted as a function of proton kinetic energy.

--- The maximum energy transferable from a proton to a knock-on electron, plotted as a function of proton kinetic energy.

(b) —— The probability, per incident pion of producing an effective knock-on electron in an upstream lucite Cerenkov counter, plotted as a function of pion kinetic energy.

--- The maximum energy transferable from a pion to a knock-on electron, plotted as a function of pion kinetic energy.

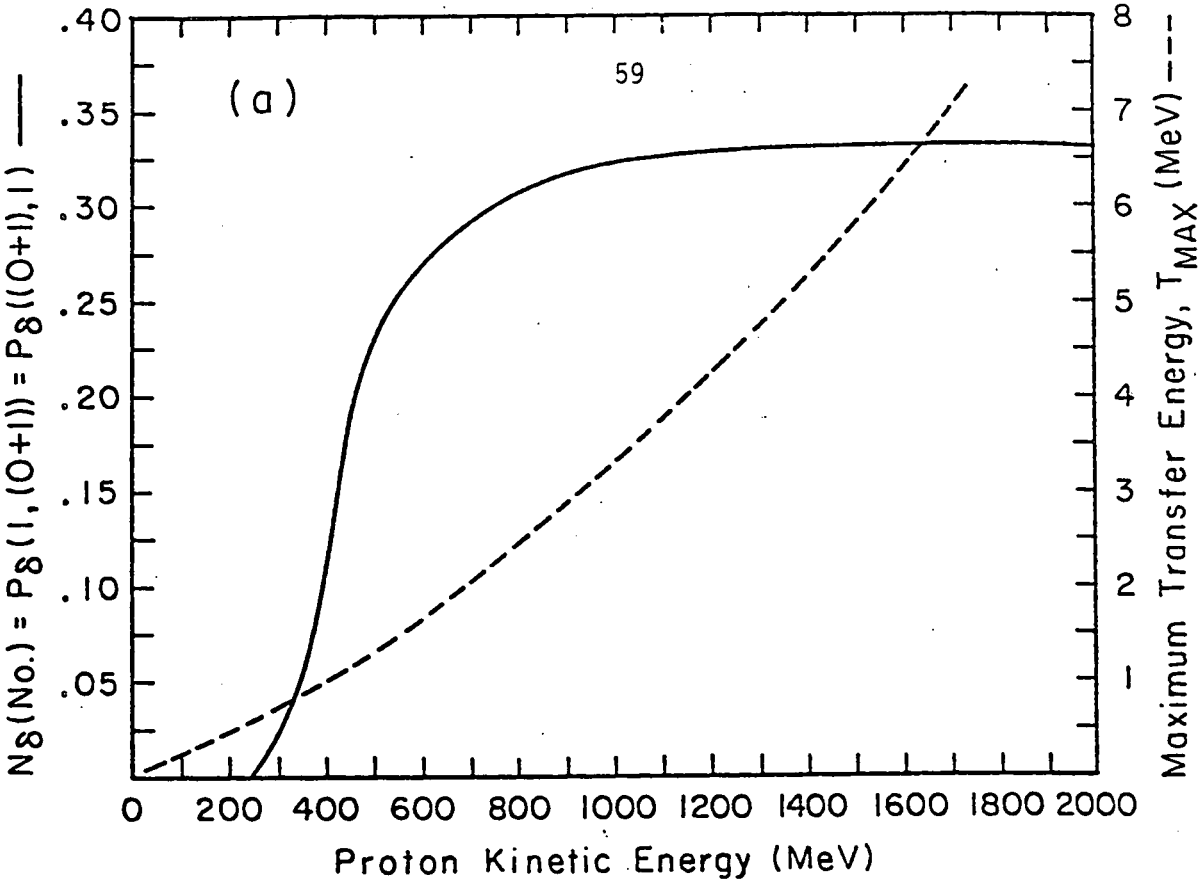
(a)
$N_\delta(No.) = P_\delta(1,(O+1)) = P_\delta((O+1),1)$ ——
Maximum Transfer Energy, T_{MAX} (MeV) ---
.40
.35
.30
.25
.20
.15
.10
.05
8
7
6
5
4
3
2
1
0 200 400 600 800 1000 1200 1400 1600 1800 2000
Proton Kinetic Energy (MeV)

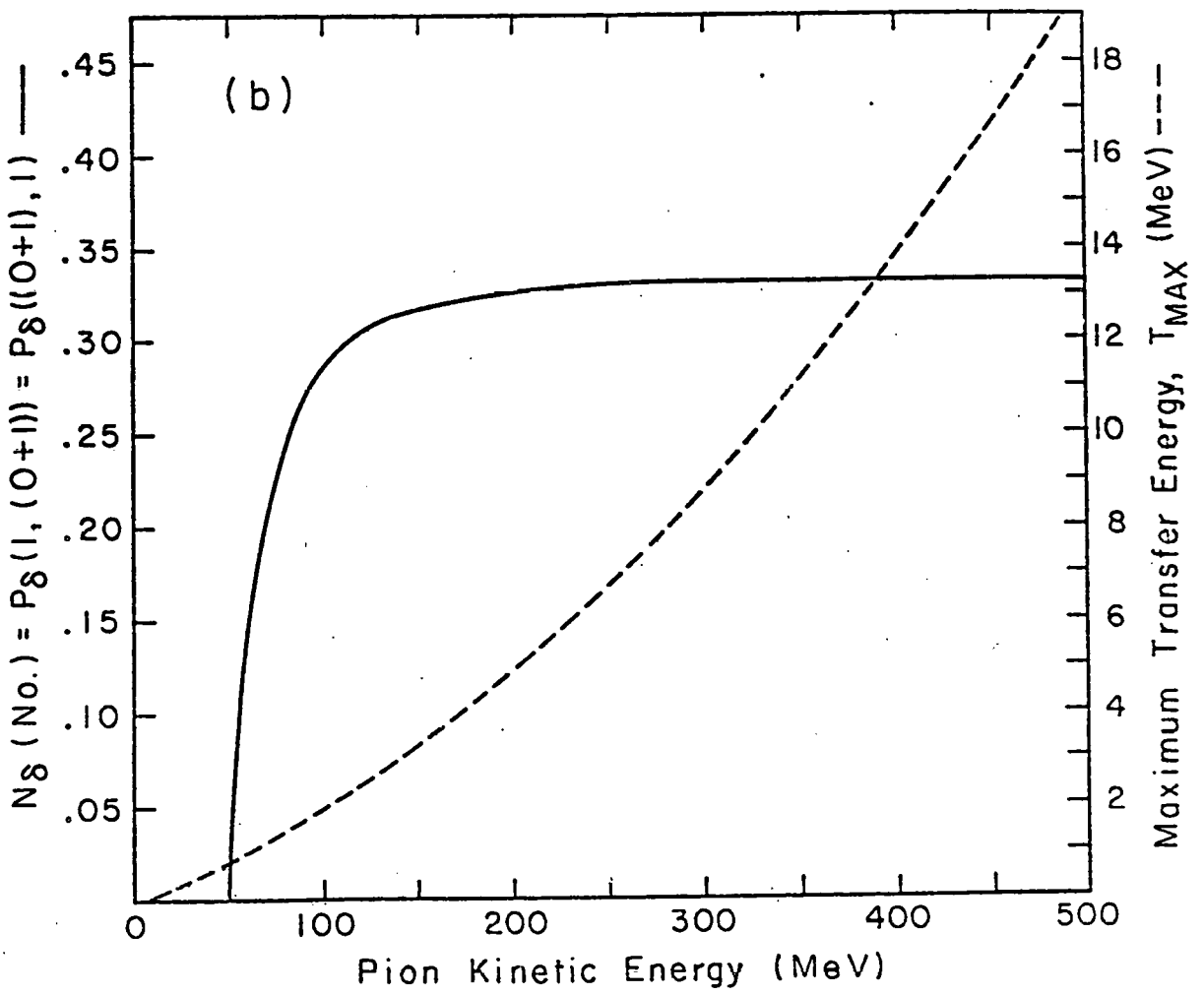
(b)
$N_\delta(No.) = P_\delta(1,(O+1)) = P_\delta((O+1),1)$ ——
Maximum Transfer Energy, T_{MAX} (MeV) ---
.45
.40
.35
.30
.25
.20
.15
.10
.05
18
16
14
12
10
8
6
4
2
0 100 200 300 400 500
Pion Kinetic Energy (MeV)

proton to produce a false (0+1),1) or (1,(0+1)) signature due to knock-on electrons, it was assumed once again that in the present experiment the proton spectra for the $^{12}C + ^{208}Pb$ reactions might be characterized by an exponential having a decay constant of $\cong$ (115 MeV)$^{-1}$, ((120 MeV)$^{-1}$ for $^{40}Ar + ^{208}Pb$). The knock-on electron probability curve shown in Fig. 20 was then weighted using the exponential decay presumed to characterize the proton energy spectra in order to determine that, on the average, .0092 effective knock-on electrons would be produced per incident proton, or equivalently, .92% of all protons entering an upstream lucite Cerenkov counter should have produced a count by this mechanism. Furthermore, for the protons entering the acceptance of an upstream lucite Cerenkov telescope,

$$P_{\delta}(1,1) = P_{\delta}(1,(0+1)) \times P_{\delta}((0+1),1) \cong (.0092)^2 \qquad (11)$$

or $\cong$ .008% should have produced false (1,1) signatures due to this source of background. Using the multiplicity information provided by the dE/dx counter system, it was therefore possible to estimate and subtract the spurious (1,1) signature rate due to this source of error.

A similar analysis for charged pions below the effective Cerenkov threshold in the upstream lucite detectors ($\cong$ 68% of the total spectrum) indicated that in this instance approximately 3.9% of the subthreshold charged pions incident upon an upstream lucite Cerenkov counter should have been detected by this mechanism. Specifically, the magnitude of the false (1,1) and (0,1) signature rates for an upstream Cerenkov telescope would be expressed

$$R_\delta(1,1) = P_\delta(1,(0+1)) \times P_\delta((0+1),1) \times \langle N_{\pi^\pm}\rangle_{effective}$$

$$\cong (.039)^2(.026)\langle N_{\pi^\pm}\rangle \sim 4\times10^{-5}\langle N_{\pi^\pm}\rangle \quad (12)$$

and

$$R_\delta(0,1) = P_\delta((0+1),1) \times (1-P_\delta(1,(0+1)))\times\langle N_{\pi^\pm}\rangle_{effective}$$

$$\cong (.039)(.96)(.026)\langle N_{\pi^\pm}\rangle \sim 1\times10^{-3}\langle N_{\pi^\pm}\rangle \quad (13)$$

respectively, where the factor .026 accounts for the solid angle of the counter ($\cong$ .48 sr), and the fact that subthreshold pions represent $\cong$ 68% of the total spectrum. Charged pions above the effective Cerenkov threshold were found to be $\cong$ 30.8% efficient (Fig. 20) for producing an effective knock-on electron ($\gtrsim$.84 MeV) although in this case account also had to be taken of the probability that a given pion would be detected directly. Therefore, if the average efficiency of an upstream lucite Cerenkov counter is assumed to be $\varepsilon \cong 70\%$ for detecting a charged pion directly, the corresponding (1,1) and (0,1) spurious background rates for energetic charged pions would be expressed,

$$R_\delta(1,1) = [(1-\varepsilon)^2 P_\delta((0+1),1)P_\delta(1,(0+1))]\langle N_{\pi^\pm}\rangle_{effective}$$

$$\cong (.30)^2(.308)^2(.012)\langle N_{\pi^\pm}\rangle \sim 1\times10^{-4}\ \langle N_{\pi^\pm}\rangle, \text{ and} \quad (14)$$

$$R_\delta(0,1) = [(1-\varepsilon)^2 P_\delta((0+1),1)(1-P_\delta(1,(0+1)))]\langle N_{\pi^\pm}\rangle_{effective}$$

$$\cong (.3)(.3)(.31)(.69)(.012)\langle N_{\pi^\pm}\rangle \sim 2\times10^{-4}\langle N_{\pi^\pm}\rangle \quad (15)$$

respectively, where the factor .012 accounts once again for the solid angle of the detector, and the fact that only 32% of the pionic spectrum is above the effective Cerenkov threshold.

The magnitude of the false (1,1) and (0,1) signature rates due to knock-on electrons produced by protons and pions is indicated by the sample data listed in Table XII. It is observed from these results that, insofar as the (1,1) charged pion signature is concerned, the background due to knock-on electrons is small enough to be considered negligible, ranging from $\cong$ .7% of the measured rate for 1.05 GeV/n ^{12}C + ^{208}Pb, to $\cong$ .5% of the corresponding rate for 1.8 GeV/n ^{40}Ar + ^{208}Pb. With regard to the (0,1) high energy gamma ray signature, however, it appears the background due to this source of error is appreciable (e.g. 10.4% for 1.05 GeV/n ^{12}C + ^{208}Pb), and consequently, in this instance, a subtraction must be made if the response of the lucite Cerenkov telescope system is to be interpreted correctly.

Perhaps, however, the most important correction aside from the conversion of gamma rays within the target was that made to account for the spurious (1,1) background rate due to low energy gamma rays.

In the course of performing the experiment, it was determined that the lucite Cerenkov counters used to measure charged pion production were approximately 3% efficient for detecting the 1.17 and 1.33 MeV gamma rays of Co^{60}. Consequently, having observed that a large number ($\cong$ 43 for 1.05 GeV/n ^{12}C + ^{208}Pb) of low energy photons (.7 MeV $\lesssim E \lesssim$ 7 MeV) do in fact accompany a central collision of two relativistic heavy nuclei, it was found necessary to correct the measured (1,1) and (0,1) signature rates for spurious counts due to this source of background.

The manner in which a photon interacts with matter is dependent on its energy. In the 1-5 MeV range, for example, the Compton effect is

Table XII: The Production of False (1,1) and (0,1) Cerenkov Telescope Signatures Due to Knock-on Electrons

Beam Energy	1.05	2.1	1.8
Projectile Ion	^{12}C	^{12}C	^{40}Ar
Target Nucleus	^{208}Pb	^{208}Pb	^{208}Pb
$R_\pi(1,1)=R_\pi(1,1)-(R_\gamma(0,1)xR_N(1,0))$ $_{TRUE, Cut \emptyset}$ (per event)	$(.0372^{\pm}.0003)$	$(.0933^{\pm}.0006)$	$(.1828^{\pm}.0012)$
$R_\delta(1,1)$, Cut $\emptyset$ (per event)	$(.00025^{\pm}.00002)$	$(.00074^{\pm}.00003)$	$(.00087^{\pm}.00008)$
Percentage Reduction of $R_\pi(1,1)_{TRUE}$ due to Knock-on Electrons	~.67%	~.79%	~.48%
$R_\gamma(0,1)$, Cut $\emptyset$, Lead Out (per event)	$(.0684^{\pm}.0005)$	$(.1009^{\pm}.0006)$	$(.1368^{\pm}.0009)$
$R_\delta(0,1)$ due to Protons and Charged Pions, Cut $\emptyset$, Lead Out (per event)	$(.0071^{\pm}.0003)$	$(.0160^{\pm}.0006)$	$(.0193^{\pm}.0012)$
Percentage Reduction of $R_\gamma(0,1)$ Signature due to Knock-on Electrons	10.4%	15.9%	14.1%

the primary means by which a photon interacts with the matter through which it passes. Above this energy, the pair production process predominates. Since, however, it was noted in the present experiment that approximately 90% of the measured low energy gamma ray spectra typically lie below 5 MeV, Compton scattering was judged to be the primary source of low energy gamma ray background in the lucite Cerenkov telescopes.

The probability that a given photon will, in fact, interact with matter is dependent on both its energy and the chemical composition of the material in question.

Consider, for example, a collimated beam of photons of energy E and intensity I_0. The number of photons expected to interact in a given thickness of material may be calculated according to the relationship

$$(I/I_0) = \exp\left[-\frac{\mu(E)}{\rho} t\right] \qquad (16)$$

where $\mu(E)/\rho$ is the mass attenuation coefficient of the material (cm^2/gm) for a photon of energy E, and I is the intensity of the photon beam after it traverses a distance t (g/cm^2). The opacity of a particular counter, for example, for photons of energy E might therefore be readily determined if its characteristic mass attenuation coefficient were known.

Interpreting this information in the context of the present experiment, the mass attenuation coefficient for lucite ($C_5H_8O_2$) was estimated as a function of energy, using the weighting procedure suggested by equation 4 and known values of the mass attenuation coefficients for carbon, hydrogen, and oxygen. Assuming an effective thickness of $\cong$ 3.87 g/cm^2 ($\rho \cong$ 1.2 g/cm^3), it was then possible to calculate, as a function of photon

energy, the opacity expected to characterize the upstream lucite Cerenkov counters used to detect charged pions. The results are indicated by the complement of the transmission curve plotted in Fig. 21, from which it is noted that the percentage of gamma rays which interact in the upstream lucite Cerenkov detectors drops slowly from ≅ 21.9% at 1 MeV to ≅ 9.0% at 7 MeV.

It will be recalled, however, from the discussion of knock-on electrons, that although the number of gamma rays scattered in traversing a given lucite detector might be calculated according to the procedure outlined above, the only Compton scattered electrons of real interest were those which produced sufficient Cerenkov radiation to be detected with some efficiency—a constraint primarily on their energy. To estimate the false signature rate due to this source of background, it was therefore necessary to determine what electron energy constituted an effective low energy cutoff, and what fraction of the Compton scattered electrons would be produced with energies greater than or equal to that value.

To address this problem, a brief review of the kinematic consequences of the Compton effect was required.

The conventional notation associated with the Compton effect is illustrated in Fig. 22, in which a photon incident from the left is scattered through an angle θ by an electron. The electron itself recoils at an angle ϕ. Since energy and momentum must both be conserved, the wavelength of the scattered photon, λ', is related to that of the incoming photon, λ, by the expression

$$\lambda' - \lambda = \frac{hc}{m_e c^2} (1-\cos\theta), \qquad (17)$$

Fig 21.

---- The probability, $(1 - P_c(E))$, as a function of energy, that a photon will be transmitted without interaction by an upstream lucite Cerenkov counter.

..... The probability, $(P_c(E))$, as a function of energy, that a photon will be scattered in an upstream lucite Cerenkov counter due to the Compton Effect.

——— The probability, $(P(E)_{T_e > .84})$, as a function of energy, that a Compton scattered photon will produce a recoil electron having more than .84 MeV of kinetic energy in an upstream lucite Cerenkov counter.

— — The overall probability per photon, $P(E)_{(1,(0+1))} = P_c(E)\, P(E)_{T_e > .84}$, of producing a Compton scattered recoil electron having more than .84 MeV of kinetic energy in an upstream lucite Cerenkov counter, plotted as a function of gamma ray energy.

xxxx The cosine of the minimum scattering angle (θ_{min}) kinematically allowed if a photon of energy E is required to produce a Compton scattered recoil electron having more than .84 MeV of kinetic energy.

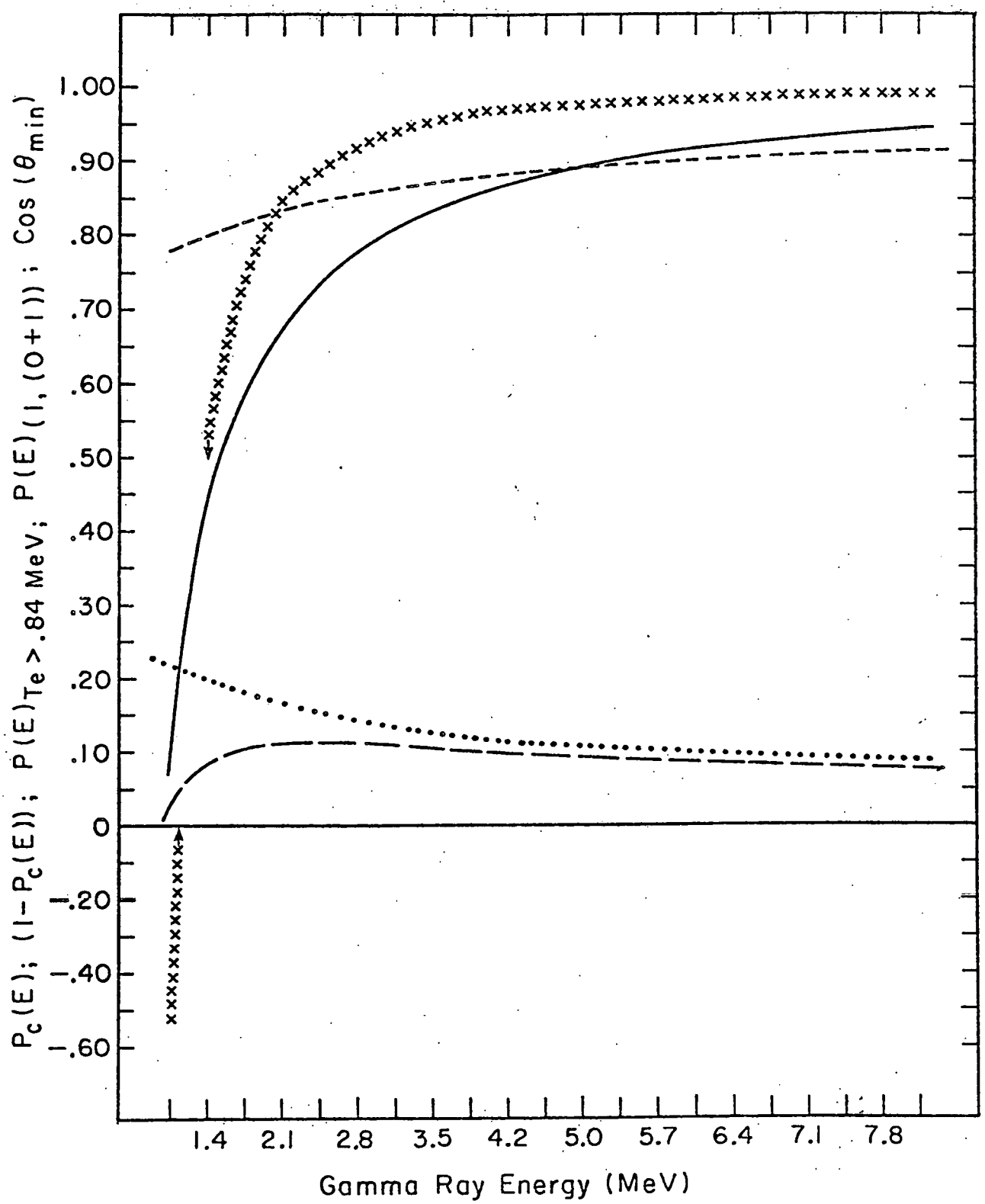
1.00
.90
.80
.70
.60
.50
.40
.30
.20
.10
0
-.20
-.40
-.60
$P_c(E)$; $(1-P_c(E))$; $P(E)_{Te>.84\ MeV}$; $P(E)(I,(O+I))$; $Cos(\theta_{min})$
1.4
2.1
2.8
3.5
4.2
5.0
5.7
6.4
7.1
7.8
Gamma Ray Energy (MeV)

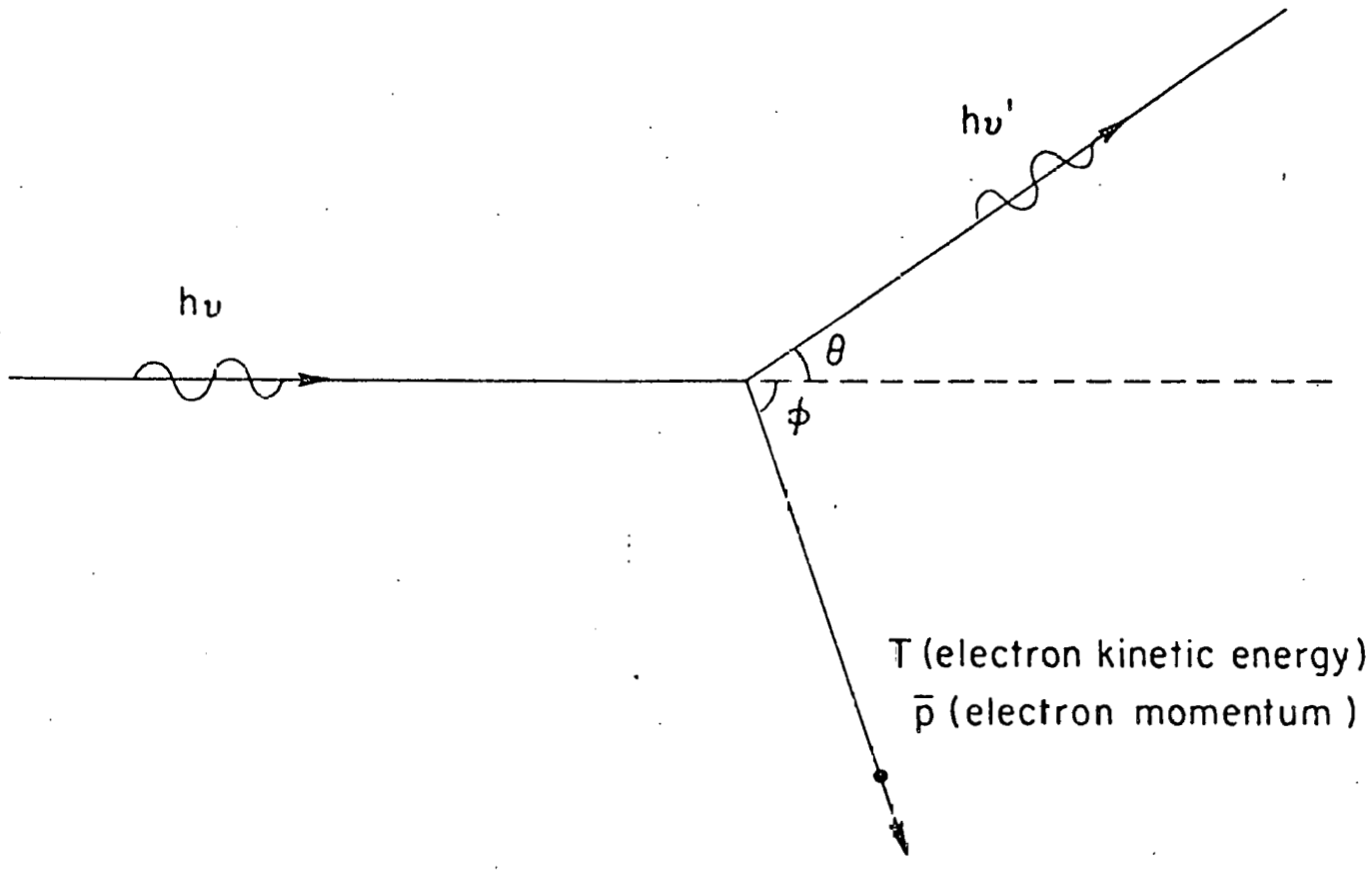

Fig. 22 The conventional notation associated with the Compton Effect. A photon incident from the left is scattered through an angle θ by an electron. The electron itself recoils at an angle ϕ.

where h is Planck's constant and m_e the mass of the electron. Equation 17 may also be rearranged to give an equivalent expression,

$$h\nu' = \frac{h\nu}{[1 + \frac{h\nu}{m_e c^2}(1-\cos\theta)]} \tag{18}$$

relating the energies of the incident and scattered photons ($h\nu$ and $h\nu'$ respectively). Furthermore, since energy which is lost by the incident photon must be transferred to the recoil electron, its energy, T_e, may be given as

$$T_e = h\nu - h\nu' = h\nu - \frac{h\nu}{1+\alpha(1-\cos\theta)} = h\nu(\frac{\alpha(1-\cos\theta)}{1+\alpha(1-\cos\theta)}), \tag{19}$$

where $h\nu/m_e c^2$ has been expressed as α for convenience.

What is noted from equations 17, 18, and 19 is that ν, T_e, and θ are uniquely related, so that if any two are known, the third may be determined. Consequently, for example, if the energy of the incident photon and the recoil electron are known, the corresponding scattering angle θ may be determined unambiguously. Furthermore, it is observed from equation 18 that as $\theta \to \pi$, the energy of the scattered photon decreases, and that of the recoil electron increases. Therefore, for a given initial photon energy $h\nu$, a low energy cutoff, T_o, imposed on the energy of the recoil electron constrains the angle of scattering, θ, to be greater than or equal to a minimum value

$$\theta_{min} = \cos^{-1}\left[1 - (\frac{T_e/h\nu}{\alpha(1-T_e/h\nu)})\right]. \tag{20}$$

The cross section, averaged over polarization for scattering a given photon into a particular solid angle, may be determined from the Klein-Nishina formula,

$$\left(\frac{d\sigma}{d\Omega}\right)_{kN} = \frac{1}{\alpha} r_o^2 \left(\frac{h\nu'}{h\nu}\right)^2 \left[\left(\frac{h\nu}{h\nu'}\right) + \left(\frac{h\nu'}{h\nu}\right) - \sin^2\theta\right], \tag{21}$$

or

$$\left(\frac{d\sigma}{d\Omega}\right)_{kN} = \frac{1}{\alpha} r_o^2 \frac{1}{(1+\alpha(1-\cos\theta))^2}\left(1 + \cos^2\theta + \frac{\alpha^2(1-\cos\theta)^2}{(1+\alpha(1-\cos\theta))}\right) \tag{22}$$

where r_o is the classical radius of the electron, α once again equals $h\nu/m_e c^2$, and the second expression was derived from the first by the substitution of equation 18. The probability, therefore, that a particular Compton event will result in the incident photon being scattered through an angle greater than or equal to some arbitrary value of θ_{min}—which is equivalent to the probability that the recoil electron will have an energy greater than or equal to the corresponding value of T_o—may be calculated by taking the ratio of the total scattering cross section which results when the range of θ is restricted to the total scattering cross section obtained when the scattering angle is unconstrained. Specifically

$$P(E)_{T_e > T_o} = \frac{\int_0^{2\pi}\int_{\theta_{min}}^{\pi} \left(\frac{d\sigma}{d\Omega}\right)_{kN} d\Omega}{\int_0^{2\pi}\int_0^{\pi} \left(\frac{d\sigma}{d\Omega}\right)_{kN} d\Omega} \tag{23}$$

where the lower limit imposed on the scattering angle, θ_{min}, is understood to imply a corresponding lower limit, T_o, on the energy of the recoil electron for a gamma ray of energy E. Interpreting this information in terms of the present experiment, one finds that if the probability of producing a Compton scattering in one of the upstream lucite Cerenkov detectors were denoted

$$P_c(E) = (1-I/I_o) = (1-\exp[(-\mu(E)/\rho)\ t_{lucite}]) \qquad (24)$$

for a gamma ray of energy E, the overall probability per incident photon of producing a spurious count due to this mechanism would be expressed

$$P(E)_{(1,(0+1))} = P(E)_{((0+1),1)} = P_c(E)P(E)_{T_e>T_o}, \qquad (25)$$

assuming the low energy cutoff T_o were known.

To find the effective low energy cutoff, T_o, germane to the present study, it was noted once again that the lucite Cerenkov detectors used in the upstream telescopes were $\cong$ 3% efficient for detecting the 1.17 and 1.33 MeV gamma rays of Co^{60}, i.e. $P(1.2)_{(1,(0+1))} \cong .03$. Furthermore, it was determined that for these photons, having an average energy of $\cong$ 1.2 MeV, the probability per incident photon of scattering due to the Compton effect was $P_c(1.2) \cong .22$ for the same lucite detectors. Consequently, by inverting equation 25 it was calculated that, in this instance, $P(1.2)_{T_e>T_o} \cong .13$, or the probability per Compton scattering of registering a count was approximately 13%. Having empirically determined, therefore, that for 1.2 MeV photons the ratio expressed in equation 23 was approximately .13, the implied low energy cutoff was found to be

$T_o \cong .84$ MeV by varying the value of θ_{min} appearing in that expression.

Using .84 MeV as the effective low energy cutoff for a recoil electron to be efficiently detected by an upstream lucite Cerenkov counter, the probability of producing such an electron, $P(E)_{T_e>.84\ MeV}$, was then calculated for each energy in the range of interest, using the procedure outlined in equation 23 and varying the value of θ_{min} appropriately (eq. 20). The results, plotted in Fig. 21 along with $\cos(\theta_{min})$, indicate that the probability, per photon, of producing a recoil electron having more than .84 MeV rises sharply from $\cong$ 2.3% at 1.0 MeV to $\cong$ 80% at 3 MeV, above which it increases slowly.

Having calculated both $P_C(E)$ and $P(E)_{T_e>.84}$ as a function of energy, equation 25 was employed to determine the overall probability per photon, $P(E)_{(1,(0+1))}$, of producing a spurious (1,(0+1)) or ((0+1),1) signature in the energy range of interest. The results of this calculation, also plotted in Fig. 21, indicate that above $\cong$ 1 MeV, the probability per photon of producing a background count by this mechanism is relatively constant, and approximately equal to 10%.

Using the calculated probabilities, $P(E)_{(1,(0+1))}$, plotted in Fig. 21 as a function of gamma ray energy, it was possible to translate the measured 90° low energy gamma ray spectra, $dN(E)/d\Omega$, associated with a given reaction into an estimated count rate, or probability, per event, of spurious (0,1) and (1,1) signatures due to this source of background. Specifically, the rate per event of background counts for the inner and outer elements of the upstream Cerenkov telescopes were calculated using the expressions,

$$R_B(1,(0+1)) = \sum_{E_\gamma} \Omega_{\hat{C}} P(E)_{(1,(0+1))} \frac{dN(E)}{d\Omega}, \quad (26)$$

and,

$$R_B((0+1),1) = \sum_{E_\gamma} \Omega_{\hat{C}} P(E)_{((0+1),1)} \frac{dN(E)}{d\Omega}, \text{ respectively,} \quad (27)$$

where $\Omega_{\hat{C}}$ denotes the solid angle of the Cerenkov counter considered, ($\cong$ .78 sr and .48 sr for the inner and outer counters). The false (1,1) and (0,1) signature rates due to Compton scattered gamma rays, (CSG), were then estimated according to the formulae,

$$R_{CSG}(1,1) = R_B((0+1),1) \times R_B(1,(0+1)) \quad (28)$$

and

$$R_{CSG}(0,1) = R_B((0+1),1) \times (1-R_B(1,(0+1))) \quad (29)$$

respectively. For purposes of illustration, the measured low energy gamma ray spectrum, $dN(E)/d\Omega$, and the spectrum effective for producing spurious (1,(0+1)) and ((0+1),1) signatures, $P(E)dN(E)/d\Omega$, are plotted in Fig. 23 for 1.05 GeV/n ^{12}C + ^{208}Pb, Cut Ø.

It should be noted at this point that, in calculating the spurious count rate according to equations 28 and 29 above, it has been tacitly assumed that gamma rays which Compton scatter and register a count in the first lucite Cerenkov detector of a given telescope, may also do so in the corresponding outer element of the counter.

This is an approximation, since it is evident that some of the photons which are Compton scattered and thereby detected in the first counter of a given telescope, will not have enough remaining energy to be detected in the second with any appreciable probability. However, it is

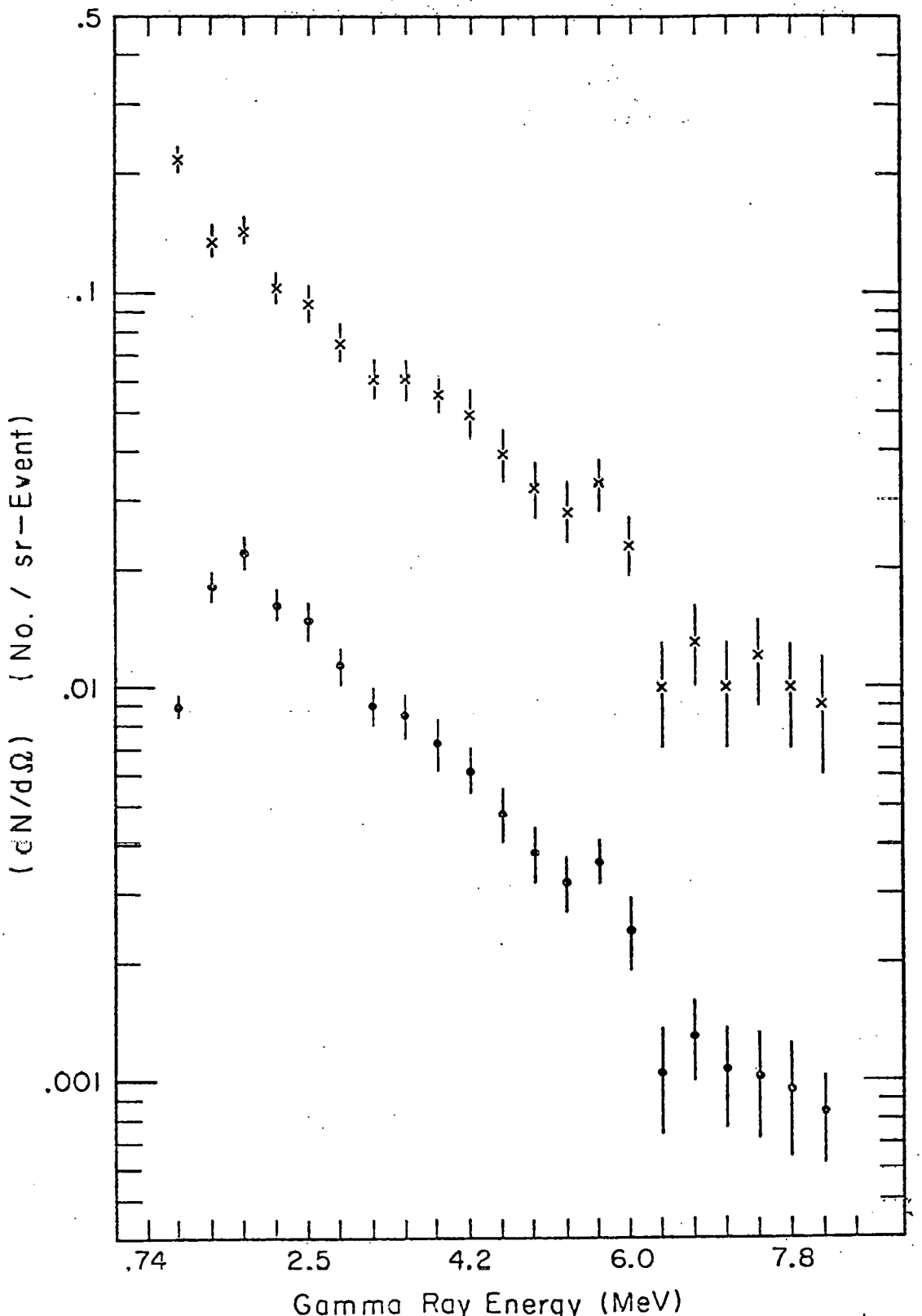

Fig 23. x – The single photon inclusive low energy γ ray spectrum, $(dN(E)/d\Omega)$, measured for central collisions of 1.05 GeV/n $^{12}C + ^{208}Pb$ (Cut ∅) at 90°

• – The low energy γ ray spectrum, $(P(E)\, dN(E)/d\Omega)$, effective for producing spurious ((1,(0+1)) and ((0+1),1) signatures due to Compton scattering

observed from Fig. 21 that the probability, per photon, of producing a background count, $P_c(E)P(E)_{T_e>.84}$, is approximately constant throughout the energy range of interest, and does not decrease appreciably until the energy of the incident gamma ray falls below ≅ 1 MeV. Furthermore, it is evident from Fig. 21 that subject to the low energy cutoff imposed on the energy of the recoil electron (≅ .84 MeV), the minimum allowable scattering angle θ_{min} decreases sharply with increasing gamma ray energy. Therefore, even for photons having energies only slightly greater than 1 MeV, the probability of a small angle scattering event resulting in minimal momentum transfer is greatly enhanced. Consequently, it is clear that, except for energies below ≅ 1 MeV, photons which scatter once in the first element of a given lucite Cerenkov telescope are just as likely to scatter in the second element of the counter, supporting the validity of this approximation.

The magnitude of the false (1,1) and (0,1) signature rates due to Compton scattered gamma rays is indicated by the sample data listed in Table XIII. It is observed from these results that, with regard to the (1,1) charged pion signature, the count rate due to this source of background decreases with increasing beam energy, ranging from ≅ 23% of the measured (1,1) signature rate for 1.05 GeV/n ^{12}C + ^{208}Pb, (Cut Ø), to ≅ 8.7% of the corresponding rate for 2.1 GeV/n ^{12}C + ^{208}Pb (Cut Ø). This result is consistent with the related observation, that the rate of low energy gamma ray production increases only slightly with increasing beam energy (from ≅42.6/event for 1.05 GeV/n ^{12}C+^{208}Pb to ≅50.4/event for 2.1 GeV/n ^{12}C + ^{208}Pb, having energies .7 MeV ≲ E ≲ 7 MeV), and as a consequence other backgrounds present, due to gamma preconversion or knock-on electrons for

Table XIII: The Production of False (1,1) and (0,1) Cerenkov Telescope Signatures Due to Compton Scattered Gamma Rays

Beam Energy (GeV/n)	1.05	2.1	1.8
Projectile Ion	^{12}C	^{12}C	^{40}Ar
Target Nucleus	^{208}Pb	^{208}Pb	^{208}Pb
$R_\pi(1,1)=R_\pi(1,1)-(R(0,1)xR_N(1,0))$, Cut Ø TRUE (per event)	$(.0372\pm.0003)$	$(.0933\pm.0006)$	$(.1828\pm.0012)$
$R_{CSG}(1,1)^*$, Cut Ø (per event)	$(.0084\pm.0003)$	$(.0081\pm.0003)$	$(.0227\pm.0008)$
Percentage Reduction of $R_\pi(1,1)_{TRUE}$ due to $R_{CSG}(1,1)$	22.6%	8.7%	12.4%
$R_\gamma(0,1)$, Cut Ø, Lead Out (per event)	$(.0684\pm.0005)$	$(.1009\pm.0006)$	$(.1368\pm.0009)$
$R_{CSG}(0,1)^*$, Cut Ø, Lead Out (per event)	$(.0632\pm.0017)$	$(.0623\pm.0017)$	$(.0951\pm.0025)$
Percentage Reduction of $R_\gamma(C,1)$ Signature due to $R_{CSG}(0,1)$	92.4%	61.7%	69.5%

* CSG stands for Compton scattered gamma rays

example, constitute a higher percentage of the total. With regard to the (0,1) high energy gamma ray signature, it appears that when the lead converters were removed from the upstream Cerenkov telescopes, the observed count rate was due almost entirely to Compton scattered gamma rays, the estimated background ranging from = 92.4% of the measured (0,1) coincidence rate for 1.05 GeV/n ^{12}C + ^{208}Pb to ≅ 62% of the corresponding rate for 2.1 GeV/n ^{12}C + ^{208}Pb. Consequently, in this instance, the spurious signature rate due to Compton scattered gamma ray background must be treated quite carefully in order to interpret the response of the lucite Cerenkov telescope system correctly.

Using a Monte Carlo program developed to estimate the effective acceptance of each detector system, it was determined by throwing 1 computational charged pion per event that given the inclusive π^- momentum distribution measured by Nagamiya[2] for .8 GeV/n ^{12}C + ^{208}Pb, an upstream lucite Cerenkov telescope would have detected ≅ .56% of all the charged pions thrown. Similar calculations using 2.1 GeV/n ^{12}C + $^{208}Pb \rightarrow \pi^-$ + Y, and 1.8 GeV/n ^{40}Ar + $^{208}Pb \rightarrow \pi^-$ + Y streamer chamber measurements[3] yielded corresponding efficiencies of .69% and .86% respectively. Assuming therefore the .8 GeV/n efficiency to remain applicable at 1.05 GeV/n, the intermediate efficiency data listed in Table XIV as a function of beam energy and projectile mass were estimated by interpolating between the .8 GeV/n and 2.1 GeV/n results.

Using the efficiency data listed in Table XIV, and taking all the corrections discussed above into account, the rate of high energy (≳ 70 MeV) charged pion production measured by the upstream lucite Cerenkov

TABLE XIV: The Estimated Total Absolute Efficiency of an Upstream Lucite Cerenkov Telescope for Detecting Charged π Mesons

Beam Energy (GeV/n)	Projectile Ion	Target Nucleus	Estimated Total Absolute Efficiency for Detecting $\pi^{\pm}$ Mesons (%)
1.05	^{12}C	^{208}Pb	.56
1.3	^{12}C	^{208}Pb	.59
1.5	^{12}C	^{208}Pb	.62
1.7	^{12}C	^{208}Pb	.64
1.9	^{12}C	^{208}Pb	.67
2.1	^{12}C	^{208}Pb	.69
1.8	^{40}Ar	^{208}Pb	.86

telescope system was translated, for each reaction under study, into an average number of $\pi^{\pm}$ mesons produced per central collision. The results have been presented in Table XV as a function of beam energy, projectile mass, and multiplicity cut. For reference, the associated absolute $\pi^{\pm}$ production cross sections have been noted there as well. The errors shown for the $\langle N_{\pi^{\pm}} \rangle$ results reflect the error due to counting statistics. For the absolute cross section data which have been presented, the errors shown include an additional 7% error in trigger cross section.

Upon inspection of these data, it would appear that, for the $^{12}C + ^{208}Pb$ reaction, the number of charged $\pi^{\pm}$ mesons produced per central collision exhibits a generally smooth increase from $\cong (2.53 \pm .18)$ at 1.05 GeV/n (Cut Ø), to $\cong (7.35 \pm .34)$ at 2.1 GeV/n (Cut Ø). For 1.8 GeV/n $^{40}Ar + ^{208}Pb$, the corresponding rate of production is $(8.73 \pm .75)$.

Overall, these results compare favorably with those of similar streamer chamber experiments,[3] although discrepancies do exist. It is noted, for example, that assuming the rate of π^{+} production is approximately equal to that for negative pions, the rate of π^{-} production previously reported for 2.1 GeV/n $^{12}C + Pb_3O_4$, $(1.79 \pm .16)$, implies a total $\pi^{\pm}$ production rate only half that measured in the present experiment. However, it is also observed with regard to the 2.1 GeV/n $^{12}C + Pb_3O_4$ result, that the trigger used was "inelastic", rejecting only the most noninteractive collisions. Consequently, since the rate of pion production is in general thought to be a moderately strong function of impact parameter, the relatively large discrepancy discussed above may be a reflection of differing trigger criteria. The rate of π^{-} production previously

TABLE XV: $\langle N_{\pi^\pm} \rangle$; Lucite Cerenkov Telescope System

Beam Energy (GeV/n)	Projectile Ion	Target Nucleus	Cut IV		Cut Ø		Cut I		Cut II		Cut III	
			$\langle N_{\pi^\pm} \rangle$	$\sigma_{\pi^\pm}$ (mb)	$\langle N_{\pi^\pm} \rangle$	$\sigma_{\pi^\pm}$ (mb)	$\langle N_{\pi^\pm} \rangle$	$\sigma_{\pi^\pm}$ (mb)	$\langle N_{\pi^\pm} \rangle$	$\sigma_{\pi^\pm}$ (mb)	$\langle N_{\pi^\pm} \rangle$	$\sigma_{\pi^\pm}$ (mb)
1.05	^{12}C	$^{20\varepsilon}Pb$	(2.03±.21)	(177±22)	(2.53±.18)	(751±74)	(2.64±.21)	(653±68)	(2.80±.21)	(380±38)	(4.29±.55)	(41±6.0)
1.3	^{12}C	$^{20\varepsilon}Pb$	(3.35±.31)	(534±62)	(3.93±.27)	(1568±152)	(4.09±.29)	(1283±124)	(4.58±.37)	(623±65)	(3.70±1.12)	(58.9±18.2)
1.5	^{12}C	$^{20\varepsilon}Pb$	(3.71±.25)	(698±67)	(5.02±.25)	(2480±207)	(5.20±.27)	(1879±158)	(5.89±.31)	(948±82)	(7.24±.57)	(163±16.8)
1.7	^{12}C	$^{20\varepsilon}Pb$	(4.75±.29)	(1166±104)	(5.89±.30)	(3544±297)	(6.23±.32)	(2849±238)	(5.95±.37)	(1494±125)	(7.92±.66)	(253±27.4)
1.9	^{12}C	$^{20\varepsilon}Pb$	(5.39±.30)	(1531±133)	(6.52±.33)	(4527±376)	(7.01±.40)	(3611±315)	(7.67±.47)	(1910±166)	(7.78±.70)	(310±35)
2.1	^{12}C	$^{20\varepsilon}Pb$	(5.79±.29)	(2125±176)	(7.35±.34)	(5887±476)	(7.91±.37)	(4835±396)	(8.87±.44)	(2270±189)	(9.99±.73)	(373±37)
1.8	^{40}Ar	$^{20\varepsilon}Pb$	(5.21±.61)	(4387±527)	(8.73±.75)	(11696±1040)	(9.51±.82)	(8040±721)	(12.06±1.05)	(3752±339)	(13.89±1.48)	(846±93)

reported for 1.8 GeV/n $^{40}Ar + Pb_3O_4$, ($\cong$ 5.6 per event), tends to support this conclusion, since in this instance the trigger used was much more restrictive ($b \leq 4.5$ fm in an ideal geometric picture), and the implied rate of $\pi^{\pm}$ production ($\cong$ 11.2 per event) much closer to that listed in Table XV, being only slightly greater than the Cut Ø rate measured in the current study, and approximately equal to the corresponding Cut II rate of $\pi^{\pm}$ production, (12.06 ± 1.05).

A second observation afforded by the data presented in Table XV, also noted in the π° production data presented in the previous sections, is that as the charged particle multiplicity increases, and the collision becomes more central, the rate of $\pi^{\pm}$ production increases substantially. Furthermore, this effect becomes more pronounced as the beam energy and/or projectile mass are raised, being only slightly evident for 1.05 GeV/n $^{12}C + ^{208}Pb$ ($2.03 \pm .21 \rightarrow 4.29 \pm .55$), somewhat more apparent for 2.1 GeV/n $^{12}C + ^{208}Pb$ ($5.79 \pm .29 \rightarrow 9.99 \pm .73$), and quite dramatic for 1.8 GeV/n $^{40}Ar + ^{208}Pb$ ($5.21 \pm .61 \rightarrow 13.89 \pm 1.48$). Both these trends were also apparent in the π° production measurements made with the NaI and lead-glass systems, and it would therefore appear they are real and important. Once again, however, the origin of this behavior is not entirely clear. It is possible, for example, that as the impact parameter of the collision decreases the average number of nucleon-nucleon collisions increases. Furthermore, since the nucleon-nucleon scattering cross section in this energy range is thought to decrease slowly with increasing beam energy, it may also be true that as the bombarding energy is raised, the impact parameter of the collision becomes increasingly crucial in determining the

number of nucleon-nucleon collisions which occur, and the resultant rate of pion production which is observed. It is also possible that, since the "explosiveness" of the collision is thought to increase as the impact parameter decreases, the "survival rate" for pions which are produced increases as well.

Using the $\pi^{\pm}$ production measurements presented in Table XV, the ratio of the average number of charged pions produced per central collision to the corresponding average total number of charged fragments produced per central collision was calculated for each reaction and multiplicity cut under study. The results are presented in Table XVI as a function of beam energy and projectile mass. The errors shown reflect the error due to counting statistics. Upon inspection of these data, two interesting observations can be made.

The first is that the ratio reported in Table XVI for 2.1 GeV/n ^{12}C + ^{208}Pb (Cut Ø), (.22±.02), is close to that implied by the π^- ratio measured by Fung et al.[3] for 2.1 GeV/n ^{12}C + Pb_3O_4 ($\langle N_{\pi^-}\rangle/\langle N_{charge}\rangle$ = .101±.006), if in fact the rate of π^+ production is approximately equal to that for negative pions. Consequently, it would appear the results of the present study compare favorably with those of the latter, although the agreement is not as good for 1.8 GeV/n ^{40}Ar + ^{208}Pb. In this instance, the ratio reported in Table XVI (.15±.02), is somewhat lower than that expected (≅ .208±.004 for 1.8 GeV/n ^{40}Ar + Pb_3O_4), though not perhaps exceptionally so in view of the large number of secondary charges undoubtedly produced which were not associated with the primary interaction, and which could not be isolated in the current study.

Table XVI: $\langle N_{\pi^{\pm}} \rangle / \langle N_{chg} \rangle$; The Ratio of the Average Number of Charged Pions Produced per Event to the Average Total Number of Charged Fragments Produced per Event

Beam Energy (GeV/n)	Projectile Ion	Target Nucleus	Cut IV $\langle N_{\pi^{\pm}} \rangle / \langle N_{chg} \rangle$	Cut Ø $\langle N_{\pi^{\pm}} \rangle / \langle N_{chg} \rangle$	Cut I $\langle N_{\pi^{\pm}} \rangle / \langle N_{chg} \rangle$	Cut II $\langle N_{\pi^{\pm}} \rangle / \langle N_{chg} \rangle$	Cut III $\langle N_{\pi^{\pm}} \rangle / \langle N_{chg} \rangle$
1.05	^{12}C	^{208}Pb	(.11±.02)	(.11±.01)	(.11±.01)	(.10±.01)	(.11±.02)
1.3	^{12}C	^{208}Pb	(.15±.02)	(.14±.02)	(.14±.01)	(.13±.02)	(.09±.03)
1.5	^{12}C	^{208}Pb	(.16±.02)	(.17±.02)	(.16±.02)	(.16±.02)	(.16±.02)
1.7	^{12}C	^{208}Pb	(.20±.02)	(.19±.02)	(.18±.02)	(.18±.02)	(.16±.02)
1.9	^{12}C	^{208}Pb	(.21±.02)	(.20±.02)	(.19±.02)	(.18±.02)	(.15±.02)
2.1	^{12}C	^{208}Pb	(.22±.02)	(.22±.02)	(.21±.02)	(.20±.02)	(.18±.02)
1.8	^{40}Ar	^{208}Pb	(.11±.02)	(.15±.02)	(.15±.02)	(.14±.02)	(.13±.02)

Perhaps the most interesting observation, however, is that, within statistics, the ratio of the number of charged pions produced per central collision to the total number of charged fragments produced per central collision depends almost entirely on the beam energy of the reaction, showing little, if any, relation to the associated charged particle multiplicity. This result suggests that beam energy is by far the most important factor in determining the number of pions produced per nucleon, and that perhaps the increased number of pions observed in high multiplicity, low impact parameter collisions is due primarily to an increase in the number of nucleon-nucleon collisions.

Finally, using the $\pi^{\pm}$ production measurements made with the lucite Cerenkov telescope system, and the π° production rates derived from the lead-glass Cerenkov detectors (Table VI), the ratio of the average number of charged pions to the average number of neutral pions produced per central collision, $\langle N_{\pi^{\pm}} \rangle / \langle N_{\pi^{\circ}} \rangle$, was examined as a function of beam energy, projectile mass, and charged particle multiplicity. The results are presented in Table XVII, the errors shown being due to counting statistics. What is noted from these data is that for the $^{12}C + ^{208}Pb$ reaction the ratio of charged pions to neutral pions produced per central collision is $\cong$ 2.4-2.7, and appears to be approximately constant, independent of both the energy of the collision and the associated charged particle multiplicity. Projectile mass does appear to influence the relative charge state abundance, however, the corresponding ratio for 1.8 GeV/n $^{40}Ar + ^{208}Pb$ being substantially lower ($\cong$ 1.65) than that noted for $^{12}C + ^{208}Pb$.

If one assumes that individual projectile nucleon-target nucleon

Table XVII: $\langle N_{\pi^\pm}\rangle/\langle N_{\pi^\circ}\rangle$; The Ratio of the Average Number of Charged Pions Produced per Event to the Average Number of Neutral Pions Produced per Event

Beam Energy (GeV/n)	Projectile Ion	Target Nucleus	Cut IV $\langle N_{\pi^\pm}\rangle/\langle N_{\pi^\circ}\rangle$	Cut Ø $\langle N_{\pi^\pm}\rangle/\langle N_{\pi^\circ}\rangle$	Cut I $\langle N_{\pi^\pm}\rangle/\langle N_{\pi^\circ}\rangle$	Cut II $\langle N_{\pi^\pm}\rangle/\langle N_{\pi^\circ}\rangle$	Cut III $\langle N_{\pi^\pm}\rangle/\langle N_{\pi^\circ}\rangle$
1.05	^{12}C	^{208}Pb	$(2.28^{\pm}.27)$	$(2.56^{\pm}.22)$	$(2.61^{\pm}.24)$	$(2.69^{\pm}.25)$	$(4.29^{\pm}.70)$
1.3	^{12}C	^{208}Pb	$(2.40^{\pm}.26)$	$(2.60^{\pm}.23)$	$(2.62^{\pm}.23)$	$(2.84^{\pm}.28)$	$(2.14^{\pm}.68)$
1.5	^{12}C	^{208}Pb	$(2.49^{\pm}.21)$	$(2.99^{\pm}.22)$	$(2.97^{\pm}.22)$	$(3.15^{\pm}.24)$	$(3.34^{\pm}.35)$
1.7	^{12}C	^{208}Pb	$(2.48^{\pm}.20)$	$(2.69^{\pm}.19)$	$(2.67^{\pm}.19)$	$(2.83^{\pm}.21)$	$(2.88^{\pm}.31)$
1.9	^{12}C	^{208}Pb	$(2.45^{\pm}.19)$	$(2.52^{\pm}.18)$	$(2.55^{\pm}.19)$	$(2.56^{\pm}.19)$	$(2.29^{\pm}.25)$
2.1	^{12}C	^{208}Pb	$(2.35^{\pm}.17)$	$(2.52^{\pm}.17)$	$(2.52^{\pm}.17)$	$(2.51^{\pm}.18)$	$(2.67^{\pm}.26)$
1.8	^{40}Ar	^{208}Pb	$(1.21^{\pm}.15)$	$(1.63^{\pm}.16)$	$(1.62^{\pm}.16)$	$(1.68^{\pm}.17)$	$(1.69^{\pm}.21)$

collisions are the dominant means by which pion production procedes, and that the first such collision is by far the most efficient in this regard, then, noting that the pp, pn, and nn collision cross sections are approximately equal in the energy range of interest, the relative abundance of the three pion charge states can be estimated if the relative probability of producing a given charge state in a particular type of nucleon-nucleon collision is known. These probabilities have been estimated in Table XVIII, using symmetry arguments and interpolation for 2 GeV nucleon-nucleon collision data.[10] Assuming they are approximately constant from 1.05 to 2.1 GeV/n, and noting as well that for the ^{12}C + ^{208}Pb target-projectile combination the relative probability of pp, nn, and pn collisions indicated by a straightforward charge to mass ratio argument is $\cong$ .20:.30:.5, the estimated $\pi^+:\pi^\circ:\pi^-$ production ratio is $\cong$ .33:.28:.29. Consequently, for a ^{12}C projectile incident upon a target of ^{208}Pb, one would expect the ratio of the number of charged pions to the number of neutral pions produced per central collision to be $\langle N_{\pi^\pm}\rangle/\langle N_{\pi^\circ}\rangle \cong 2.6$. A similar analysis for the ^{40}Ar + ^{208}Pb target-projectile system yields a $\pi^+:\pi^\circ:\pi^-$ charge state ratio of $\cong$ .32:.28:.40, which once again results in an estimated charged pion to neutral pion production ratio of $\cong$ 2.6.

Having determined that one might expect the ratio $\langle N_{\pi^\pm}\rangle/\langle N_{\pi^\circ}\rangle$ to be approximately 2.6 for ^{12}C + ^{208}Pb, it is interesting to note that the ratio measured experimentally does indeed lie in this range. This result could be an indication that for ^{12}C + ^{208}Pb, individual target nucleon-projectile nucleon collisions occurring in the fast primary stages of the reaction dominate the observed production of charged and neutral

TABLE XVIII: The Probability for a Given Type of Nucleon-Nucleon Collision of Producing a Particular Pion Charge State

Type of Nucleon-Nucleon Collision	Approximate Probability of Producing a π^+ Meson	Approximate Probability of Producing a π° Meson	Approximate Probability of Producing a π^- Meson
pp	2/3	2/9	1/9
nn	1/9	2/9	2/3
pn	1/3	1/3	1/3

pions, though to be sure of this conclusion, a more sophisticated estimate of the $\langle N_{\pi^\pm}\rangle/\langle N_{\pi^\circ}\rangle$ ratio expected theoretically would undoubtedly be required.

It is also interesting to note that the observed ratio for $^{40}Ar + ^{208}Pb$ is substantially lower than that observed for $^{12}C + ^{208}Pb$, as well as that predicted for the $^{40}Ar + ^{208}Pb$ reaction itself. This result is due, to some degree, to a partial saturation of the upstream Cerenkov telescope system resulting from the high average charged pion multiplicity associated with the $^{40}Ar + ^{208}Pb$ reaction. However, since the estimated Cut Ø and Cut I charged pion production rates for $^{40}Ar + ^{208}Pb$ are only 15-20% higher than the corresponding rates for 2.1 GeV/n $^{12}C + ^{208}Pb$, the reduced $\langle N_{\pi^\pm}\rangle/\langle N_{\pi^\circ}\rangle$ ratio observed for the former reaction is not thought to result primarily from counter saturation. Even, for example, if the results of a similar streamer chamber experiment[3] are used ($\langle N_{\pi^-}\rangle \cong 5.6$) to estimate the rate of charged pion production, the $\langle N_{\pi^\pm}\rangle/\langle N_{\pi^\circ}\rangle$ ratio which results ($\cong$ 1.7-1.9) is still substantially lower than that predicted. Consequently one is led to consider the possibility that the reduced ratio for $^{40}Ar + ^{208}Pb$ is real and important, and an indication perhaps that in this instance the collision dynamics are fundamentally different than those for $^{12}C + ^{208}Pb$. Once again, however, to be sure of this conclusion would require further experimentation with an improved detector system.

For completeness, the two particle azimuthal angle correlation function,

$$\left(\frac{d^2\sigma}{d\phi_1 d\phi_2} \Big/ \left(\frac{d\sigma}{d\phi_1}\right)\left(\frac{d\sigma}{d\phi_2}\right)\right) \qquad (30)$$

measured for energetic charged pions and intermediate energy protons is

plotted in Fig. 24(a-g) and Fig. 25(a-c), respectively.

It will be recalled from previous work that, for each central collision trigger, cuts were taken on pulse height in the dE/dx counter system, so that a given scintillator could only register the passage of a charged particle if its energy was in a specified range. By cutting on very small pulse heights, (pions $\gtrsim$ 140 MeV, protons $\gtrsim$ 900 MeV), it was assumed the charges selected would be primarily energetic pions. A further classification was made as to the number of scintillators registering a count in a given event. Events of the same useful "multiplicity" were then examined for azimuthal correlations. For example, to investigate the correlation behavior between energetic pions, events in which two fast charges were observed were studied by plotting the relative angle ($\leq 180^{o}$) between them, to see if any angular region might be favored. Since this procedure becomes much more complicated when more than two charged particles are observed, only events with a useful multiplicity of 2 were selected for study. This technique was used to study two-particle azimuthal correlations for pions ($E \gtrsim 140$ MeV), and intermediate energy protons (200 MeV $\lesssim E \lesssim$ 600 MeV).

It is pointed out that information from the Cerenkov telescope arrays could not be used in this instance, since the azimuthal angle subtended by a given Cerenkov telescope was much larger than that subtended by a dE/dx scintillator strip. Consequently, use of the Cerenkov information would bias the measurement of the relative angle between fast charges towards small azimuthal angles, since, for example, adjacent scintillators subtending the same angular region as a single Cerenkov telescope might both register a pion, even if only one had actually been present.

Fig 24. The two-particle azimuthal correlation function

$$\left(\frac{d^2\sigma}{d\phi_1 d\phi_2} \Big/ \left(\frac{d\sigma}{d\phi_1}\right)\left(\frac{d\sigma}{d\phi_2}\right)\right)$$

measured for pairs of energetic charged particles observed for a) 1.05 GeV/n $^{12}C + ^{208}Pb$, b) 1.3 GeV/n $^{12}C + ^{208}Pb$, c) 1.5 GeV/n $^{12}C + ^{208}Pb$, d) 1.7 GeV/n $^{12}C + ^{208}Pb$, e) 1.9 GeV/n $^{12}C + ^{208}Pb$, f) 2.1 GeV/n $^{12}C + ^{208}Pb$, g) 1.8 GeV/n $^{40}Ar + ^{208}Pb$, plotted as a function of the relative azimuthal angle between the two charged particles of a pair.

h) The first $(d^2\sigma/d\phi_1 d\phi_2)/(d\sigma/d\phi_1)(d\sigma/d\phi_2)$ data point measured for each $^{12}C + ^{208}Pb$ reaction, plotted as a function of beam energy.

i) The first $(d^2\sigma/d\phi_1 d\phi_2)/(d\sigma/d\phi_1)(d\sigma/d\phi_2)$ data point measured for 1.8 GeV/n $^{40}Ar + ^{208}Pb$.

Fig 25. The two-particle azimuthal correlation function

$$\left(\frac{d^2\sigma}{d\phi_1 d\phi_2} \Big/ \left(\frac{d\sigma}{d\phi_1}\right)\left(\frac{d\sigma}{d\phi_2}\right)\right)$$

measured for pairs of intermediate energy charged particles for a) .4 GeV/n $^{12}C + ^{208}Pb$, b) 1.05 GeV/n $^{12}C + ^{208}Pb$, c) 2.1 GeV/n $^{12}C + ^{208}Pb$, plotted as a function of the relative azimuthal angle between the two charged particles of a pair.

Fig. 24

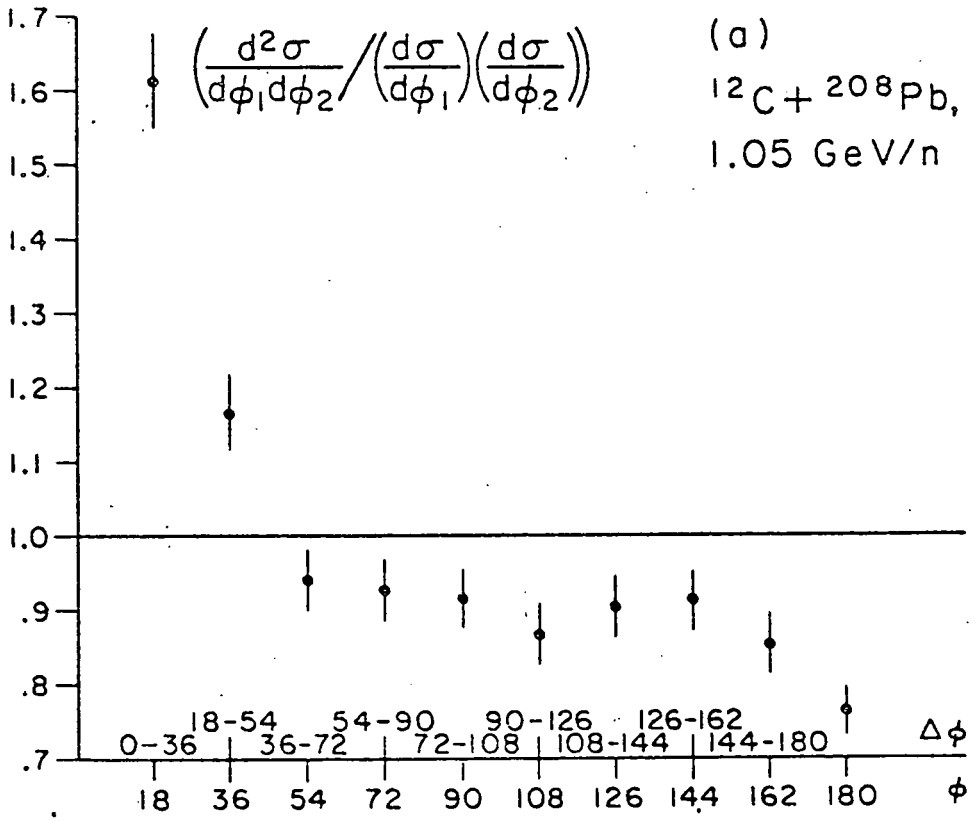
$\left(\frac{d^2\sigma}{d\phi_1 d\phi_2}\Big/\left(\frac{d\sigma}{d\phi_1}\right)\left(\frac{d\sigma}{d\phi_2}\right)\right)$
(a)
$^{12}C + ^{208}Pb$,
1.05 GeV/n
1.7
1.6
1.5
1.4
1.3
1.2
1.1
1.0
.9
.8
.7
0-36
18-54
36-72
54-90
72-108
90-126
108-144
126-162
144-180
Δφ
18 36 54 72 90 108 126 144 162 180
φ

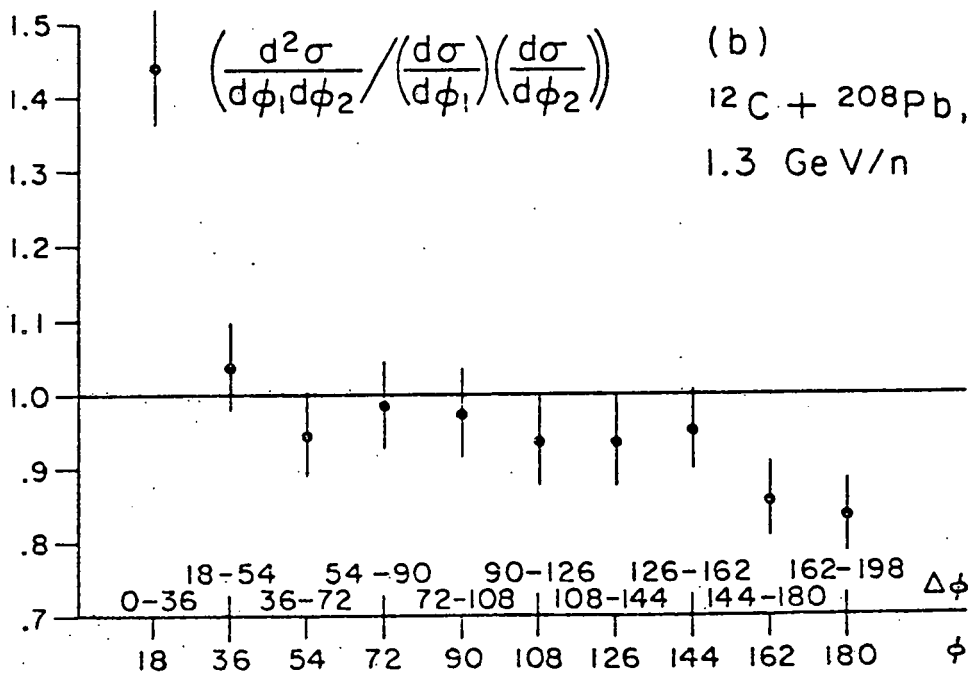
$\left(\frac{d^2\sigma}{d\phi_1 d\phi_2}\Big/\left(\frac{d\sigma}{d\phi_1}\right)\left(\frac{d\sigma}{d\phi_2}\right)\right)$
(b)
$^{12}C + ^{208}Pb$,
1.3 GeV/n
1.5
1.4
1.3
1.2
1.1
1.0
.9
.8
.7
0-36
18-54
36-72
54-90
72-108
90-126
108-144
126-162
144-180
162-198
Δφ
18 36 54 72 90 108 126 144 162 180
φ

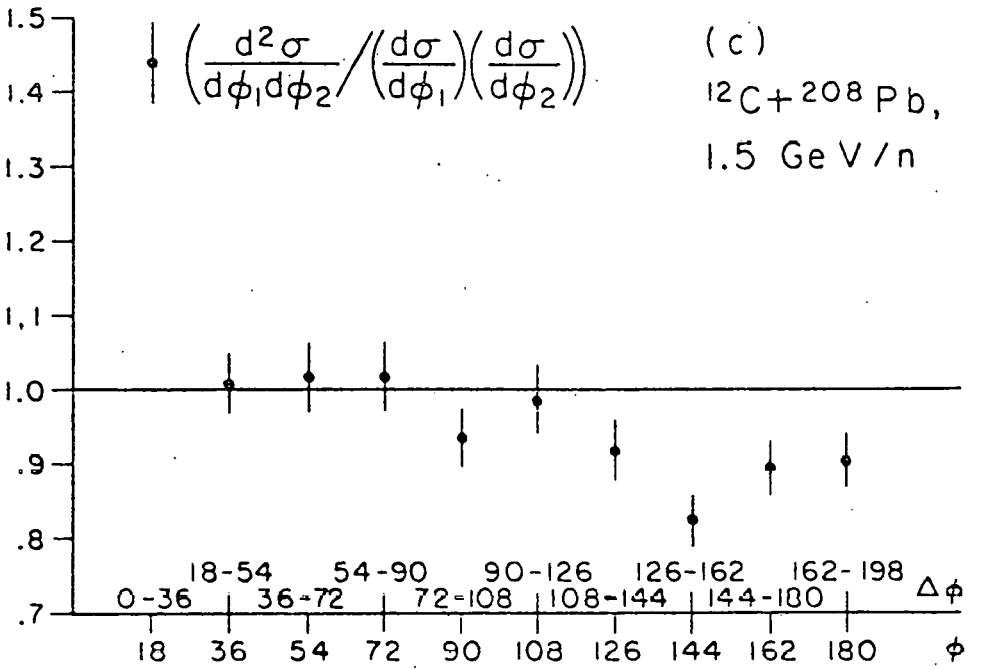
$\left(\frac{d^2\sigma}{d\phi_1 d\phi_2}\Big/\left(\frac{d\sigma}{d\phi_1}\right)\left(\frac{d\sigma}{d\phi_2}\right)\right)$
(c)
$^{12}C + ^{208}Pb$,
1.5 GeV/n
1.5
1.4
1.3
1.2
1.1
1.0
.9
.8
.7
18-54
54-90
90-126
126-162
162-198
0-36
36-72
72-108
108-144
144-180
Δφ
18 36 54 72 90 108 126 144 162 180
φ

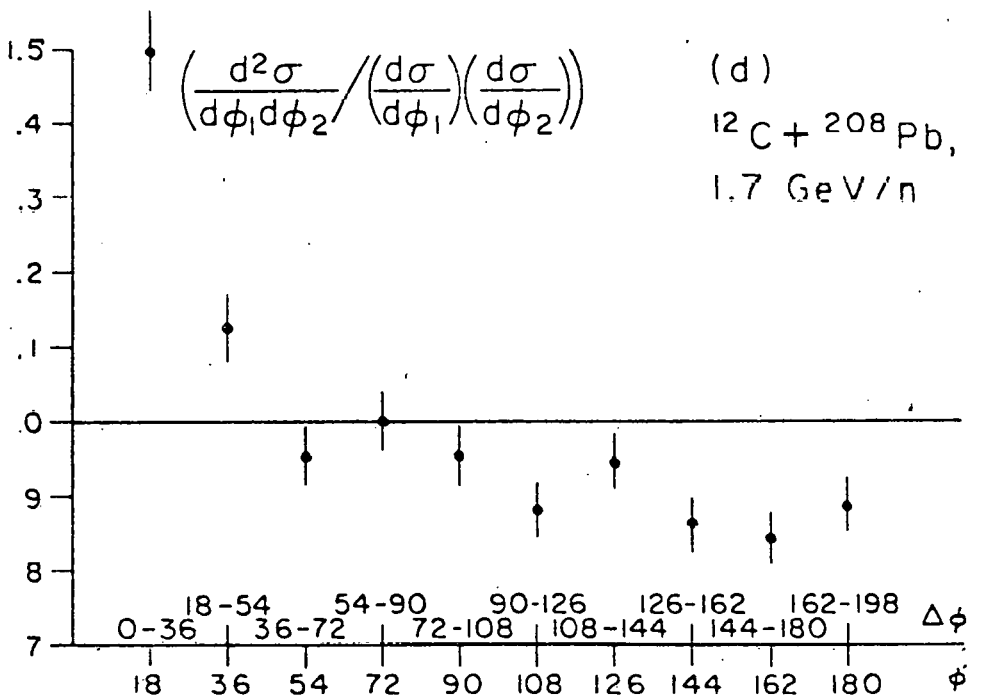
$\left(\frac{d^2\sigma}{d\phi_1 d\phi_2}\Big/\left(\frac{d\sigma}{d\phi_1}\right)\left(\frac{d\sigma}{d\phi_2}\right)\right)$
(d)
$^{12}C + ^{208}Pb$,
1.7 GeV/n
1.5
.4
.3
.2
.1
0
9
8
7
18-54
54-90
90-126
126-162
162-198
0-36
36-72
72-108
108-144
144-180
Δφ
18 36 54 72 90 108 126 144 162 180
φ

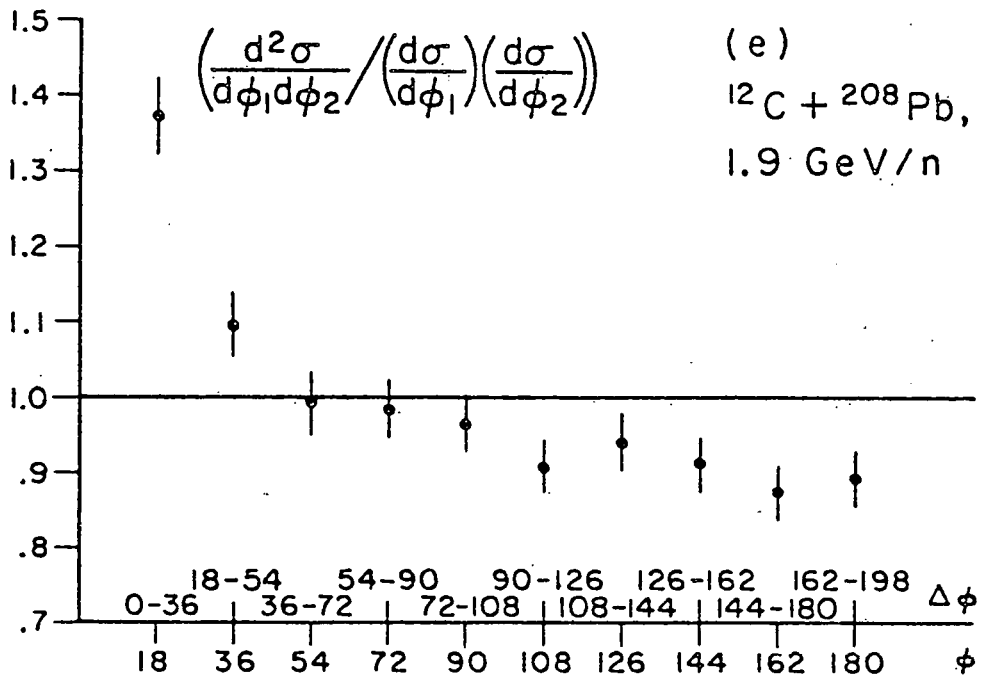
$\left(\frac{d^2\sigma}{d\phi_1 d\phi_2}\Big/\left(\frac{d\sigma}{d\phi_1}\right)\left(\frac{d\sigma}{d\phi_2}\right)\right)$
(e)
$^{12}C + ^{208}Pb$,
1.9 GeV/n
1.5
1.4
1.3
1.2
1.1
1.0
.9
.8
.7
0-36
18-54
36-72
54-90
72-108
90-126
108-144
126-162
144-180
162-198
Δφ
18 36 54 72 90 108 126 144 162 180
φ

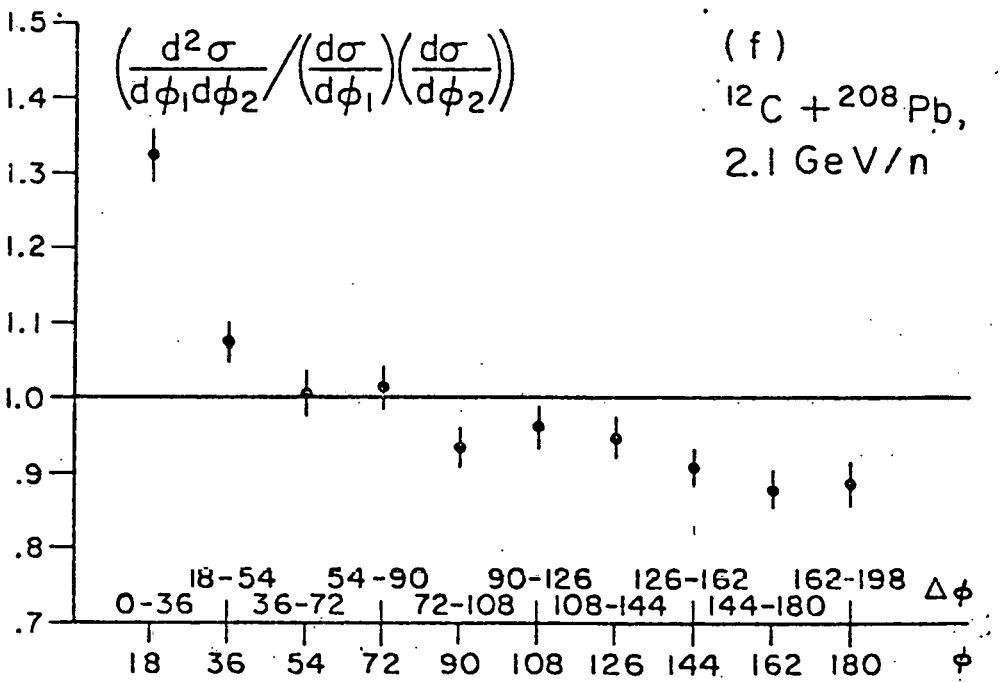
$\left(\frac{d^2\sigma}{d\phi_1 d\phi_2}\Big/\left(\frac{d\sigma}{d\phi_1}\right)\left(\frac{d\sigma}{d\phi_2}\right)\right)$
(f)
$^{12}C + ^{208}Pb$,
2.1 GeV/n
1.5
1.4
1.3
1.2
1.1
1.0
.9
.8
.7
0-36
18-54
36-72
54-90
72-108
90-126
108-144
126-162
144-180
162-198
Δφ
18 36 54 72 90 108 126 144 162 180
φ

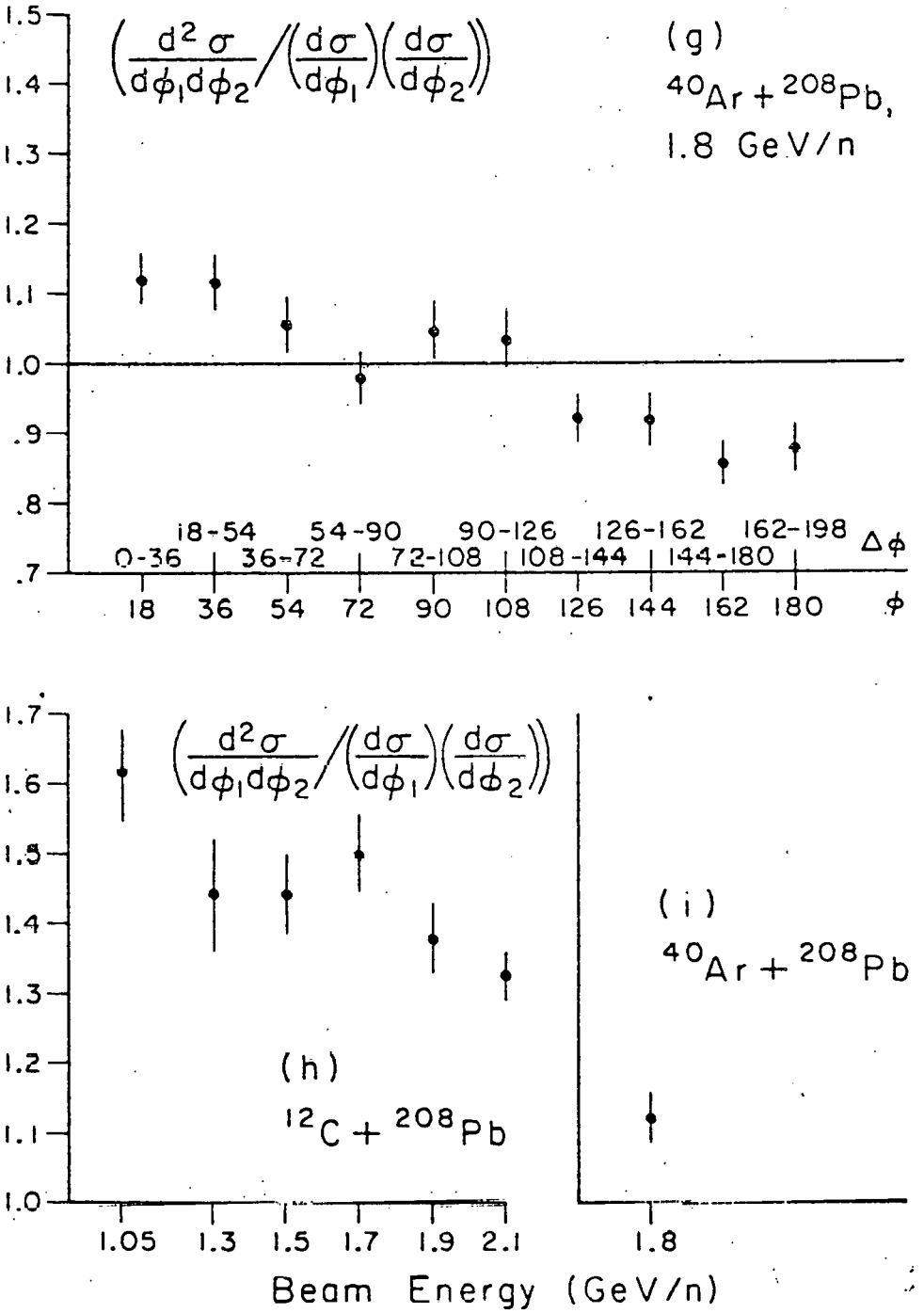
$\left(\frac{d^2\sigma}{d\phi_1 d\phi_2}\Big/\left(\frac{d\sigma}{d\phi_1}\right)\left(\frac{d\sigma}{d\phi_2}\right)\right)$
(g)
$^{40}Ar + ^{208}Pb$,
1.8 GeV/n
1.5
1.4
1.3
1.2
1.1
1.0
.9
.8
.7
18-54
54-90
90-126
126-162
162-198
0-36
36-72
72-108
108-144
144-180
Δφ
18 36 54 72 90 108 126 144 162 180
φ
$\left(\frac{d^2\sigma}{d\phi_1 d\phi_2}\Big/\left(\frac{d\sigma}{d\phi_1}\right)\left(\frac{d\sigma}{d\phi_2}\right)\right)$
(h)
$^{12}C + ^{208}Pb$
(i)
$^{40}Ar + ^{208}Pb$
1.7
1.6
1.5
1.4
1.3
1.2
1.1
1.0
1.05 1.3 1.5 1.7 1.9 2.1
1.8
Beam Energy (GeV/n)

Fig. 25

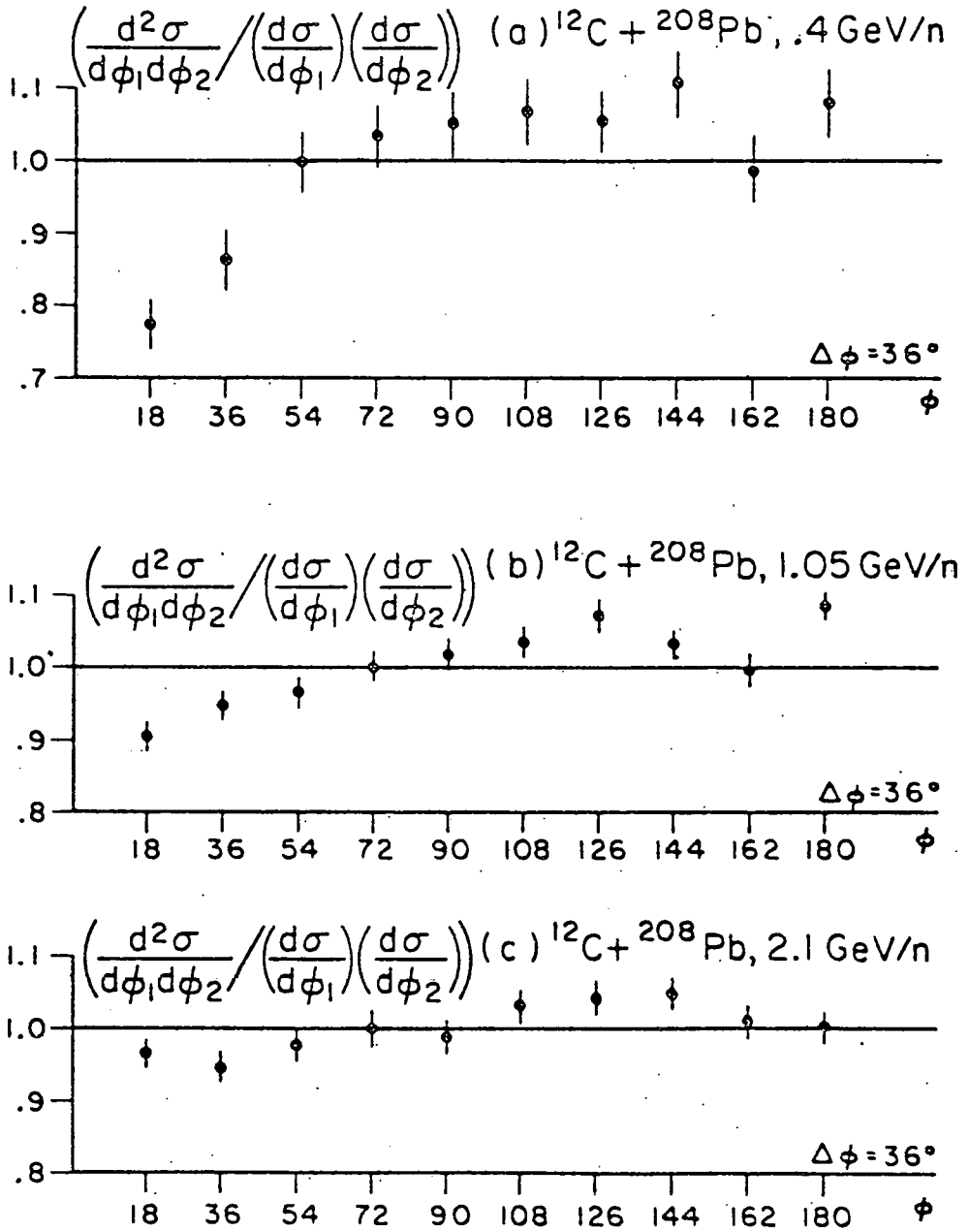
$\left(\frac{d^2\sigma}{d\phi_1 d\phi_2}\Big/\left(\frac{d\sigma}{d\phi_1}\right)\left(\frac{d\sigma}{d\phi_2}\right)\right)$
(a) $^{12}C + ^{208}Pb$, .4 GeV/n
(b) $^{12}C + ^{208}Pb$, 1.05 GeV/n
(c) $^{12}C + ^{208}Pb$, 2.1 GeV/n
1.1
1.0
.9
.8
.7
$\Delta\phi = 36°$
18 36 54 72 90 108 126 144 162 180
ϕ

It is also noted that particle identification was not possible in the present experiment and, as a result, pairs of like sign pions could not be distinguished from those of opposite charge. Consequently, any conclusions drawn from these data are subject to the presence of a residual background of $\pi^+\pi^-$ pairs, even though there is recent evidence[11] which suggests that pions of opposite sign are truly uncorrelated and would not obviate the observed correlation behavior.

The positive correlation evident in Fig. 24(a-g) for pairs of energetic charged particles of small relative azimuth is interpreted to be a consequence of the positive Bose correlation expected for like sign pairs of charged pi mesons. It is apparently quite narrow, the correlation function expressed above being substantially greater than unity only for the first data point of each graph, or relative angles of $\Delta\phi \leq 36^{o}$.

The main source of background to the measured correlation behavior presented in Fig. 24(a-g) was judged to be knock-on electrons, a given knock-on electron producing a false count when it passed through one scintillator, and the fast charge which "produced" the electron passed through that adjacent to it. The magnitude of the background due to this source of error was estimated to range from $\cong$ 11% of the first data point value for 1.05 GeV/n ^{12}C + ^{208}Pb, to $\cong$ 25% of the corresponding rate for 2.1 GeV/n ^{12}C + ^{208}Pb. The estimated background for 1.8 GeV/n ^{40}Ar + ^{208}Pb was $\cong$ 22% of the first data point value.

These estimates were prepared by taking the known geometry of the dE/dx counter system into account, and assuming that the spectra of pions passing through it were characterized by an exponential decay of $\cong$ $(70\ MeV)^{-1}$.

However, due to uncertainty, for example, in the minimum effective electron energy corresponding to the minimum production angle required to effectuate the side by side scintillator signature ($\cos^2\theta = T_e/T_{max}$) the precise magnitude of the background due to knock-on electrons could not be calculated. Consequently, since it was not possible to isolate knock-on electrons directly, no correction has been applied to the data of Fig. 24(a-g), even though the background estimates presented above are thought to be approximately correct. Were this not the case and the background due to knock-on electrons substantially greater than that estimated, the observed small angle correlation would be expected to increase with increasing beam energy, the level of background due to this source of error being greater for the higher energy reactions.

The conversion of gamma rays within the target was estimated not to contribute any substantial background in this instance, due to the kinematics of pair production, the π° momentum distribution thought to be effective, and the fact that for any shower which had progressed even marginally beyond the initial stages of development, the pulse height observed in the dE/dx scintillators would not be correct. Consequently, no correction was made to account for gamma ray conversion. Once again, were this judgement in error and the background due to gamma ray conversion substantial, the positive small angle correlation evident in Fig. 24(a-g) would be expected to increase with increasing beam energy.

The significance of the positive small angle correlation observed for pairs of energetic charged particles is difficult to ascertain due to the limited angular resolution of the dE/dx counter system ($\Delta\phi_{min} \cong 36^o$),

and the large region of polar angle over which it integrated ($\theta \cong 32^{o}$-161^{o}). Furthermore, Gyulassy has recently suggested[12] that any correlation of this nature is ambiguous, unless the complete final state configuration can be observed and dynamic correlations eliminated. Consequently, in view of these facts and the observation that more precise correlation data for 1.8 GeV/n ^{40}Ar + ^{208}Pb already exist,[13] no attempt was made to analyze these data further. The main significance of these results in the context of the present experiment would therefore appear to be that, under the appropriate constraints, the experimental apparatus is indeed capable of separating protons and pions, lending support to the validity of the spectral data presented.[14]

One behavior which was thought to be of interest was that, with increasing beam energy or projectile mass, the observed correlation for energetic charged particles of small relative azimuth was substantially reduced (Fig. 24(h-i)). This observation would tend to indicate that either some level of coherent pion production had become apparent, or the size of the pion emitting source had become larger and the strength of the correlation expected for like sign pairs correspondingly weaker. It was found, however, by Monte Carlo technique, that the increase in the average proton and pion multiplicities observed as a function of beam energy and projectile mass in the present experiment are more than sufficient to obviate this result, the observed correlation expected to decrease approximately with the square root of the charged particle multiplicity due to the increase probability of observing an uncorrelated pair, and decrease faster yet due to the increased influence of coincidence summing.

The two-particle azimuthal correlation function measured for

intermediate energy charged particles is presented in Fig. 25(a-c).

The data presented in Fig. 25(a-c) are thought to result primarily from pairs of protons, since the energy threshold required to enter the dE/dx counter system largely precluded the observation of heavy charged particles, statistical fission fragments, etc. The only appreciable source of background in this instance was considered to be intermediate energy pions, which should in any event have contributed $\lesssim$ 20% of the data sample examined, judging by the $\pi^{\pm}$ production measurements presented earlier. Unfortunately, however, although the background due to charged pions may not be entirely negligible, particle identification was not possible in the present experiment and, since this source of error could not be isolated directly, no correction to account for it has been applied to the data presented.

One observation which is immediately apparent upon inspection of these results is that, having made a different cut in the range of pulse heights accepted by the dE/dx counter system, the observed correlation behavior changes dramatically from the enhanced probability noted previously for pion pairs of small relative azimuth to the negative anticorrelation observed in Fig. 25(a-c) for the same angular region. It is concluded from this observation that the correlation behavior measured in the present experiment is real and important, and not merely an artifact of the detector system. It is also noted, however, that the nature of the curves shown in Fig. 25 is not entirely understood.

When these data were first obtained, it was thought before normalization that the correlation observed for .4 GeV/n ^{12}C + ^{208}Pb, for example,

represented the sharp nucleon knockout correlation predicted by Koonin[15] at $\phi = \pi$, broadened perhaps by nuclear shadowing, or the large kinematic region integrated over by the dE/dx counter system. However, upon completion of the normalization, it was determined that although there is a slow broad rise for large relative azimuthal angles, the primary feature of the data is an anticorrelation for small relative ϕ.

This behavior is not completely understood. While pairs of protons should be anticorrelated at small relative momenta due to fermi statistics, and this observation has, in fact, been reported[16,17] for relativistic heavy ion collisions, the anticorrelation expected would be smaller and narrower than observed in the present experiment, especially in view of the limited resolution of the measuring apparatus. Furthermore, if the dE/dx counter system were indeed sensitive enough to measure the proton anti-correlation due to fermi statistics, one would also expect to observe a strong positive correlation at intermediate relative azimuth due to the effects of positive nucleon-nucleon interactions. Since this is not the case, one is led to consider the possibility that the observed behavior is due to a mechanism not considered, or a combination of complicated processes, making the correct interpretation of these results difficult to ascertain. The one trend apparent in the data of Fig. 25(a-c) which is thought to be understood is that the decreased magnitude of the correlation observed for 1.05 and 2.1 GeV/n $^{12}C + {}^{208}Pb$ results from the increased charged particle multiplicity characterizing those interactions.

Consequently, the significance of the azimuthal correlation behavior observed for pairs of intermediate energy charged particles is unclear.

Since the complete final state configuration cannot be observed, it is possible, for example, that collision dynamics play an important role in determining the correlation behavior which will be observed. Alternatively, the correlation shown in Fig. 25(a-c) may be real, but badly distorted due to trigger criteria, limited detector resolution, or the large region of polar angle subtended by the dE/dx counter system. Unfortunately, however, although conjecture as to the nature of the observed correlation is possible, it is impossible to proffer a decisive interpretation of these data without further experimentation with an improved detector system.

It is concluded from these analyses that, for $^{12}C + ^{208}Pb$, the rates of both $\pi^{\pm}$ and π° production increase smoothly as a function of increasing beam energy, showing no signs of either extraordinary pion production or unusual production thresholds within the estimated error of the data. Furthermore, the $\pi^{\pm}, \pi^{\circ}$ production data derived from the present experiment appear in general to compare favorably with those of previous work in this field. The rate, per event, of charged and neutral pion production increases substantially for high multiplicity, low impact parameter collisions, although the corresponding rate, for example, of charged pions produced per charged fragment does not. This suggests that the increased pion production observed for collisions characterized by high charged particle multiplicities is due primarily to an increase in the number of nucleon-nucleon collisions and not to any fundamental change in the production mechanism. That the increase observed for high multiplicity events becomes more dramatic with increasing beam energy may be due to the fact that in this energy range the nucleon-nucleon scattering

cross section decreases slowly with increasing energy, and as a consequence the impact parameter of the collision may become much more crucial in determining the number of nucleon-nucleon collisions which occur. Although in general the average energy of the characteristic pion spectra, for example, does appear to decrease for high multiplicity events, there is no primary evidence to suggest that, for a given projectile, these events are more equilibrated in any thermodynamic sense, and the observation noted above would appear simply to indicate increased energy sharing among the hadronic participants of the collision. Consequently, overall these preliminary results appear to be consistent with a cascade process such as that described by Cugnon.[18] The only observation which is not in obvious agreement with the above conclusion is that the observed ratio $\langle N_{\pi^{\pm}} \rangle / \langle N_{\pi^{o}} \rangle$ for $^{40}Ar + ^{208}Pb$ appears to be substantially lower than that for $^{12}C + ^{208}Pb$ ($\cong$ 1.7 vs. 2.6), indicating that perhaps the means of pion production for the former reaction is fundamentally different from that for the latter. However, to be sure of this conclusion would require further experimentation with an improved detector system.

There appears to be a large number of low energy gamma rays ($\cong$ 50/event for 2.1 GeV/n $^{12}C + ^{208}Pb$ having energies .7 MeV $\lesssim E \lesssim$ 7 MeV) associated with the collision of two relativistic heavy ions. However, despite a secondary dependence on charged particle multiplicity, the observed gamma ray yield appears to be largely independent of beam energy as well as other details of the collision. Therefore, it might be concluded that either the fragmentation of the target is limited in the energy range of interest, or the gamma rays observed are produced in a fast initial stage of the

reaction by a mechanism for which subsequent details of the collision are of no consequence. Nucleon-nucleon bremsstrahlung, however, is not thought to account for the entire gamma ray yield, since the production rate for $^{40}Ar + ^{208}Pb$ is not large enough compared to that for $^{12}C + ^{208}Pb$ to justify that conclusion. Consequently, the primary gamma ray production mechanism remains unidentified, in this instance, and because of the large particle backgrounds generally present in relativistic heavy ion collisions, a large solid angle, multiple element counter experiment will probably be necessary before substantial progress can be made in this area.

REFERENCES:

1. J. Gosset, H. H. Gutbrod, W. G. Meyer, A. M. Poskanzer, A. Sandoval, R. Stock, G. D. Westfall, Phys. Rev. C16, 629 (1977).

2. S. Nagamiya, private communication.

3. S. Y. Fung, W. Gorn, G. P. Kiernan, F. F. Liu, J. J. Lu, Y. T. Oh, J. Ozawa, R. T. Poe, L. Schroeder, H. Steiner, Phys. Rev. Lett. 40, 292 (1978); A. Sandoval, R. Stock, H. E. Stelzer, R. E. Renfordt, J. W. Harris, J. P. Brannigan, J. V. Geaga, L. J. Rosenberg, L. S. Schroeder, K. L. Wolf, Phys. Rev. Lett. 45, 874 (1980); J. J. Lu, doctoral dissertation; J. J. Lu, D. Beavis, S. Y. Fung, W. Gorn, A. Huie, G. P. Kiernan, R. T. Poe, G. Vandalen, Phys. Rev. Lett. 46, 898 (1981).

4. J. Cugnon et al., Nucl. Phys. A352, 505 (1981); J. Cugnon, D. Kinet, J. Vandermeulen, to be published.

5. G. F. Bertsch, Phys. Rev. C15, 713 (1977).

6. T. Shibata, H. Ejiri, J. Chiba, S. Nagamiya, K. Nakai, R. Arnholt, H. Bowman, J. G. Ingersoll, E. A. Rauscher, J. O. Rasmussen, Nucl. Phys. A308, 513 (1978); J. B. Cumming, R. W. Stoenner, P. E. Haustein, Phys. Rev. C14, 1554 (1976).

7. L. Madansky and Y. K. Lee, "Nuclear Moments and Nuclear Structure," Annual Report DOE/ER/03274-1 (1980), unpublished.

8. W. H. Barkas and M. J. Berger, NAS-NRC Publ. no. 1133 (1964), p. 103.

9. Particle Data Group, LBL, "Review of Particle Properties," Physics Letters 75B (1978).

10. J. P. Vary, Phys. Rev. Lett. 40, 295 (1978).

11. C. Ezell, L. J. Gutay, A. T. Laasanen, F. T. Dao, P. Schübelin and F. Turkot, Phys. Rev. Lett. 38, 873 (1977).

12. M. Gyulassy and S. K. Kauffmann, Phys. Rev. Lett. 40, 298 (1978).

13. S. Y. Fung, W. Gorn, G. P. Kiernan, J. J. Lu, Y. T. Oh, and R. T. Poe, Phys. Rev. Lett. 41, 1592 (1978).

14. T. Hallman, Thesis, The Johns Hopkins University (1982), unpublished.

15. S. E. Koonin, Phys. Rev. Lett. 39, 680 (1977).

16. A. M. Poskanzer, Invited Paper for the International Conference on Nuclear Structure, Tokyo (1977).

17. F. Zarbakhsh, A. L. Sagle, F. Brochard, T. A. Mulera, V. Perez-Mendez, R. Talaga, I. Tanihata, J. B. Carroll, K. S. Ganezer, G. Igo, J. Oostens, D. Woodard and R. Sutter, Phys. Rev. Lett. 46, 1268 (1981).

18. J. Cugnon, D. Kinet, J. Vandermeulen, Nucl. Phys. A379, 553 (1982); see also reference 4 above.

CERN ALPHA-ALPHA WORK

L. Madansky

L. Madansky was a member of the R807 collaboration at CERN in which experiments were performed studying the various aspects of alpha-alpha, alpha-p and p-p collisions.

The results of the analysis, mainly carried out in collaboration with the members of the Pennsylvania group (S. Frankel et al.) have been published or are in press. They are "Very High Central Multiplicity 63 GeV-63 GeV $\alpha\alpha$ Interactions," T. Åkesson et al., Physics Letters 110B 344 (1982); "Hadronization of Excited Nucleons in Nuclear Collisions at ISR Energies," T. Åkesson et al., submitted to Nuclear Physics B; and "Multiplicity Distributions in p-Alpha and Alpha-Alpha Collisions in the CERN ISR," T. Akesson et al., submitted to Nuclear Physics. The published paper is characteristic of the results, namely, that they are understood as simple products of multiple collisions with no evidence of collective effects.

THE ANOMALON EXPERIMENT (E630: Koontz et al.)

T. Hallman and L. Madansky

An experiment to search for the radiative decay of the so-called anomalon that is produced in heavy-ion reactions was proposed by a LBL group (R. Koontz, G. Roche, L. Schroeder, H. Pugh, G. Krebs). The main point of the experiment was to detect protons, deuterons and other light elements from reactions of ^{12}C with various nuclear targets and to study the gamma rays in the region (~100 MeV) that were coincident with such particles. Any unusual states that were associated with the excited target for the projectile fragment that would decay via gamma radiation could, in principle, be an independent signature of the anomalon, which has been seen only in emulsion experiments. The Hopkins group and others (J. Carroll, T. Mulera, T. Hallman, L. Madansky) was invited to join the collaboration and set up a NaI gamma detector similar to the ones used in previous experiments that were designed to study high energy gamma production in heavy ion collisions.

The projectiles were detected with an array of solid state counters. The gamma-ray system consisted of a 1" NaI converter followed by a scintillator to detect the converted electrons, and followed by two 5" thick NaI cylinders of approximately 12" diameter. A veto counter rejected spurious events in which charged particles may have accompanied the gamma rays. The 5" detector absorbed the shower with good resolution and the split provided an additional means for rejecting neutron events which produced abnormal pulse height distributions in the two counters. The experiment was run in the late spring and the results are being analyzed at this time.

The very preliminary results indicate that the gamma-ray spectrum associated with either protons or deuterons, as determined by the charged particle telescopes, looks very much like one from pi-zero production for the most part. A detailed study is underway to establish cross sections so that, within the experimental statistics and the expected pi-zero production, some limits on radiative anomalon decay can be established. The main analysis is being carried out at LBL and some quantitative results will be available in the near future.

The Neutron and Charged Particle Emission Following μ^--capture in ^{165}Ho

E. McIntyre, T. Hallman, Y. K. Lee, R. Levin, L. Madansky, G. Mason* and B. Olaniyi*

μ^--capture in nuclei has been intensively studied in the past, and much of our insight into weak interactions came from such investigations.[1] The μ^--capture is also used as a probe of nuclear interactions through such phenomena as muonic x-rays, collective nuclear excitation, and particle emissions.[2] Recently the energetic components of both neutron and proton emission following μ^--capture in medium-heavy nuclei have become the focus of attention[3] since the origin and nature of such energetic components are not explainable on the basis of available theories of μ^--capture or nuclear de-excitation processes. It may be necessary to take a fresh look at the pionic processes in the nucleus. These may be taken into account in the weak hadronic current in order to explain energetic proton emission.[4]

Review of Experimental Situations

The surprisingly high neutron energy component was first suggested by an unpublished report,[5] in which the neutron spectra from Pb was reported to have an exponential form with a decay constant $E_0 = 12 \pm 1$ MeV up to the neutron energy of 50 MeV. Subsequently, Schröder et al.[6] reported a neutron spectrum up to 20 MeV which was in essential agreement with Krieger's result. More data were reported for lighter nuclei by Sundelin et al.[7] for neutron energies up to 50 MeV with a decay constant of 7 MeV.

---

* University of Victoria and TRIUMF, Canada

Sundelin's result for the neutron energy measurements depends on the unfolding of pulse height spectra from the scintillation counter which is at best a difficult procedure.

Energetic charged particle emission was first reported by Russian groups.[8,9] The latest measurement by Krane et al.[10] reports proton spectra between 40 and 70 MeV for several targets with the decay constant of $E_0 = 9.9 \pm 1.1$ MeV for Pb. The best theoretical effort by Singer et al.,[11] based on pre-equilibrium models using phenomenological nucleon-momentum distribution falls far short of explaining the energetic proton components. An additional puzzle is the fact that the proton spectra of Krane et al.[10] have the same slope as the high-energy neutron spectra. These experimental results indicate a capture mechanism based on many-body processes, similar to that in nuclear photo-disintegration and in π^--capture, in which high energy nucleons are emitted.

Review of Theoretical Interpretations

In order to explain the unusually energetic proton and neutron spectra, a hydrodynamic model was proposed by T. Kozlowsky et al.,[12] in which the nuclear muon capture process was studied as an excitation of the analogues of various harmonics of the multipole giant resonance, using the hydrodynamic model of the nucleus. Amado et al.[13] tried a phenomenological model in which an ad hoc "nuclear recoil function" was introduced that characterized the ability of the target nucleus to absorb the momentum. The "nuclear recoil function" was then assumed to be dominated by the minimum possible value of the momentum carried by the nuclear debris.

A comprehensive discussion of both neutron and proton spectra following μ^--capture was given by Singer[3] in which the capturing nucleus was treated as consisting of quasi-free nucleons moving in a momentum-dependent potential and having a phenomenological effective nucleon-momentum distribution. The model accounts well for the observed particle emission rates, but the calculated nuclear excitation function still lacks in strength in the high-energy tail.

A novel and parameter-free approach to μ^--capture was introduced by Bernabeu. The key point was the deep connection between axial μ^--capture and π^--capture.[4] The μ^--capture probability Γ can be written as $\Gamma \sim \vec{V}^2 + \vec{A}^2 + A_0^2$ where V_μ and A_μ are the hadronic vector and axial vector currents. In the limit $|\vec{q}| \to 0$, we have, from the PCAC hypothesis

$$q_0 A_0 \sim \langle X|\phi_\pi|N\rangle \quad \text{for the nuclear transition } N \to X,$$

ϕ_π being the pion field. Hence, the term A_0 can be obtained by the extrapolation of the S-wave pion absorption amplitude from the physical pion mass m_π to the mass m_μ. This provided a lower limit for the quantity $d\Gamma_{N\to X}/dq^2$ at $|\vec{q}| = 0$. This leads to the conclusion that about 1% of the capture event should have an energy transfer of more than 80 MeV. This conclusion means that there are strong reasons to believe correlated nucleons are emitted in μ^--capture.

Experimental Method

Difficulty with the particle detection following μ^--capture lies mainly in the low counting rate and the severe background. We try to overcome these problems by using the best slow μ^--beam with a good duty cycle,

large-volume scintillators, and by including coincident gamma rays in the trigger.

For the neutron spectra the time-of-flight method is far superior to the method of unfolding pulse height spectra.[7] The neutron counters, previously described in connection with the π^--capture experiment,[14] are used with the addition of charged particle counters. Unlike the case of the π^--capture experiment, the telescope signal for μ^--stop cannot be used for the time-zero because of the long lifetime of the μ^- in the 1s atomic state. It was decided to use the nuclear γ-rays following μ^--capture as the time-zero signal. It is also crucial that such nuclear gamma rays should be resolved and identified.

For the charged particle, the pulse height spectra give good energy resolution for energetic protons and deuterons (> 30 MeV), but time-of-flight measurement gives superior results in the low energy region. Both methods were used simultaneously. A dE/dx counter was used to distinguish particles.

The time-of-flight system consisted of 12 large plastic scintillators (NE110, Nuclear Enterprise) with the dimension of 24" x 6" x 3" at the flight path of 5 ft. A dE/dx counter of ¼" thickness made of plastic scintillator (NE110) was placed as a shield in front of the main counters. The geometry of the system with respect to the μ^- beam is shown in Figure 1. The long scintillators are viewed from both ends by 58DVP photomultipliers in a position-sensitive and mean-time mode.[14]

During our initial runs we tried various NaI(Tl) counters as well as Ge(Li) counters as the time-zero counters. The Ge(Li) counters gave a

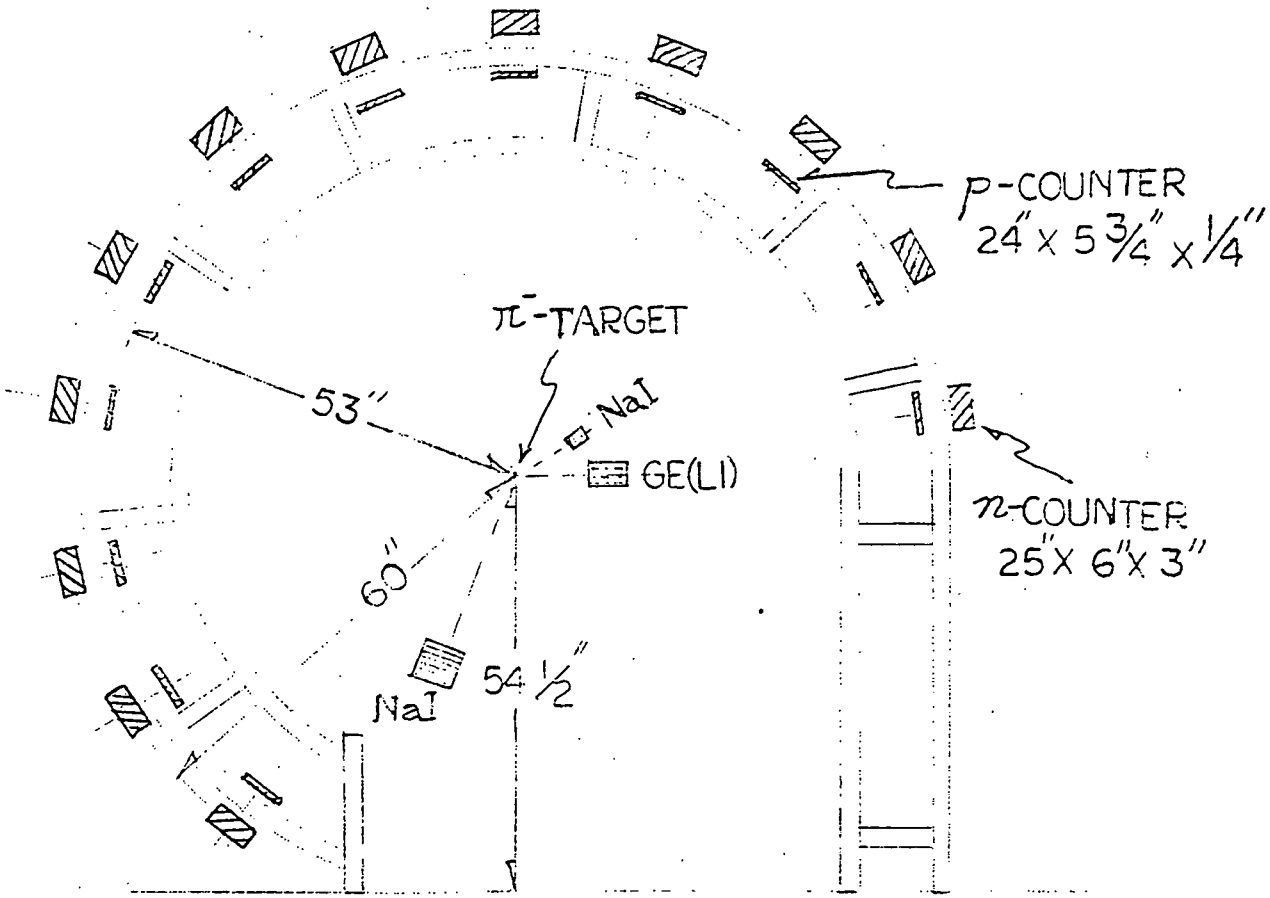

Figure 1. Geometry of the neutron and charged particle counters in the plane perpendicular to the beam. The tubular aluminum frame does not eclipse the counters.

time resolution of 6 nanoseconds at best for 200 keV γ rays, and this called for a neutron flight path of at least 15' for 10% energy resolution for 80 MeV neutrons. This is a viable alternative for a future experiment if high resolution for γ-ray energy is required, but we chose to use a 2"x2" NaI(Tl) counter as the time-zero counter with a timing resolution of 2 nanoseconds.

The multiple particle counter system, which is a careful compromise of efficiency, timing and background consideration, was originally worked out for the π^--capture experiment.[14] It is capable of angular correlation and particle-particle correlation. The latter feature is necessary in order to determine the crucial signature of the back-to-back neutrons as a result of the participation of π^- in the process of μ^--capture,[4] discussed above.

The μ^--beam was obtained at the recently developed slow μ-channel at the TRIUMF.[15] The μ^- beam was at 55 MeV/c and the three-element telescope and the target combination produced 20,000/sec stopped μ^- in the target. The last element of the telescope was used as the veto counter. The target was metallic ^{165}Ho 300 mg/cm^2 in thickness, which was placed in the beam at such an angle that allowed only one of the neutron counters to be severely eclipsed by absorption in the target. The thickness of the target was a compromise between a good stopping rate and tolerable self-absorption of protons in the target.

The μ^- are selected from background π^- and e^- using the time-of-flight with respect to micro-structure of the accelerator beam. As shown in Figure 2, the event gate serves as the main trigger for CAMAC. It

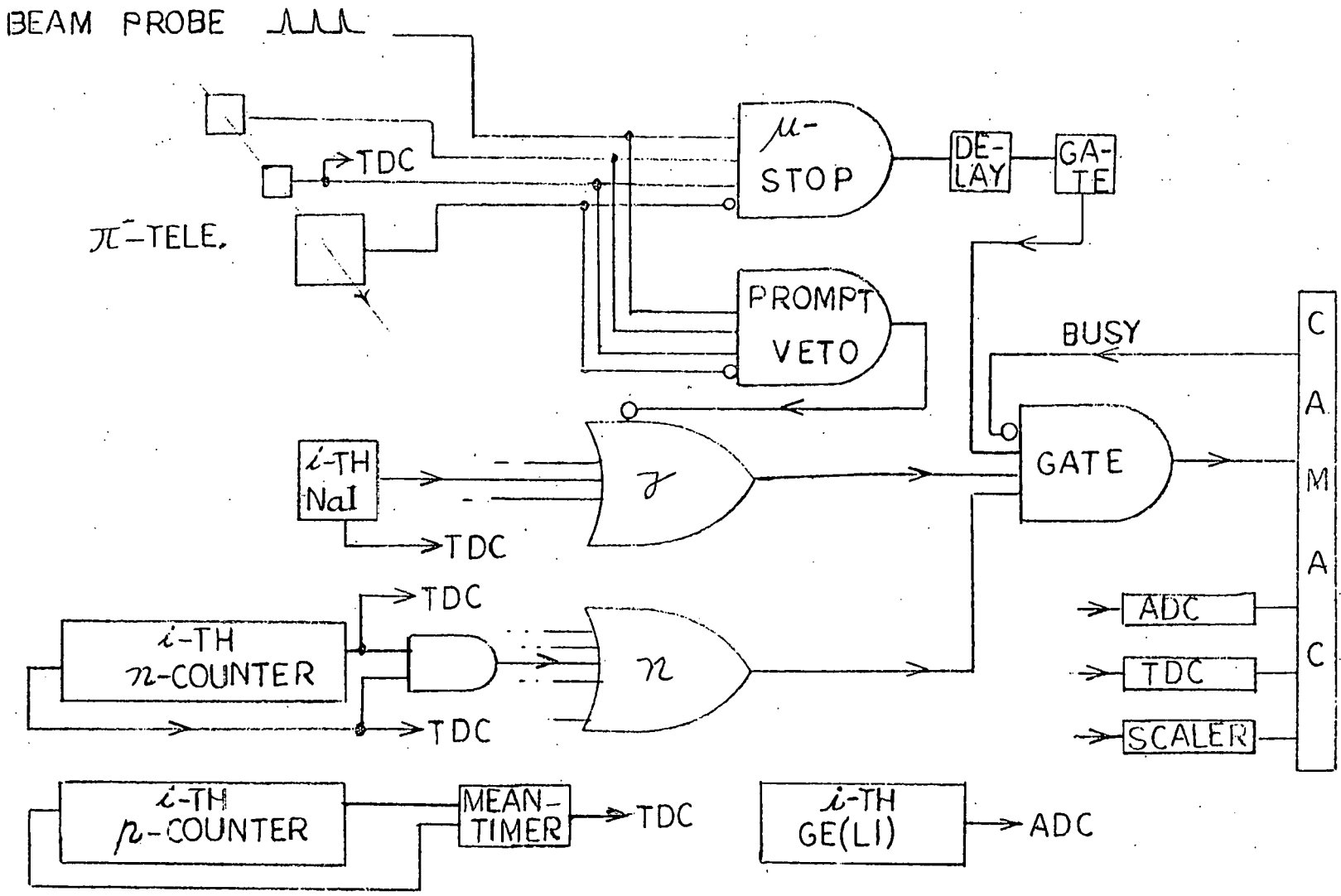

Figure 2: Electronics schematic. Connections to discriminators, scalers, and ADC's are mostly omitted for clarity.

is enabled by a delayed gate from the μ^-stop telescope signal in order to eliminate prompt photons, which were mostly muonic and target x-rays. This event gate required at least one neutron counter and the NaI(Tl) time-zero counter to fire. The event gate provided the common start signals for all of the time-to-digital converters for telescopes, NaI(Tl) counters, n- and p-counters. In Figure 2 individual connections of each counter anodes and dynodes to TDC's and ADC's are not included for simplicity.

Each channel for the n-counters and the telescope counters was provided with a constant fraction discriminator in order to achieve sub-nanosecond timing resolution. Each proton counter, which was also viewed by two phototubes from both ends, was provided with leading edge discriminators and electronic meantimers with 2 nanosecond resolution. The timing spread for the p-counter was mainly due to pulse height-dependent walk, and we are hopeful that a software walk compensation can substantially reduce the spread.

Data Acquisition and Preliminary Analysis

The μ^--capture experiment was intended to provide a spectra of energetic protons and neutron. These spectra were obtained in the following manner. Proton and neutron counters were considered in pairs (see Fig. 1), the proton counter acting as a charged particle veto for the neutron counter. A signal in the neutron counter was considered to be due to a neutron if the proton counter did not detect the passage of a particle. In the situation where the proton counter did register a count in coincidence with the neutron counter, examination of the pulse height

in each provided a means of distinguishing a charged particle from a neutron which interacted in the ¼" proton counter. (Based on relative thickness, a detected neutron has ~10% choice of interacting in the proton counter.) The 3" thick neutron counter acted approximately as a total energy dump detector. The ¼" proton counter then acted as a ΔE measurement. (Charged particles of less than ~35 MeV are totally absorbed in the ¼" thick proton counter and so are <u>not</u> seen by this method.) A scatter plot comparing pulse height in the neutron counter with that in the proton counter shows small pulse heights associated with neutron interaction in the ¼" scintillator as well as a clearly defined band of counts ahowing the $\Delta E/E$ relation between pulse heights in the two counters for charged particles. This was an efficient technique of identifying protons with energy greater than ~35 MeV. A 2"x2" NaI crystal was used to detect γ rays from the nuclear μ capture and served as a time-zero for ToF (time-of-flight) measurements. The portion of the delayed γ-ray spectrum of interest is shown in Figure 3. This region of the spectrum contains several dysprosium γ-rays. The prompt muonic x-rays were suppressed by the electronic logic system. If a γ-ray fell into this region of the NaI spectrum, then the neutron counter data was added to the neutron spectrum. The neutron spectrum from μ capture on Ho is presented in Figure 4. A background subtraction has been made on the assumption that the spectrum greater than 105 MeV is spurious. This fixes an approximate level of background counts per MeV which has been subtracted out of the neutron spectrum.

Although the last run on μ^--capture was meant to be exploratory, we were able to obtain preliminary results for both neutron and proton

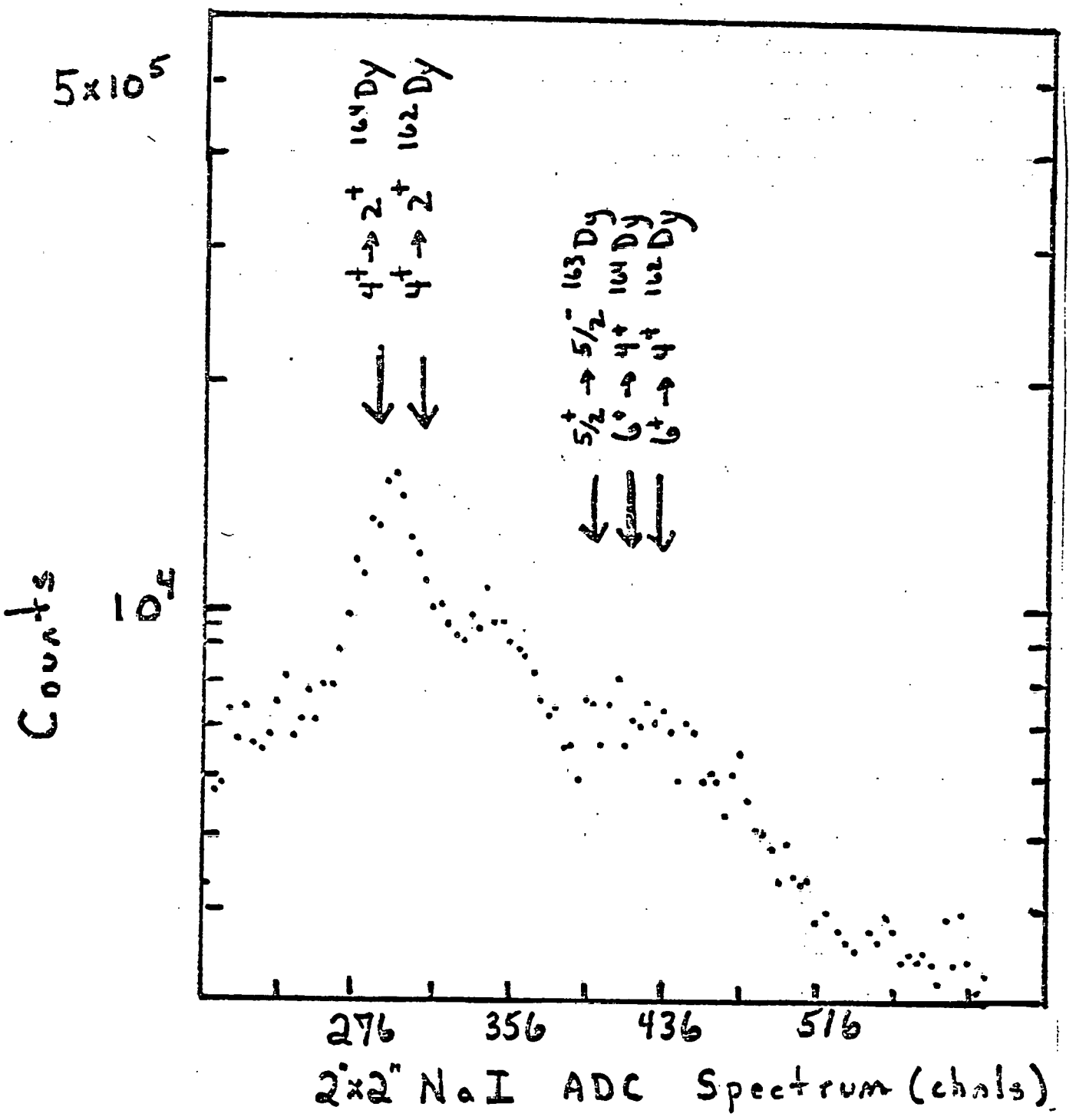

Figure 3: The Delayed Photon Spectrum in the Time-Zero Counter (NaI, 2" x 2")

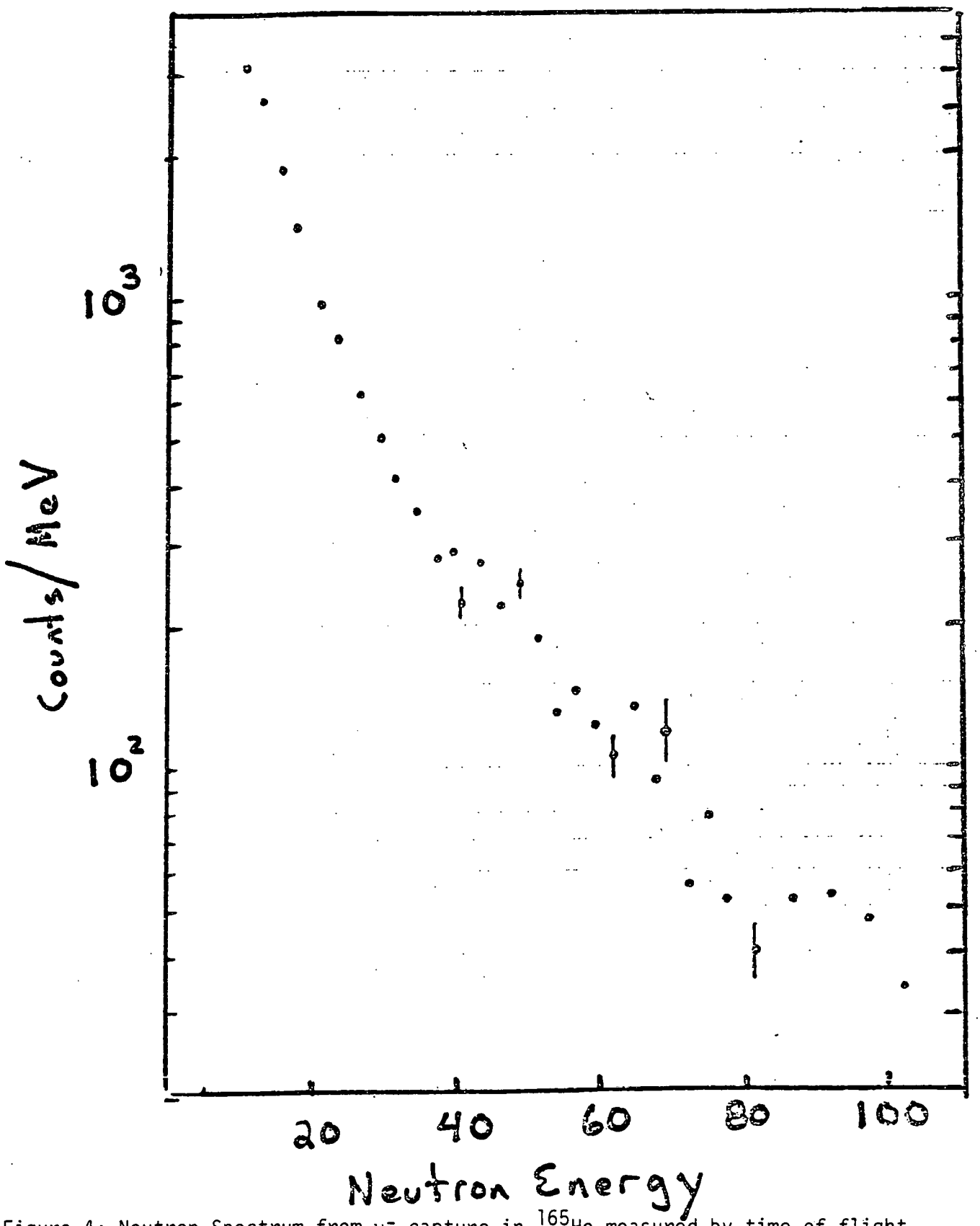

Figure 4: Neutron Spectrum from μ^--capture in ^{165}Ho measured by time-of-flight. The time-zero includes mainly ($4^+ \rightarrow 2^+$) transitions in ^{164}Dy and ^{162}Dy.

emission spectra. The neutron spectrum obtained by time-of-flight is shown in Figure 4. An increase in statistics, more careful pulse-height cuts in each counter, the effect of absorption in dE/dx counters and counter efficiency are some of the areas yet to be worked on. However, we could see two exponential components: $E_0 = 5.1 \pm 0.8$ MeV extending from 11 to 32 MeV, and $E_0 = 11.9 \pm 1$ MeV extending from 32 to 80 MeV. The second decay constant is to be compared to Krieger's result of $E_0 = 12 \pm 1$ MeV for Pb.

The proton spectrum measured by TOF is shown in Figure 5. During the last run the energy dump counter was included in the trigger so that those charged particle events where the particle stopped in the dE/dx counter are not measured. Therefore, the proton spectrum is valid only above ~35 MeV, since that was the energy required to "punch through" the proton counter. No peaks in the NaI spectra were identified as being due to Tb, which would result from proton emission after μ^- capture. Hence, the proton spectra was collected in coincidence with any pulse above the noise in the 2"x2" NaI crystal. There is a large drop in the proton spectra below ~40 MeV, due to the absorption of the proton in the proton counter.

This spectra gives a slope of $E_0 = 14 \pm 2$ MeV extending up to 90 MeV, which is to be compared to the result of $E_0 = 9.9 \pm 1.1$ MeV for Pb, extending from 40 to 80 MeV reported by Krane.[10] The inability to identify the specific γ-rays from the final isotope of Tb is a source of uncertainty but γ-ray data on ^{164}Tb are not available. (Unidentified peaks in the Ge(Li) spectra from μ capture [Figure 6] may correspond to Tb gamma rays). As the analysis progresses, we can use the pulse height

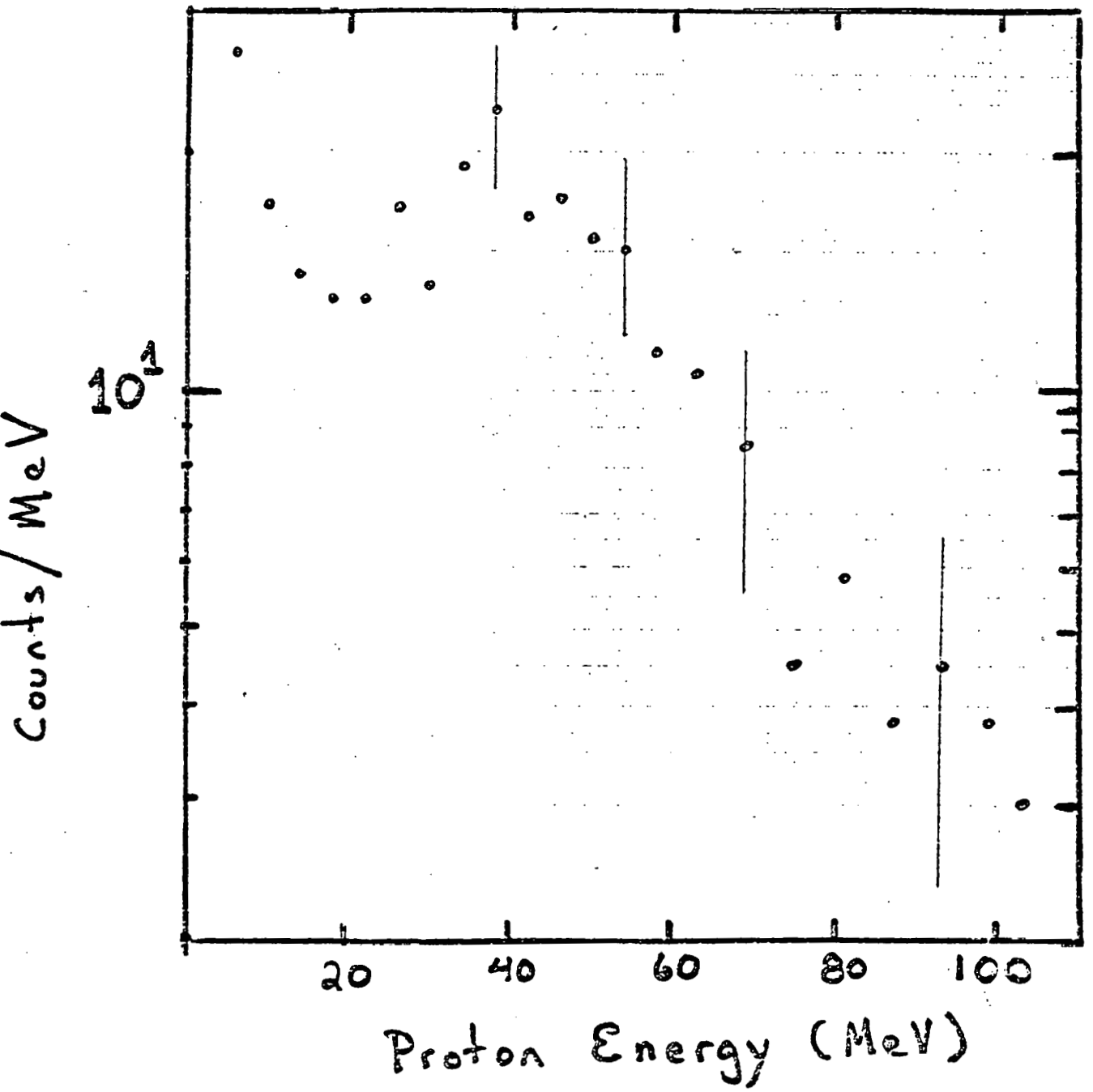

Figure 5: Proton Spectrum from μ^--capture in ^{165}Ho Measured by Time-of-Flight. The range below 35 MeV is to be ignored because of the effect of the dF/dx counter.

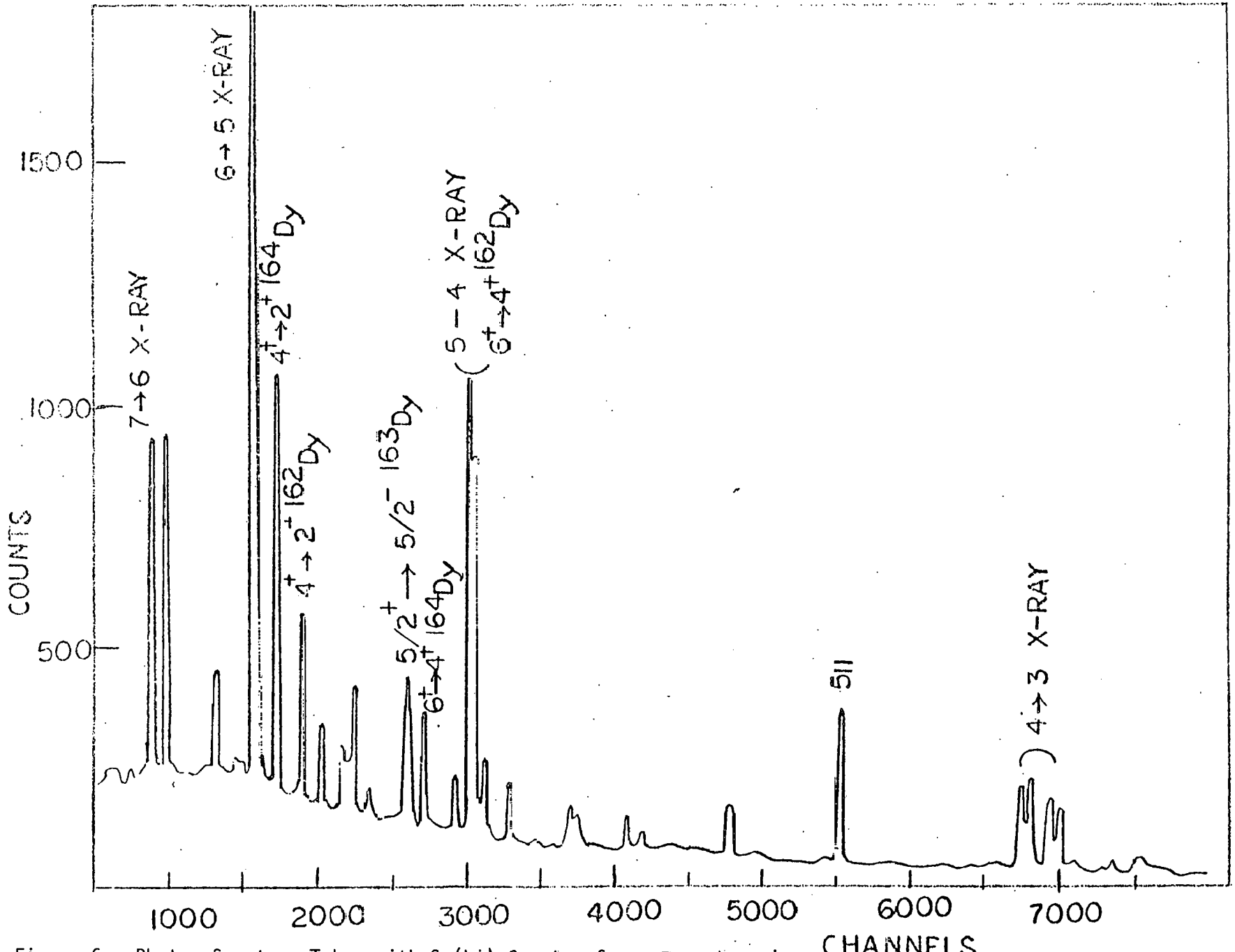

Figure 6: Photon Spectrum Taken with Ge(Li) Counter from μ^--capture in ^{165}Ho

information in the combination of dE/dx and energy dump detectors to determine the charged particle energy accurately. In the future we should employ a target for which the nuclear physics of the daughter nucleus with Z-2 is well known.

We should not draw any firm conclusion at the present moment as to the nature of the energetic components of charged particle emission in μ^--capture. The most important observation at this stage would be that the slope of the exponential decay of both neutron and proton spectra is of the same magnitude, and there is one additional exponential component below 32 MeV in the neutron spectra.

REFERENCES:

1. N. C. Mukhopadhyay, Physics Report 30C, 1 (1977).
2. H. Überall, "Springer Tracts in Modern Physics," Vol. 71 (Springer-Verlag, 1974), p. 1.
3. M. Lifshitz and P. Singer, Phys. Rev. C22, 2135 (1980).
4. J. Bernabeu, T. E. O. Ericson and C. Jarlskog, Phys. Lett. 69B, 161 (1977).
5. M. H. Krieger, Thesis, Columbia University, 1969 (unpublished); also Columbia University Report, No. NEVIS-172 (1969).
6. W. U. Schröder et al., Z. Phys. 26B, 57 (1974).
7. R. M. Sundelin and R. M. Edelstein, Phys. Rev. C7, 1037 (1973).
8. Yu. G. Budyashov et al., Sov. Phys.-JETP 33, 11 (1971).
9. M. P. Balandin et al., Sov. J. Nucl. Phys. 28, 297 (1978).
10. K. S. Krane et al., Phys. Rev. C20, 1873 (1979).
11. M. Lifshitz and P. Singer, Phys. Rev. C22, 2135 (1980).
12. T. Kozlowski and A. Glinski, Nucl. Phys. A305, 368 (1978).
13. P. Singer, N. C. Mukhopadhyay, R. D. Amado, Phys. Rev. Letters 42, 162 (1979).
14. L. Madansky and Y. K. Lee, Annual Progress Report for DOE, DOE/ER/02374-2, 1981, p. 91.

The Neutron, Charged Particle, and γ-ray Correlation in π^--capture in ^{165}Ho and ^{181}Ta

E. McIntyre, T. Hallman, R. Levin, Y. K. Lee, L. Madansky and G. Mason*
and B. Olaniyi*

The investigation of the π^--capture in medium heavy nuclei is now in its final phase of analysis after the latest run at the TRIUMF during May and June, 1982. We continue to study the neutron and proton spectra in coincidence with discrete nuclear gamma rays, to exhibit correlations of the spectra to neutron multiplicity and residual nuclear states. We finished the examination of the data from the previous runs carried out during 1981, and the results are published.[1] In our early data a discrete component in the pre-compound neutron spectra is resolved for the first time, and its correlation to the population of high spin nuclear states is observed.

The major improvements and modification in the latest run during 1982 were the addition of charged particle counters, which acted also as charged particle shields for the neutron counters; inclusion of an additional Ge(Li) counter for a higher efficiency and possible photon-photon correlation; better beam optics and targeting for a higher stopping rate of π^-. The upgraded experiment was presented to the TRIUMF as a new experiment for a sufficient running time and higher priority, and was approved as Experiment 211. In order to accommodate higher yields, the event trigger requirements were also tightened. Sufficient statistics were accumulated in order to

---

* University of Victoria, and the TRIUMF, Canada

determine the shape and intensity of the discrete component of the exclusive neutron spectra, the n-n-γ ray correlations, and the n-γ angular distributions.

During the latest run at TRIUMF we also measured the photon-photon correlation with a particular emphasis on the lineshape study of the quadrupole split pionic x-ray as a function of neutron multiplicity. The data are still under analysis, but the rationale for the experiment, which intends to detect the correlation between the neutron multiplicity and the orientation of the atomic orbit of π^- with respect to the deformed nucleus, is given at the end of this chapter.

Purpose of the Experiment

Recently progress in understanding the de-excitation process in heavy ion collisions[2,3] has given new insight into the nuclear processes involved in π^--capture. Several choices of target nuclei exist, ^{165}Ho and ^{181}Ta, for example,[4,5] for which nuclear properties of residual isotopes are well understood from heavy ion physics.[6]

The experiment described below is an effort to make more exclusive measurements of the π^--capture process by identifying the reaction channel leading to a particular nuclear state of a definite isotope. This goal is achieved by using an efficient time-of-flight system for neutrons in coincidence with discrete nuclear gamma rays. Peaks at the high energy end of exclusive neutron spectra in ^{165}Ho are resolved, and they reveal a strong effect on the population of high spin nuclear states. This is the first measurement where the neutron multiplicity, the angular momentum of the

residual nuclei, and the neutron spectra are correlated to exhibit the resolved details of pre-compound neutron emission, as well as the effects of nuclear structure.

In this study we address ourselves to three categories of questions. The first one is about the primary process of capture of the π^- by nucleons. It seems that the majority of π^- are captured by a correlated pair of nucleons. Our data indicates that the nuclear structure plays an important role in determining the nature of the correlated nucleon pairs, and the n-γ ray correlation can supply a partial answer to the location of the capture events and the spectra of the primary nucleons.

The second question concerns the de-excitation of highly excited nuclei which occurs primarily by emission of fast and slow neutrons, and in some cases charged particles. We believe that n-(γ-ray) correlation studies provide the most detailed information of this process, which is often discussed as "pre-equilibrium" particle emission. The third category involves the nuclear physics of the γ-ray emitting states of the residual nuclei. Our data show that there is a complex correlation between the neutron spectra and the final nuclear states, which can be effectively studied by the present approach.

The current results are timely in view of the recent intensive efforts to describe the broad category of pre-compound emission by several different models.[7,8,9] Decisive experiments to resolve the ambiguity in such models are beginning to appear in terms of channel-defined measurements.[10] The π^--capture in medium heavy nuclei offers a particularly important opportunity to make such measurements since an experimentally

clear time-zero signal is available from the stopped π^-, and a wide range of residual isotopes and nuclear states of high spin are reached.

Experimental Arrangements

The present experiment was carried out with the slow beam from the M13 Channel at the TRIUMF accelerator. The details of the major components of the time-of-flight apparatus were described previously in our Annual Report for 1981,[11] and the description of the new counters for the charged particles is given in connection with the μ^--capture experiment in the preceding chapter of the present report. Briefly, twelve large plastic scintillators (NE110, 24" x 6" x 3") were employed in a time-of-flight system with a flight path of 5 $\pm$ 0.25 ft. The counters were spaced to measure the angular distribution at steps of 23 $\pm$ 5°. Both ends of each neutron counter were viewed by individual phototubes. The data from each counter were utilized in a mean-time mode achieving overall timing resolution better than 1 ns.

The charged particle counters were ¼" thick, subtending the same solid angle as the neutron counter. Two Ge(Li) gamma-ray detectors were placed approximately 2' from the target in the plane defined by the neutron detectors. The background signals in the neutron counters due to electrons and γ-rays were effectively eliminated by the time-of-flight information. In the neutron spectra the background due to protons was eliminated through identification of residual isotopes by its coincident γ-rays, and by the vetoes generated by the charged particle counter.

Results

The experiment was carried out in two separate stages. The first stage involved shake-down runs during November of 1980, and data-taking runs during February of 1981, using two metallic targets of ^{165}Ho and ^{181}Ta. The results of these measurements were analyzed mostly for the neutron spectra in coincidence with readily observed γ-rays from the ground state band (g.s.b., from now on) transitions of even-even isotopes. Residual nuclear states with spins up to 8$\hbar$ were studied.

Our final runs during the second stage were carried out during May, 1982, with the addition of charged particle counters, another Ge(Li) detector, and with a significant increase in π^--stop rate. In order to accommodate the increased data rate, the event trigger requirement was tightened to reduce background events and to favor events involving fast neutrons over thermal neutrons. The experiment was limited to the ^{165}Ho target only, but sufficient beam time was allocated to achieve the quality and statistics of the data to enable the inclusion of $(12^+ \rightarrow 10^+)$ and $(10^+ \rightarrow 8^+)$ transitions, particle-particle correlations, and particle-γ ray correlations.

We finished the factor of 20 compression of our original data tapes from the latest runs, and started the analysis of spectra and correlation on a VAX 11/780, using the CERN histogramming package HBOOK. The completion of the data analysis and interpretation will take us well into the middle of next year. The results of the analysis of the data from our 1981 run was partly finished and presented in the previous annual report,[11] and has been recently published.[1]

Figure 1. Summary of early (1981) data. Neutron spectra in coincidence with ($4^+ \rightarrow 2^+$) and ($8^+ \rightarrow 6^+$) transitions in the g.s.b. for various neutron multiplicites for ^{165}Ho and ^{181}Ta targets. Lines are drawn to guide the eye.

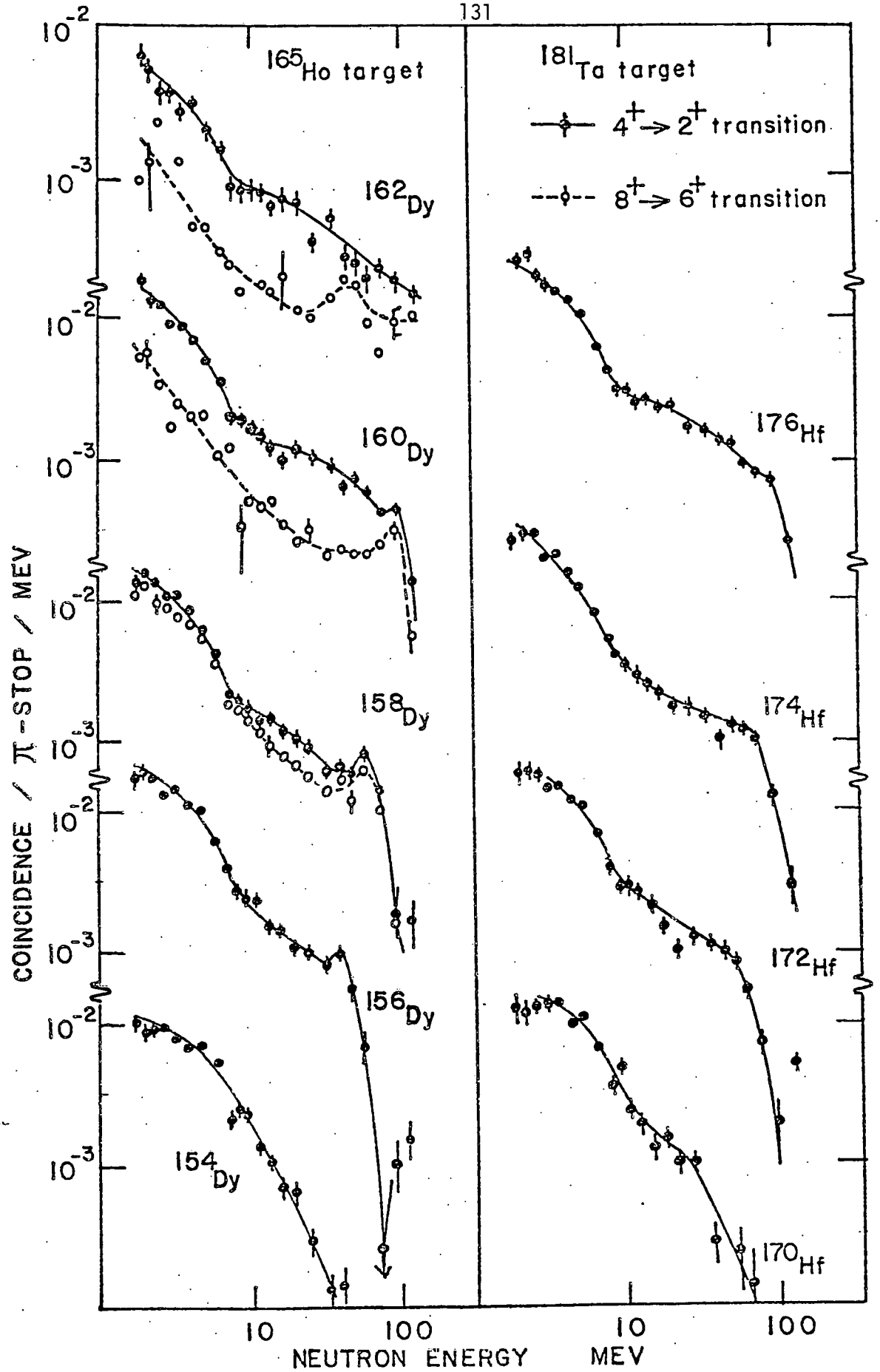
165Ho target
181Ta target
4+ → 2+ transition
8+ → 6+ transition
162Dy
160Dy
158Dy
156Dy
154Dy
176Hf
174Hf
172Hf
170Hf
COINCIDENCE / π-STOP / MEV
NEUTRON ENERGY MEV
10
100

FIG. 1

Interpretation of the Early Data on ^{165}Ho and ^{181}Ta

In Figure 1, the neutron spectra in coincidence with the $(4^+ \rightarrow 2^+)$ g.s.b. transitions for two targets are shown. The corresponding $(8^+ \rightarrow 6^+)$ gsb data are also shown for a few cases. These spectra have features which are absent in inclusive neutron spectra.[12] For the ^{165}Ho target, peaks are observed at the high energy end of the spectrum for three neutron multiplicities. The peaks are enhanced for the $(8^+ \rightarrow 6^+)$ transitions for ^{160}Dy. Such peaks are almost unrecognizable for the ^{181}Ta target, but the origin of this effect is not known.

In order to understand the presence and the shift in position of the peak for different neutron multiplicity (M_n), we evaluate the situation where one fast neutron is emitted from the nucleus, leaving an excitation energy corresponding to the peak of the excitation function for the (p,xn)-reaction with $x = M_n - 1$. If we use the tabulation[13] of the values for $(E_m - E_{thres})$ where E_m is the excitation energy for the maximum probability for $(M_n - 1)$ neutron emission, and the E_{thres} is the threshold energy for the (p,xn)-reaction, then we can evaluate the energy of the fast neutron to be

$$E_n = M_\pi c^2 + Q(M_n) - BE(\pi) - (E_m - E_{thres}),$$

where M_π and $BE(\pi)$ are the pion mass and binding energy, respectively, and $Q(M_n)$ is the Q-value for the M_n neutron emission from the nuclear mass table.[14] The results are listed in Table I. The agreement in positions is encouraging, but the mechanism favoring such a simple process is not clear, especially in view of the absence of such peaks for the ^{181}Ta target.

Table I. Peak Neutron Energy

Isotopes	M_n	$Q(M_n)$ MeV	$E_m - E_{thres}$ MeV	E_n Calculated MeV	E_n Observed MeV
^{162}Dy	3	-20	9 ± 2	110 ± 2	-
^{160}Dy	5	-35	15 ± 2	89 ± 2	97 ± 12
^{158}Dy	7	-50	17 ± 5	72 ± 5	62 ± 6
^{156}Dy	9	-67	32 ± 7	40 ± 7	44 ± 4
^{154}Dy	11	-83	44 ± 7	12 ± 7	-

The above observation leads to the general picture of de-excitation based on the capture of π^- by a quasi-deuteron on the surface of the nucleus. One neutron has a large probability for escaping with a small final state interaction, and the other neutron will start a series of nuclear reactions. Such a view in its extreme form was sometimes taken by authors in the past. Mukhopadhyay[15] was able to fit the inclusive neutron spectra by assuming one of the primary neutron escaped without a final state interaction at all, if a certain nucleon momentum distribution was assumed inside the nucleus. In the related field of inelastic scattering of nucleons, Hüfner and co-authors assume that single scattering dominates nucleon-nucleus inclusive cross-sections for energies between 15 and 100 MeV and successfully calculates the spectra for fast neutrons.[16,17]

In the more familiar (p,xn)-reactions the excitation function of each multiplicity is rather sharply defined (within 20 MeV FWHM) for a given incident proton energy.[10] If we combine this observation with the assumption that one of the primary neutrons in π^--capture tends to escape with a minimum of scattering, one can see the importance of the energy of the first neutron emission in determining the neutron multiplicity. The pre-equilibrium calculation[7] based on four initial exciton numbers is not able to describe these aspects, and incorporation of the special features of the surface capture is expected to be crucial.

In addition to the discrete feature of neutron spectra, the nuclear spin-dependence of the neutron multiplicity and spectral shape should be a challenge to more detailed pre-equilibrium calculations. The conjecture that the intermediate region in the neutron spectra (e.g.

10 MeV < E < 80 MeV for ^{160}Dy) is due to more than one pre-equilibrium neutron emission is now being tested by analyzing the latest data for a n-n correlation experiment in coincidence with γ rays.

Preliminary Results of Latest Run with ^{165}Ho Target

Data from Experiment 211, obtained in May 1982, has been partially analyzed. The results presented here for the π capture data are based on approximately 500,000 events. A factor of two improvement in statistics can be expected when the full set of data is analyzed. The present data can be considered to be of higher quality than the previous data, in that a larger fraction of the data is due to high energy neutron events. This was achieved by raising the bias level on the neutron counter to eliminate a larger fraction of thermal neutrons.

The data has been analyzed in the following fashion. Gamma ray spectra from the Ge(Li) counters allowed the determination of the final state. This amounted to a knowledge of the neutron multiplicity of the reaction (e.g. ^{154}Dy has a neutron multiplicity M_n = 11) and the spin of the emitting nuclei. The spin observed in a particular event is not, however, necessarily the highest spin created in the reaction, since several gamma rays are emitted as the nuclei de-excites through the ground state band (g.s.b.).

The discrimination level (baseline) of the neutron counter (in MeV_{ee}) was determined, which fixed the efficiency of the individual neutron counter at each neutron energy. (The efficiency of the neutron counter as a function of baseline and neutron energy was calculated by computer Monte

Carlo simulation.[18]) The absolute efficiency of the two Ge(Li) detectors was also determined. Knowledge of these efficiencies allowed the assignment of a weight factor to coincidences between a neutron of a particular energy and a gamma ray of a particular energy. A count in the neutron detectors was considered to be due to a neutron if its proton counter did not fire. These weight factors were used to fill a scatter plot of neutron energy versus gamma ray energy. Such a scatter plot can be considered to consist of gamma ray peaks associated with each neutron energy. An estimate of the background to each peak allowed the calculation of the gamma ray intensity for each neutron energy. The intensity of the gamma ray peaks at each neutron energy is the neutron spectra associated with the particular gamma peak.

Figure 2(a b) shows such neutron spectra associated with particular gsb transitions in ^{160}Dy (M_n=5), and Figure 3 shows the same for ^{158}Dy (M_n=7). The spectra are plotted as Counts/MeV against neutron energy. To increase the signal to noise ratio, the spectra are computed only for channels between the ½ power points of the Ge(Li) peak. The ratio of total area to the area between the ½ power points will be used to give Count/MeV/π-stop for each spectra. The lines on the graph are hand drawn and should only "guide the eye".

Comparison of these spectra in Figure 2 suggests the following. All the spectra show a sharp cutoff in neutron energy, at approximately 90 MeV. This represents a high energy component in the spectra, which becomes relatively more important for the "high spin" spectra. This is because there are fewer neutrons in the 15-70 MeV range for the high spin associated spectra. Comparison of the ($8^+ \rightarrow 6^+$) and the ($6^+ \rightarrow 4^+$) spectra

bears out this observation. It is reasonable to connect the high energy neutron with the generation of high spin states. Examination of Figure 3(b) shows that, for the ^{158}Dy associated spectra (M_n=7) the 15-70 MeV region is only depleted for the $12^+ \rightarrow 10^+$ transition. The ^{158}Dy spectra exhibit peaks at approximately 65 MeV neutron energy.

Spectra such as these have been generated for dysprosium isotopes 154, 156, 158, 160, 162, corresponding to neutron multiplicities 11, 9, 7, 5 and 3. It is possible to sum the neutron spectra corresponding to all the gamma rays of a particular isotope, giving a spectra associated with that isotope. Alternately, it is possible to sum over all isotopic gamma rays of a particular spin, given the neutron spectra associated with the creation of a particular spin. Consider first the "spin summed" neutron spectra for particular isotopes, displayed in Figure 4(a and b). For ^{162}Dy, the midenergy component (from 15 to 70 MeV) dominates the spectrum, suggesting that the low neutron multiplicity (M_n=3) of this final state is created when both neutrons of the capturing quasi-deuteron escape with a substantial fraction of the pion energy. This scenario gives two energetic neutrons, enhancing the midenergy range of the spectrum and leaving only a small portion of the available pion rest mass energy to remove the third neutron from the excited nucleus.

The ^{160}Dy and ^{158}Dy spectra exhibit peaks at about 90 and 65 MeV respectively. In these cases, it may be that the final neutron multiplicity (and thus the isotope) is determined by emission of an energetic neutron. The remaining energy (from the 140 MeV available from the pion mass) may be used to evaporate additional neutrons. Therefore, the energy carried away

by the energetic neutron determines the final state neutron multiplicity. This is reasonable to suppose in moving from ^{160}Dy to ^{158}Dy, the shift in the high energy peak provides approximately 25 MeV which can be used to remove two additional neutrons. If the energies of these two peaks are plotted against the mass number, and a straight line is drawn through them, the prediction of peaks at ~110 MeV in the ^{162}Dy spectra, ~40 MeV in the ^{156}Dy and ~15 MeV in the ^{154}Dy spectra can be made. Examination of Figure 4 shows that the ^{162}Dy spectra begins its dropoff at ~110 MeV. (Any peak in this spectra may be masked by the large midenergy neutron component.) Furthermore, there is a broad bulge in the ^{156}Dy spectra at about 35-40 MeV. It is difficult to argue that the ^{154}Dy spectra exhibits any peak at ~15 MeV, but its presence may be masked by the large number of neutrons below 20 MeV. Finally it should be noted that the ^{156}Dy and ^{154}Dy spectra exhibit a small shoulder at ~70 MeV neutron energy. Since the Q value for this channel is 83 MeV, it is safe to consider this small hump to be due to insufficient background subtraction.

Next consider the "multiplicity summed" neutron spectra, Figure 5(a and b), where, for example, the $12^+ \rightarrow 10^+$ spectra for all isotopes has been summed. Comparison of the $12^+ \rightarrow 10^+$ spectra with the $4^+ \rightarrow 2^+$ indicates that a high energy component (~80 MeV) is relatively more important in the high spin case. This is consistent with the model of spin generation by the escape of a high energy neutron from the nuclear surface.[19] The high energy component becomes less prominent as the spin decreases. In the case of the $2^+ \rightarrow 0^+$ transition, there is again a small enhancement at high energy. This may correspond to back-to-back emission of energetic neutrons which

leaves no net angular momentum, but enhances the probability of observing an energetic neutron.

Strong Perturbation of Pionic X-ray Studied in Coincidence with γ-rays

During the π^--capture experiment described above, multiple Ge(Li) counters were used not only to increase the counting statistics but explicitly to allow measurement of the photon-photon correlation. During the run of May 1982, two 12-hour shifts were dedicated to the photon-photon correlations by relaxing the requirement of particle detection in the trigger.

We consider the nuclear gamma ray as a signature of neutron multiplicity, and in turn consider the neutron multiplicity to be related to the orientation of the pionic orbital with respect to the axis of the highly deformed nucleus. In the Ta and Ho targets, the pionic $5 \rightarrow 4$ x-ray transition is split into two peaks by the quadrupole effects due to the deformed nuclei. Schematically, one peak corresponds to the pions skirting around the equator of the cigar-shaped nucleus and the other peak corresponds to the pions skimming the poles of the nuclei.

If the $5 \rightarrow 4$ x-ray is studied in coincidence with a gamma ray which originates from π^--capture in the interior of the nucleus, then a variation of the lineshape might be observed. A good candidate for such a gamma ray is the 4^+ to 2^+ transition of ^{154}Dy. For this isotope the neutron multiplicity is 11, and consideration of energy conservation alone suggests that both members of the capturing pair of nucleons are absorbed in the nucleus. This is more likely to happen if the capture occurs in the interior of the

Figure 2. Neutron spectra in coincidence with various transitions in the g.s.b. in ^{160}Dy.

Figure 3. Neutron spectra in coincidence with various transitions in the g.s.b. in ^{158}Dy.

Figure 4. Neutron spectra for various neutron multiplicities. All observed γ-rays from the g.s.b. of each isotope are summed.

Figure 5. Neutron spectra in coincidence with various transitions in the g.s.b. For each spin-parity sequence, $I^+ \rightarrow I'^+$, the spectra for all neutron multiplicities are summed.

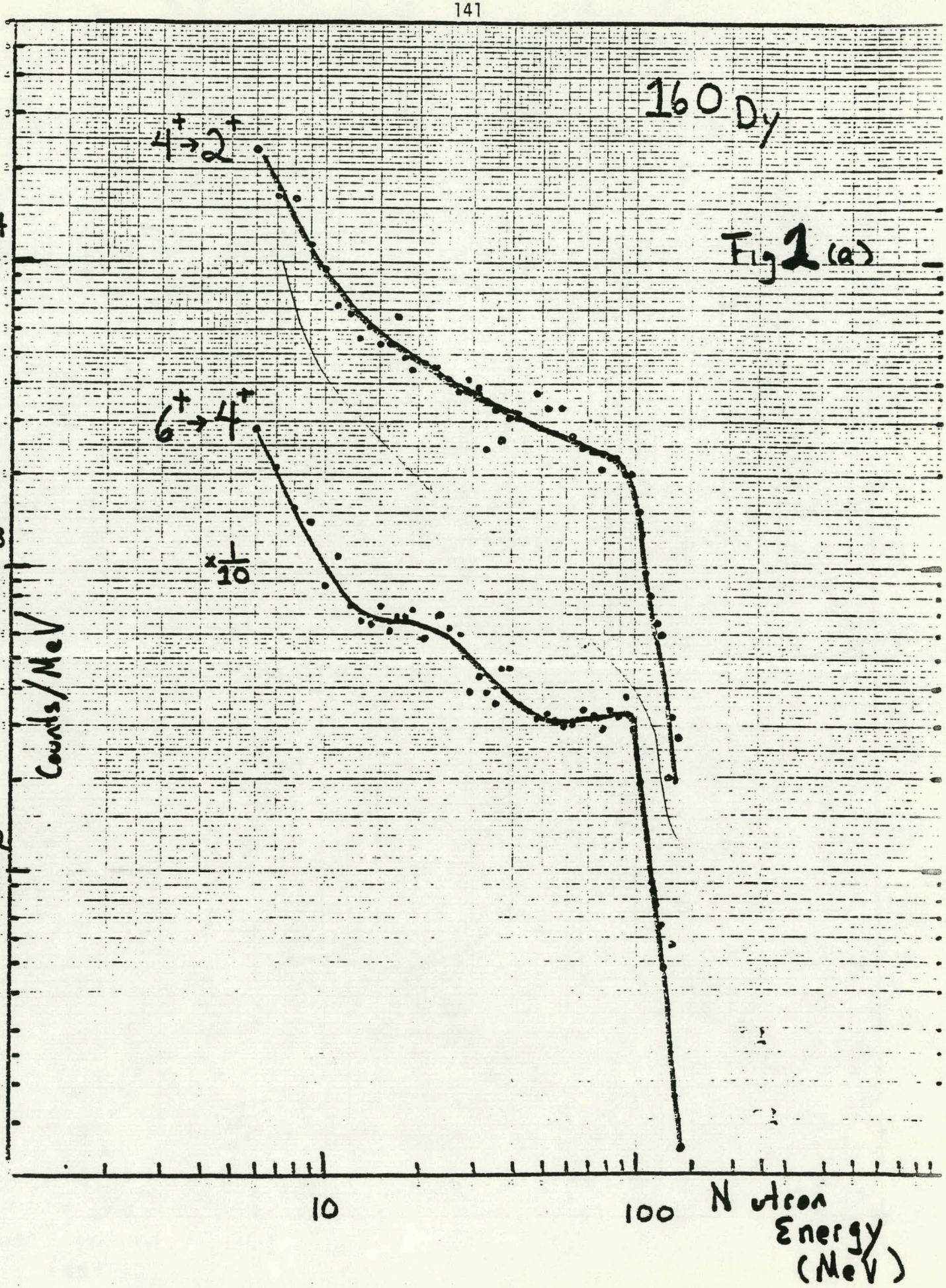
160 Dy
4+ → 2+
6+ → 4+
× 1/10
10⁴
10³
10²
Counts/MeV
10
100
Neutron Energy (MeV)

Fig 1 (a)

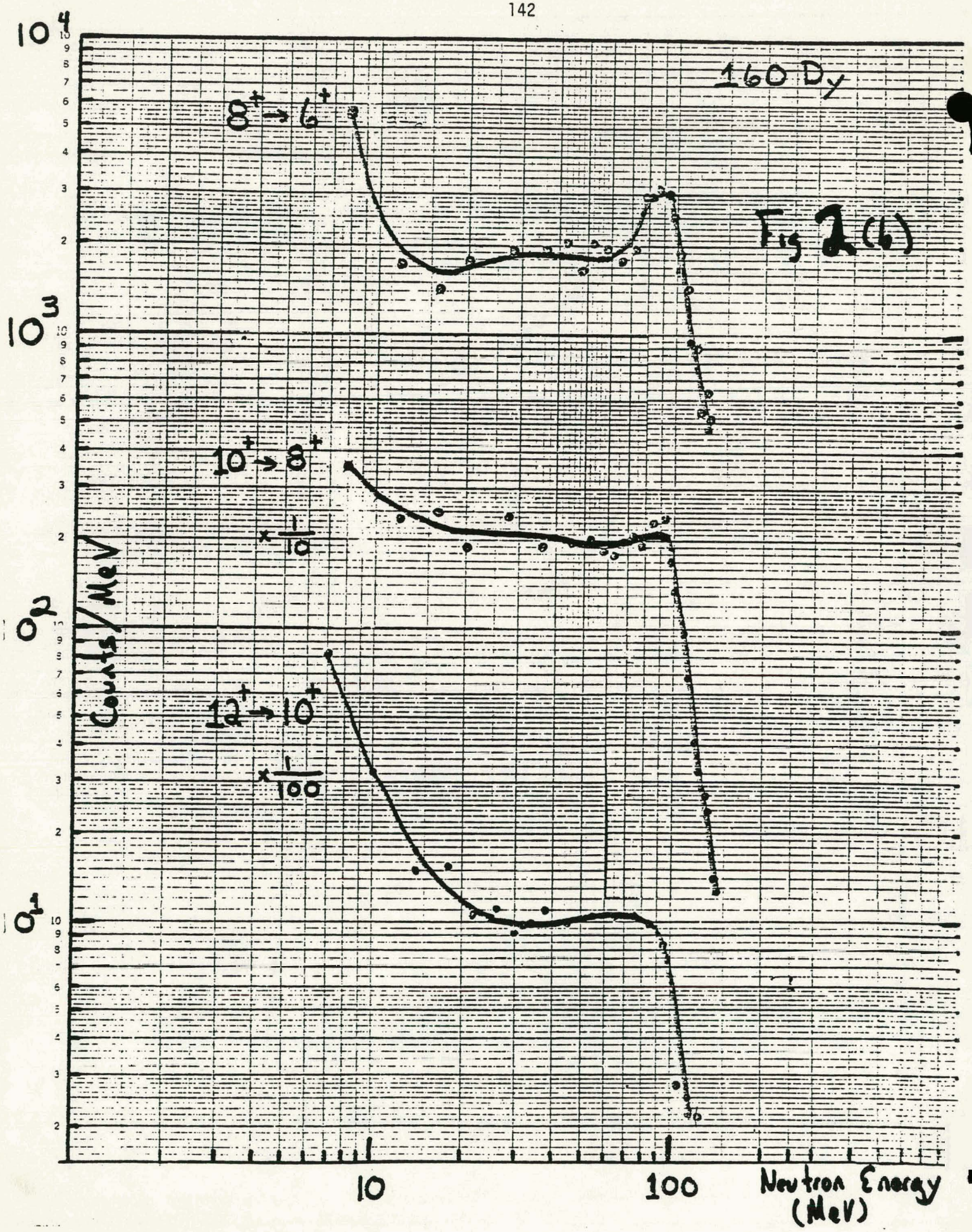
160 Dy
8+ → 6+
10+ → 8+
× 1/10
12+ → 10+
× 1/100
Counts/MeV
10
100
Neutron Energy (MeV)

Fig 2(b)

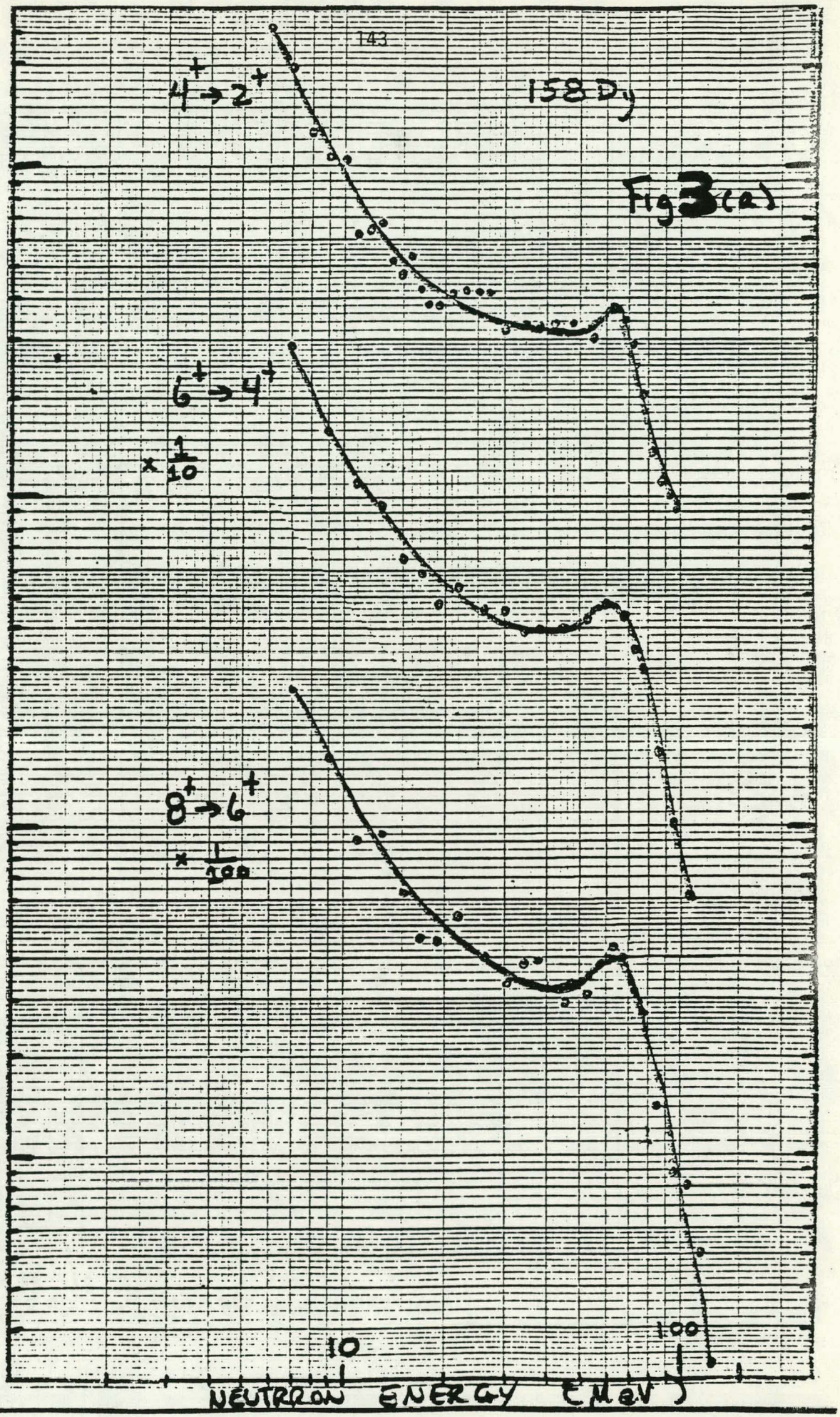
158Dy
4+ → 2+
6+ → 4+
× 1/10
8+ → 6+
× 1/100
Counts/MeV
10⁴
10³
10²
10¹
10
100
NEUTRON ENERGY (MeV)

Fig 3(a)

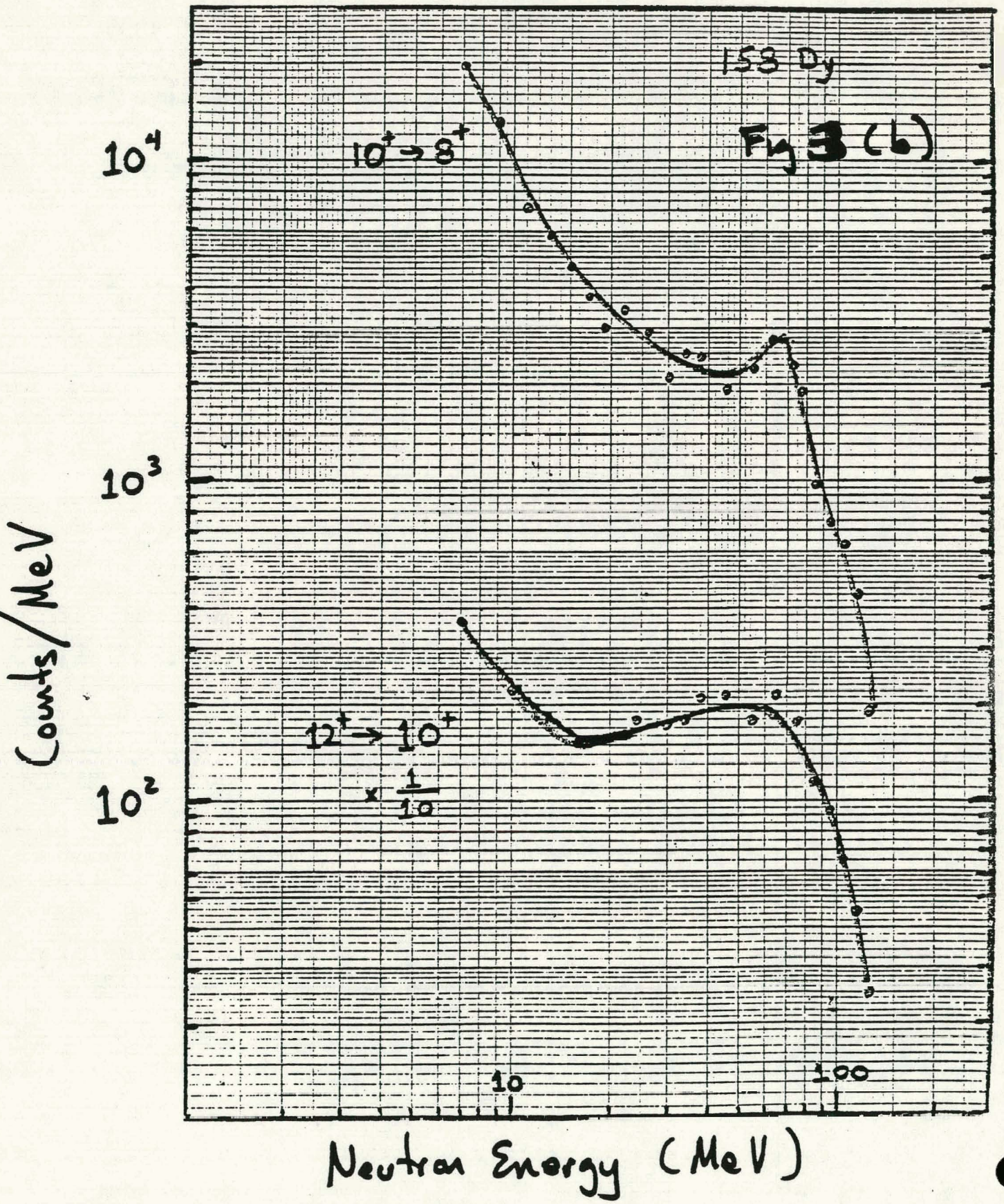
153 Dy
Fig 3 (b)
$10^+ \rightarrow 8^+$
$12^+ \rightarrow 10^+$
$\times \frac{1}{10}$
10^4
10^3
10^2
Counts/MeV
10
100
Neutron Energy (MeV)

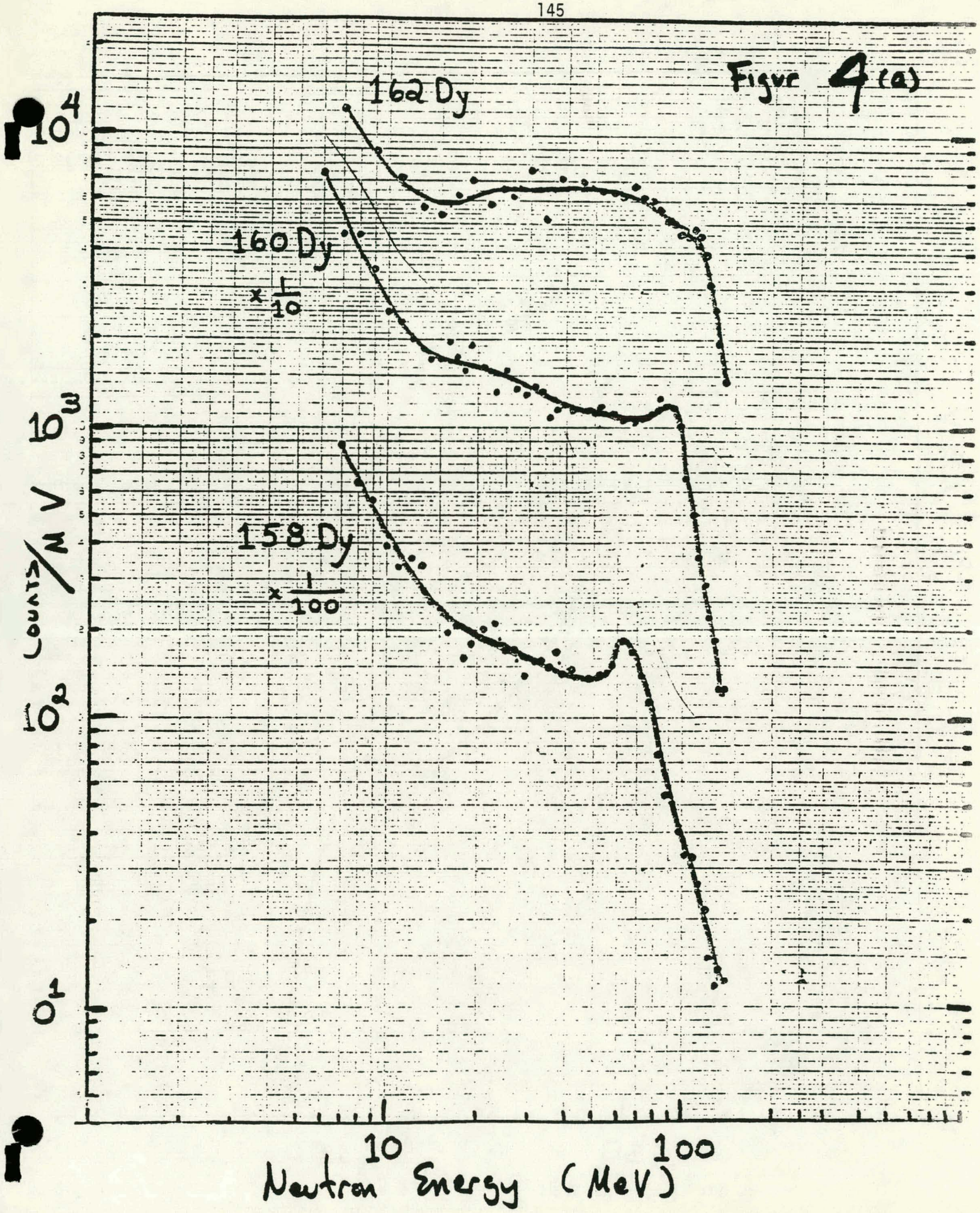
Figure 4 (a)
162 Dy
160 Dy
x 1/10
158 Dy
x 1/100
10⁴
10³
10²
10¹
Counts/MeV
10
100
Neutron Energy (MeV)

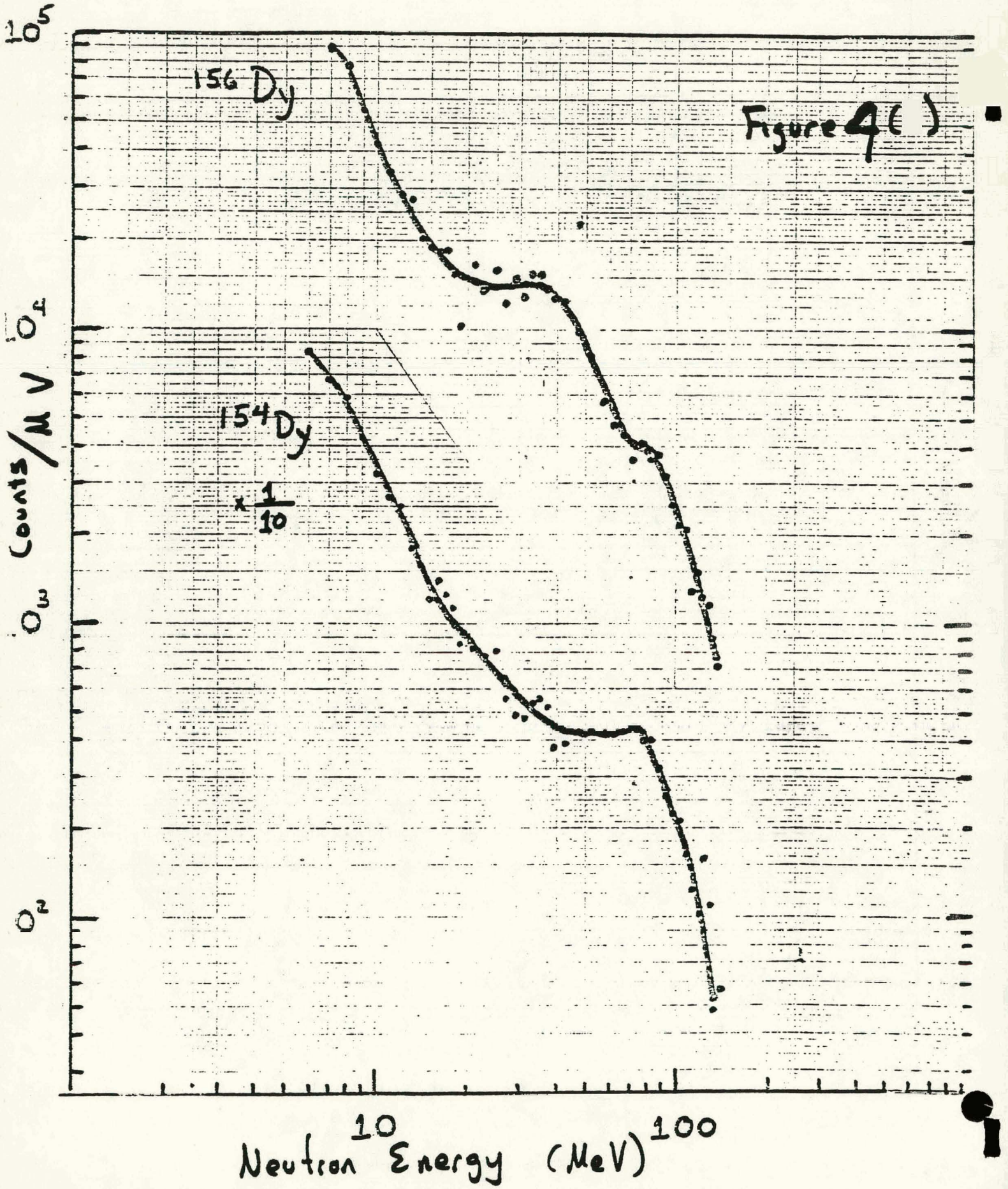
10^5
10^4
10^3
10^2
Counts/MeV
^{156}Dy
^{154}Dy
$\times \frac{1}{10}$
10
100
Neutron Energy (MeV)

Figure 4( )

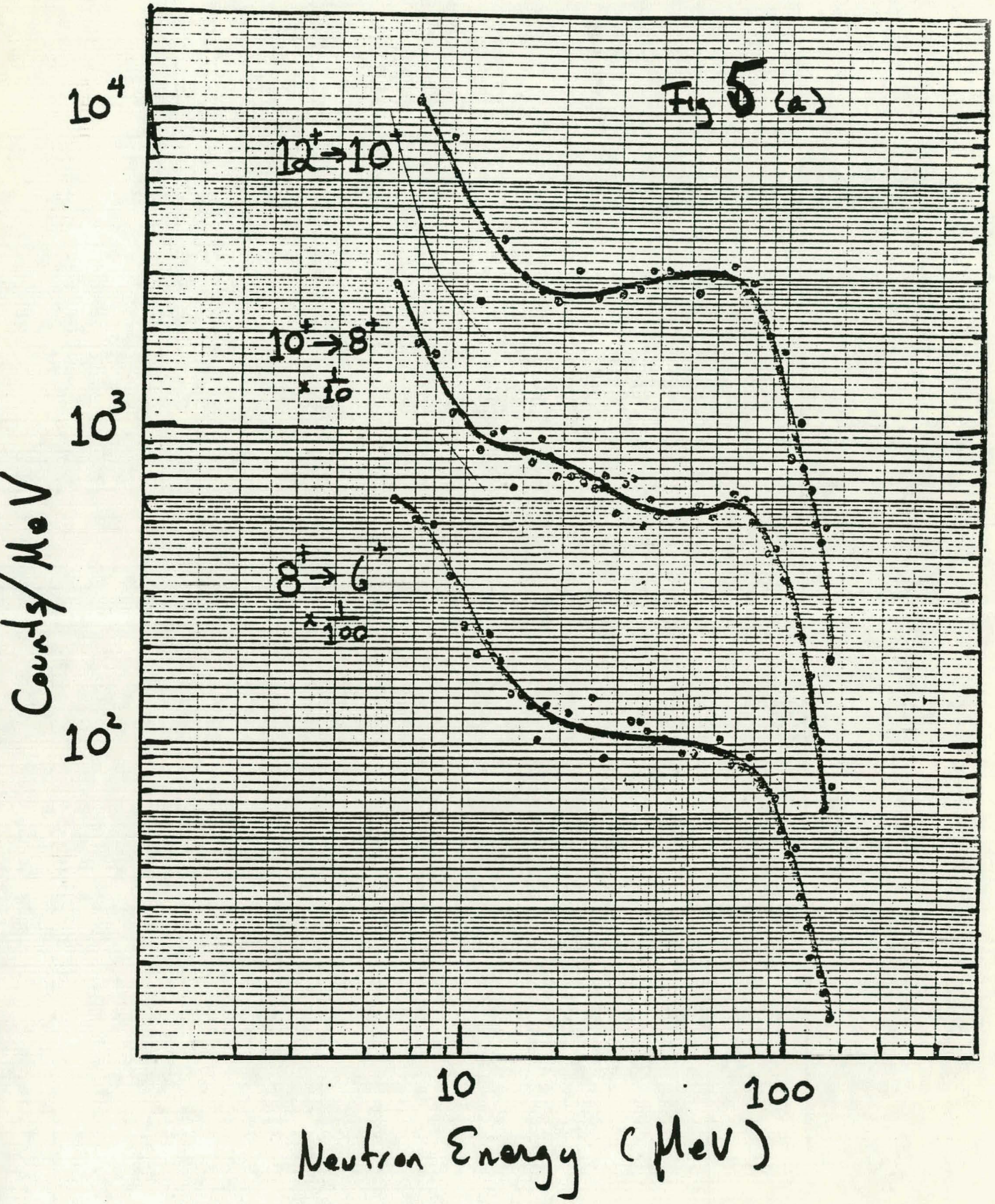
Fig 5 (a)
$12^+ \rightarrow 10^+$
$10^+ \rightarrow 8^+$
$\times \frac{1}{10}$
$8^+ \rightarrow 6^+$
$\times \frac{1}{100}$
10^4
10^3
10^2
Counts/MeV
10
100
Neutron Energy (MeV)

Fig 5 (b)

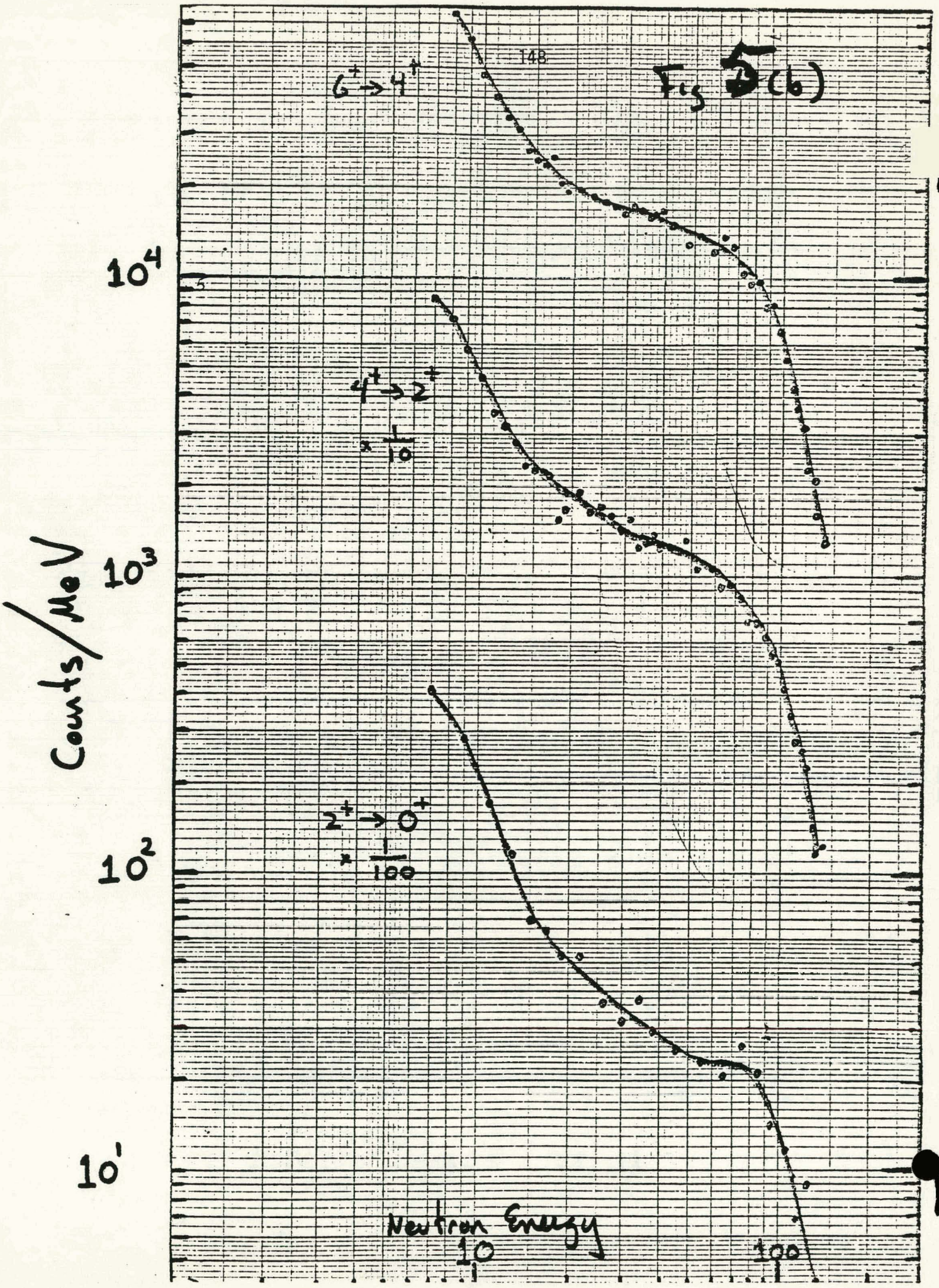
6+ → 4+
4+ → 2+
× 1/10
2+ → 0+
× 1/100
Counts/MeV
10⁴
10³
10²
10¹
Neutron Energy
1.0
10

deformed nucleus.

The data for the target of ^{165}Ho is now under analysis. If such effects are observed, it is certainly worthwhile to study other targets. One immediate candidate is ^{181}Ta for which the overlap of pion wavefunction with the nuclear matter is larger. The effects, if observed, will be an important correction to the quadrupole shift studies of pionic x-rays, and a novel method of microscopically studying the nuclear deformation and pionic interaction with nuclear matter.

REFERENCES:

1. R. Levin, T. J. Hallman, Y. K. Lee, E. McIntyre, Jr., L. Madansky and B. Olaniyi, Phys. Letters 114B, 427 (1982).
2. W. U. Schroder et al., Ann. Rev. Nucl. Sci. 27, 467 (1977).
3. V. S. Buttsev et al., Sov. J. Part. Nucl. 11, 358 (1980).
4. R. Beetz et al., Z. Phys. A286, 215 (1978).
5. P. Ebersold et al., Phys. Lett. 58B, 428 (1975).
6. R. O. Sayer et al., At. Data Nucl. Data Tables 15, 85 (1975).
7. M. Blann, Ann. Rev. Nucl. Sci. 25, 428 (1975).
8. E. Gadioli et al., Nucl. Phys. A256, 414 (1976).
9. A. S. Iljinov, Nucl. Phys. A268, 513 (1976).
10. H. Eijiri et al., Nucl. Phys. A305, 167 (1978).
11. L. Madansky and Y. K. Lee, Annual Progress Report for the DOE, DOE/ER/02374-2, 1981, p. 91.
12. W. Dey et al., Helv. Phys. Acta 49, 778 (1976).
13. Landolt-Börnstein, New Series I, Vol. 5b, ed. H. Schopper (Springer, Berlin, 1974).
14. V. S. Shirley and C. M. Lederer, eds., Nuclear Wallet Cards, The Isotope Project, Lawrence Berkeley Lab. (1979), unpublished.
15. Mukhopadhyay et al., Nuclear Phys. A319, 448 (1979).
16. H. C. Chiang and J. Hüfner, Nucl. Phys. A349, 466 (1980).
17. W. Q. Chao, F. Hachenberg, and J. Hüfner, Nucl. Phys. A384, 24 (1982).
18. N. R. Stanton, "GRACE Monte Carlo Neutron Detector Efficiency Program" Ohio State University COO-1545-92.
19. M. P. Locher and F. Myhrer, Helv. Phys. Acta 49, 123 (1976).

LIST OF PUBLICATIONS DURING THIS CONTRACT PERIOD:

T. Åkesson, M. G. Albrow, S. Frankel, L. Madansky et al., "Very High Central Multiplicity 63 GeV-63 GeV $\alpha\alpha$ Interactions," Physics Lett. 110B, 344 (1982).

R. Levin, T. J. Hallman, Y. K. Lee, E. McIntyre Jr., L. Madansky and B. Olaniyi, "Neutron Spectra Coincident with Discrete Gamma Rays in π^- Capture on ^{165}Ho and ^{181}Ta," Physics Lett. 114B, 427 (1982).

A. F. Shor, B. Olaniyi, S. C. Cheng, G. Dugan, C. S. Wu, Y. K. Lee and A. J. Caffrey, "Rotational Excitations in Residual Nuclei Produced by Stopped Negative Pions on Targets of ^{165}Ho, ^{175}Lu, ^{176}Lu, ^{179}Hf, and ^{181}Ta," submitted to Nuclear Physics.

T. Åkesson, M. G. Albrow, S. Frankel, L. Madansky et al., "Hadronization of Excited Nucleons in Nuclear Collisions at ISR Energies," submitted to Nuclear Physics B.

T. Akesson, M. G. Albrow, S. Frankel, L. Madansky et al., "Multiplicity Distributions in p-Alpha and Alpha-Alpha Collisions in the CERN ISR," submitted to Nuclear Physics.

E. McIntyre, T. Hallman, T. Lee, R. Levin, L. Madansky and G. Mason, "Correlations between Neutrons and Gamma Rays from π^- and μ^- Capture in Holmium," paper to be presented at the 1982 Fall Meeting of the Division of Nuclear Physics, Amherst, Massachusetts.

NEUTRON SPECTRA COINCIDENT WITH DISCRETE GAMMA RAYS IN π^- CAPTURE ON ^{165}Ho AND ^{181}Ta

R. LEVIN, T.J. HALLMAN, Y.K. LEE, E. McINTYRE Jr., L. MADANSKY
Department of Physics, The Johns Hopkins University, Baltimore, MD 21218, USA

and

B. OLANIYI
TRIUMF and the University of Victoria, B.C., Canada

Received 18 December 1981
Revised manuscript received 28 April 1982

Neutron spectra from π^--capture in medium-heavy nuclei are presented in coincidence with discrete nuclear gamma rays to exhibit possible correlations of the spectra to neutron multiplicity and residual nuclear states. A discrete component in the pre-compound neutron spectra is resolved for the first time, and its correlation to the population of high spin nuclear states is observed.

Recent progress in understanding the de-excitation process in heavy ion collisions [1,2] has given new insight into the nuclear processes involved in π^--capture. Several choices of target nuclei exist, ^{165}Ho and ^{181}Ta for example [3], for which the nuclear properties of residual isotopes are well understood from heavy ion physics [4].

The experiment described below is an effort to make more exclusive measurements of the π^--capture process by identifying the reaction channel leading to a particular nuclear state of a definite isotope. This goal is achieved by using an efficient time-of-flight system for neutrons in coincidence with discrete nuclear gamma rays. Peaks at the high energy end of exclusive neutron spectra in ^{165}Ho are resolved, and they reveal a strong effect on the population of high spin nuclear states. This is the first measurement where the neutron multiplicity, the angular momentum of the residual nuclei, and the neutron spectra are correlated to exhibit the resolved details of pre-compound neutron emission, as well as the effects of nuclear structure.

The current results are timely in view of the recent intensive efforts to describe the broad category of pre-compound emission by several different models [5–7]. Decisive experiments to resolve the ambiguity in such models are beginning to appear in terms of channel-defined measurements [8]. π^--capture in medium to heavy nuclei offers a particularly important opportunity to make such measurements since an experimentally clear time-zero signal is available from the stopped π^-, and a wide range of residual isotopes and nuclear states of high spin are reached.

The present experiment was carried out with a slow pion beam at the TRIUMF. Twelve large plastic scintillators (24″ × 6″ × 3″) were employed in a time-of-flight system [9] with a flight path of 5 ± 0.25 ft. The counters were spaced to measure the angular distribution at steps of 23 ± 5°. Both ends of each neutron counter were viewed by individual phototubes. The data from each counter were utilized in a mean-time mode, achieving overall timing resolution better than 1 ns. A large Ge(Li) gamma-ray detector was placed 19″ from the target in the plane defined by the neutron detectors. Background signals in the neutron counters due to electrons and gamma rays were effectively eliminated by the time-of-flight information, and the background due to protons was elimi-

0 031-9163/82/0000–0000/$02.75

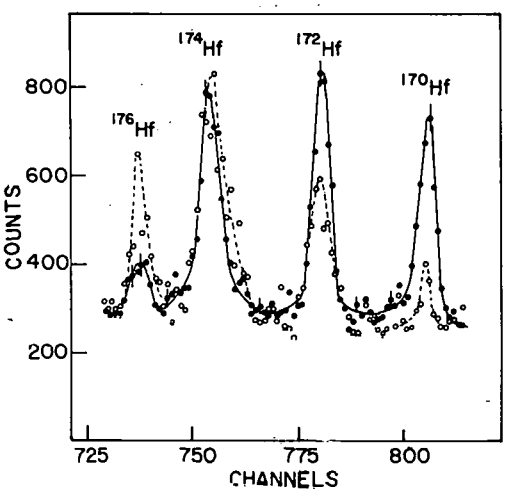

Fig. 1. The coincidence γ-ray spectra for the $(4^+ \rightarrow 2^+)$ gsb transitions with ^{181}Ta target. Solid circles are for coincidence with neutron energy <10 MeV; open circles for neutron energy >57 MeV. The spectra are normalized to the same maximum heights and the lines are drawn to guide the eye.

nated through identification of the residual isotope by its coincident gamma ray.

Data were recorded whenever the three-part coincidence of a stopped π^-, a gamma-ray signal in the Ge(Li), and at least one neutron counter occurred. The coincidence γ-ray spectra for the $(4^+ \rightarrow 2^+)$ ground-state-band (gsb) transitions with ^{181}Ta are shown in fig. 1 for various final isotopes of Hf. The solid circles correspond to the γ-rays in coincidence with high energy neutrons (>57 MeV) and the open circles with the evaporation neutrons (<10 MeV). With an increase in neutron energy, production of isotopes with lower neutron multiplicity increases sharply. Interesting variation in the isotope production patterns is noted for transitions to higher levels of the gsb.

In fig. 2, the neutron spectra in coincidence with the $(4^+ \rightarrow 2^+)$ gsb transitions for two targets are shown. The corresponding $(8^+ \rightarrow 6^+)$ gsb data are also shown for a few cases. These spectra have features which are absent in inclusive neutron spectra [10]. For the ^{165}Ho target, peaks are observed at the high energy end of the spectrum for three neutron multiplicities. The peaks are enhanced for the $(8^+ \rightarrow 6^+)$ transitions for ^{160}Dy. Such peaks are almost unrecognizable for the ^{181}Ta, but the origin of this effect is not known.

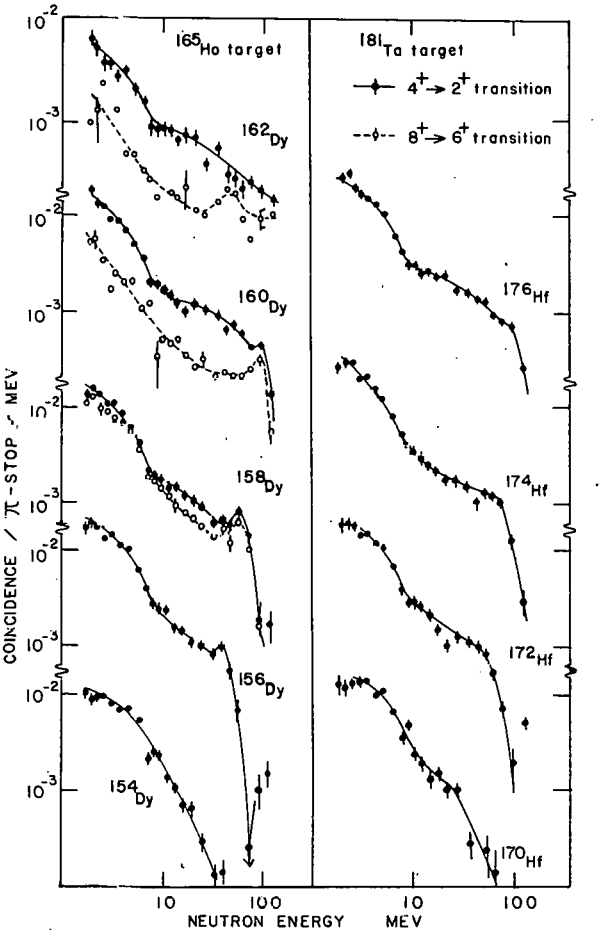

Fig. 2. Neutron spectra in coincidence with $(4^+ \rightarrow 2^+)$ and $(8^+ \rightarrow 6^+)$ transitions in the gsb for various neutron multiplicities for ^{165}Ho and ^{181}Ta targets. Lines are drawn to guide the eye.

In order to understand the presence and the shift in position of the peak for different neutron multiplicity (M_n), we evaluate the situation where one fast neutron is emitted from the nucleus leaving an excitation energy corresponding to the peak of excitation function for (p, xn)-reaction with $x = M_n - 1$. If we use the tabulation [11] of the values for $(E_m - E_{thres})$ where E_m is the excitation energy for the maximum probability for $(M_n - 1)$ neutron emission, and E_{thres} is the threshold energy for the (p, xn)-reaction, then we can evaluate the energy of the fast neutron to be:

$$E_n = M_\pi c^2 + Q(M_n) - \mathrm{BE}(\pi) - (E_{max} - E_{thres}),$$

Table 1
Peak neutron energy.

Isotopes	M_n	$Q(M_n)$ (MeV)	$E_m - E_{thres}$ (MeV)	E_n	
				calculated (MeV)	observed (MeV)
^{162}Dy	3	−20	9 ± 2	110 ± 2	–
^{160}Dy	5	−35	15 ± 2	89 ± 2	97 ± 12
^{158}Dy	7	−50	17 ± 5	72 ± 5	62 ± 6
^{156}Dy	9	−67	32 ± 7	40 ± 7	44 ± 4
^{154}Dy	11	−83	44 ± 7	12 ± 7	–

where M_π and BE(π) are the pion mass and binding energy, respectively, and $Q(M_n)$ is the Q-value for the M_n neutron emission from the nuclear mass table [12]. The results are listed in table 1. The agreement in positions is encouraging, but the mechanism favoring such a simple process is not clear, especially in view of the absence of such peaks for the ^{181}Ta target.

In fig. 2 the region between the high energy peak and the evaporation spectra may correspond to decay processes involving more than one fast neutron. Such conjecture is supported by the observation of the bulge in this region for the multiplicity of 5 (^{160}Dy), where a large amount of energy is shared among a relatively small number of particles. Fig. 2 shows that the bulge is very much reduced and the peak at the high energy end remains for the $8^+ \rightarrow 6^+$ transition for the multiplicity of 5 (^{160}Dy), indicating that the population of high-spin ($\geqslant 8^+$) is strongly correlated to the neutrons in the peak.

The above observation leads to the general picture of de-excitation based on the capture of the π^- by a quasideuteron on the surface of the nucleus. One neutron has a large probability for escaping with a small final state interaction, and the other neutron will start a series of nuclear reactions. When this is compared with the more familiar (p, xn)-reactions where the excitation function of each multiplicity is rather sharply defined (within 20 MeV FWHM) for a given incident proton energy [8], one can see the importance of the energy of the first neutron emission in determining the neutron multiplicity. The pre-equilibrium calculation [5] based on four initial exciton numbers is not able to describe these aspects, and incorporation of the special features of the surface capture is expected to be crucial.

In addition to the discrete feature of neutron spectra, the nuclear spin-dependence of the neutron multiplicity and spectral shape should be a challenge to more detailed pre-equilibrium calculations. The conjecture that the intermediate region in the neutron spectra (e.g. 10 MeV $< E <$ 80 MeV, for ^{160}Dy) is due to more than one pre-equilibrium neutron emission is now being tested by a n–n correlation experiment in coincidence with γ-rays.

The case of ^{162}Dy deserves special attention because only a few particles and gamma rays connect the initial capturing nuclei and the final ground state. Besides the fact that it involves only three neutrons, it is seen in fig. 2 that the majority of decays in ^{162}Dy do not go through the 8^+ state. Instead the 4^+ state seems to be very close to the entry state into ground state band after neutron emission. This suggests that there is a decay mechanism which carried away a large amount of energy with little change of angular momentum, such as a radiative π^--capture or back-to-back particle emission. There is, however, no obvious signature of back-to-back particle emission in the neutron spectra.

The authors gratefully acknowledge the assistance and hospitality extended to them at the TRIUMF, Canada, and the help of A.J. Caffrey during the early preparation. The project is partly supported by the US Department of Energy.

References

[1] V.S. Buttsev et al., Sov. J. Part. Nucl. 11 (1980) 358.
[2] W.U. Schroder et al., Ann. Rev. Nucl. Sci. 27 (1977) 465.

[3] R. Beetz et al, Z. Phys. A286 (1978) 215;
P. Ebersold et al., Phys. Lett. 58B (1975) 428.
[4] R.O. Sayer et al., At. Data Nucl. Data Tables 15 (1975) 85.
[5] M. Blann, Ann. Rev. Nucl. Sci. 25 (1975) 123.
[6] E. Gadioli et al., Nucl. Phys. A256 (1976) 414.
[7] A.S. Iljinov, Nucl. Phys. A268 (1976) 513.
[8] H. Ejiri et al., Nucl. Phys. A305 (1978) 167.
[9] M. Elfield et al., Nucl. Instrum. Methods 100 (1972) 237.
[10] W. Dey et al., Helv. Phys. Acta 49 (1976) 778.
[11] Landolt-Börnstein, New Series I, Vol. 5b, ed. H. Schopper (Springer, Berlin, 1974).
[12] V.S. Shirley and C.M. Ledérer, eds., Nuclear wallet cards, The isotope project, Lawrence Berkeley Lab. (1979), unpublished.

CERN-EP/82-73
10 June 1982

HADRONIZATION OF EXCITED NUCLEONS IN NUCLEAR COLLISIONS AT ISR ENERGIES

The Axial Field Spectrometer Collaboration

(BNL[1]-CERN[2]-Copenhagen[3]-Lund[4]-Pennsylvania[5]-RAL[6]-Tel Aviv[7])

T. Åkesson[4], M.G. Albrow[6], S. Almehed[4], O. Benary[7], H. Bøggild[3], O. Botner[2], H. Brody[5], V. Burkert[2], A. Di Ciaccio[1], D. Cockerill[6], S. Dagan[7], E. Dahl-Jensen[3], I. Dahl-Jensen[3], G. Damgaard[3], W.M. Evans[6], C.W. Fabjan[2], S. Frankel[5], W. Frati[5], H. Gordon[1], A. Hallgren[2], K.E. Hansen[3], B. Heck[2], H.J. Hilke[2], J.E. Hooper[3], G. Jarlskog[4], P. Jeffreys[6], G. Kesseler[2], T. Killian[1], J. v.d. Lans[2], P.R. Lindblom[5], D. Lissauer[7], B. Lörstad[4], T. Ludlam[1], L. Madansky[8], N.A. McCubbin[6], A. Melin[4], U. Mjornmark[4], R. Möller[3], W. Molzon[5], B.S. Nielsen[2], A. Nilsson[4], L.H. Olsen[2], Y. Oren[7], L. Rosselet[2], E. Rosso[2], A. Rudge[2], R.H. Schindler[2], B. Schistad[3], W.J. Willis[2], M. Winik[1], J.J. Winterberg[5], W. Witzeling[2], C. Woody[1].

ABSTRACT

Calorimeters downstream of the intersection of pα and αα beams in the ISR have been used to study the hadronization of excited nucleons. These data extend and support the conclusions from previous studies of the A-dependence of particle multiplicities in ultrarelativistic p-nucleus collisions, which provided evidence that the proton hadronizes outside the nuclear volume.

(Submitted to Nuclear Physics B)

1. Brookhaven National Laboratory, USA*
2. CERN, Geneva, Switzerland
3. Niels Bohr Institute, University of Copenhagen, Denmark
4. University of Lund, Sweden
5. University of Pennsylvania, USA*
6. Rutherford Appleton Laboratory, UK
7. University of Tel-Aviv, Israel
8. Johns Hopkins University, USA*

* Supported in part by U.S. Department of Energy

Multiplicity Distributions in p-Alpha and Alpha-Alpha Collisions in the CERN ISR

The Axial Field Spectrometer Collaboration

T. Akesson(4), M. G. Albrow(6), S. Almehed(4), O. Benary(7), H. Boggild(3), O. Botner(2), H. Brody(5), V. Burkert(2), A. di Ciaccio(1), D. Cockerill(6), S. Dagan(7), E. Dahl-Jensen(3), I. Dahl-Jensen(3), G. Damgaard(3), W. M. Evans(6), C. W. Fabjan(2), S. Frankel(5), W. Frati(5), H. Gordon(1), A. Hallgren(2), K. H. Hansen(3), B. Heck(2), H. J. Hilke(2), J. E. Hooper(3), G. Jarlskog(4), P. Jeffreys(2), G. Kesseler(2), T. Killian(1), J. v.d. Lans(2), D. Lissauer(7), B. Lorstad(4), T. Ludlam(1) L. Madansky(8), N. A. McCubbin(6), A. Melin(4), U. Mjornmark(4) R. Moller(3), W. Molzon(5), B. S. Nielsen(2), A. Nilsson(4) L. H. Olsen(3), Y. Oren(7), L. Rosselet(2), E. Rosso(2), A. Rudge(2) R. H. Schindler(2), B. Schistad(3), W. J. Willis(2), M. Winick(1), W. Witzeling(2), M. Wood(5), and C. Woody(1)

(1) Brookhaven National Laboratory
(2) CERN, Geneva, Switzerland
(3) Niels Bohr Institute, University of Copenhagen, Denmark
(4) University of Lund, Sweden
(5) University of Pennsylvania, USA
(6) Rutherford Appleton Laboratory, UK
(7) University of Tel Aviv, Israel
(8) Johns Hopkins University, USA

Abstract

Measurements of multiplicity distributions and momentum spectra in the central rapidity region in p-p, p-alpha, and alpha-alpha collisions are reported. They are better fitted to the "wounded nucleon" than to the "gluon string" model. The alpha-alpha data show poor KNO scaling to the p-p data. The <pt> of the momentum spectra, for all the reactions, are identical up to very high multiplicities.